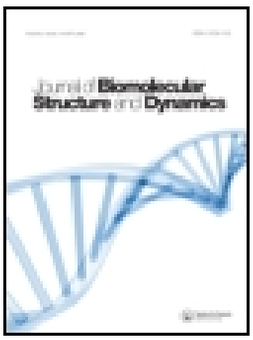

Taylor & Francis
Taylor & Francis Group

Journal of Biomolecular Structure and Dynamics

ISSN: 0739-1102 (Print) 1538-0254 (Online) Journal homepage: http://www.tandfonline.com/loi/tbsd20

Design, synthesis, MTT assay, DNA interaction studies of platinum(II) complexes

Miral V. Lunagariya, Khyati P. Thakor, Bhargav N. Waghela, Foram U. Vaidya, Chadramani Pathak & Mohan N. Patel

To cite this article: Miral V. Lunagariya, Khyati P. Thakor, Bhargav N. Waghela, Foram U. Vaidya, Chadramani Pathak & Mohan N. Patel (2016): Design, synthesis, MTT assay, DNA interaction studies of platinum(II) complexes , Journal of Biomolecular Structure and Dynamics, DOI: 10.1080/07391102.2016.1268071

To link to this article: http://dx.doi.org/10.1080/07391102.2016.1268071

Publisher: Taylor & Francis

Journal: *Journal of Biomolecular Structure and Dynamics*

DOI: http://dx.doi.org/10.1080/07391102.2016.1268071

Design, synthesis, MTT assay, DNA interaction studies of platinum(II) complexes

Miral V. Lunagariya[a], Khyati P. Thakor[a], Bhargav N. Waghela[b], Foram U. Vaidya[b], Chadramani Pathak[b] and Mohan N. Patel[a]*

[a]*Department of Chemistry, Sardar Patel University,*

Vallabh Vidyanagar–388 120, Gujarat, India.

Corresponding author. Tel.: +91 2692 226856 E-mail: jeenen@gmail.com

[b]*Department of Cell biology,*

Indian institute of advanced Research,

Gandhinagar, Gujarat, India.

E-mail: cmpathak@iiar.res.in

Abstract

The square planar Pt(II) complexes of the type $[Pt(L^n)(Cl_2)]$ (where $L^n = L^{1-3}$ = thiophene-2-carboxamide derivatives and L^{4-6} = thiophene-2-carbothioamide derivatives) have been synthesized and characterized by physicochemical and various spectroscopic studies. MIC method was employed to inference the antibacterial potency of complexes in reference to free ligands and metal salt. Characteristic binding constant (K_b) and binding mode of complexes

with calf thymus DNA (CT-DNA) were determined using absorption titration (0.76 – 1.61 × 10^5 M^{-1}), hydrodynamic chain length assay and fluorescence quenching analysis, deducing the partial intercalative mode of binding. Molecular docking calculation displayed free energy of binding in the range of -260.06 to -219.63 $kJmol^{-1}$. The nuclease profile of complexes towards pUC19 DNA shows that the complexes cleave DNA more efficiently compared to their respective metal salt. Cytotoxicity profile of the complexes on the brine shrimp shows that all the complex exhibit noteworthy cytotoxic activity with LC_{50} values ranging from 7.87 to 15.94 µg/mL. The complexes have been evaluated for cell proliferation potential in human colon carcinoma cells (HCT 116) and IC_{50} value of complexes by MTT assay (IC_{50} = 125 - 1000 µg/mL).

Keywords: Platinum(II) complexes, Cell proliferation assay, Antibacterial study, Brine shrimp cytotoxicity assay, DNA interaction study.

1. Introductions

Medicinal inorganic chemistry has been strengthened by the discovery of the anticancer properties of the coordination compound *cis*-platin by Rosenberg *et. al* in 1969, owing to its great impact in the treatment of cancer.(N. Farrell (Ed.), 1989; Rosenberg, Vancamp, Trosko, & Mansour, 1969) Since its approval in 1979, it has been used for therapeutic agent, diagnostic agent, mineral supplement and chelation therapy. Platinum metal has also been frequently incorporated into pharmaceuticals.(Guo & Sadler, 1999; Mjos & Orvig, 2014; Thompson & Orvig, 2003) For the treatment of ovarian, testicular, lung and bladder cancers, it has been an important component in chemotherapeutic treatments.(Kelland, 2007; Wheate, Walker, Craig, & Oun, 2010) Although it is found successful in the treatment of various cancers, it has several side effects like nausea, vomiting, ototoxicity and neurotoxicity that limit treatment with *cis*-platin.(Kelland, 2007; Wheate et al., 2010)

As anticancer agent's carboplatin, oxaliplatin, nedaplatin, lobaplatin and heptaplatin enclosing platinum metal have been reported.(I.H.Krakoff, 1988,; Loehrer, Williams, & Einhorn, 1988) In cancer chemotherapy, *cis*-platin and other platinum-based drugs have been greatly inspired by their clinical use for the treatment of hypercalcaemia and skeletal metastases and in geminal bisphosphonates (BPs) drug, which shows the affinity for bones and other calcified tissues(Kelland, 2007) and also being active in the development of biosensors.(Aslanoglu, Isaac, Houlton, & Horrocks, 2000) Initial investigations of the mechanism of cisplatin, as an anticancer drug, proposed that metal based drug interact with DNA, due to the covalent binding of platinum compounds to the N7 of guanine residue. Hence, it affects the replication and generation of cellular events and finally leads to the death of cancer cell.(Boulikas, 2003; Wang & Lippard, 2005) However, limitation of cisplatin is that, it has nephrotoxicity and is only partially soluble in water in its clinical application. It was observed that reaction between sulphur-containing proteins and platinum metal induces poisonous effect to carcinogenic cells and inactivate some enzymes.(Florea & Büsselberg, 2011; Kostova, 2006; N. Farrell, 2009; P. Kalyani, 2012) Hence, the synthesis of new types of platinum based complexes, whose structure and mode of action differ from those of cisplatin and bearing oxygen and sulphur donor atoms are important to prevent adverse reactions. Several platinum complexes with S-heterocyclic ligands such as thiophene, benzo[b]thiophene, benzothiazole, 2-acetyl thiophene and thiophene-2-carboxaldehyde were reported.(Ji, Shigeta, Niko, Watanabe, & Konishi, 2013; S. B. Kumar et al., 2012; M. Zala, 2011; Neto, de Lima, & Beraldo, 2006)

A series of Pt(II) complexes have been synthesized using -S, O/ -S, S donor containing heterocyclic thiophene-2-carboxamide/thiophene-2-carbothioamide

derivative ligands and characterized by elemental analysis, electronic spectra, conductance measurements, TGA, FT-IR and LC-MS spectroscopy and Pt(II) complexes to explore them as molecules of biological significance. Some of its derivatives have potent biological activities as *in vitro* cytotoxicity, antimicrobial and anticancer agents.

2. Experimental

2.1 Material and Instrumentation

All solvents and reagents used were of analytical grade. Potassium tetrachloroplatinate(II) chloride salt was purchased from S. D Fine-Chem Ltd. (SDFCL). Nutrient broth (NB), agarose, ethidium bromide (EtBr), tris-acetyl-EDTA (TAE), bromophenol blue was purchased from Himedia (India). Calf thymus (CT) DNA, thiophene-2-carbonyl chloride were purchased from Sigma Aldrich (India). Thin layer chromatography (TLC) was performed using Merck aluminium sheets coated with silica gel 60 F_{254}. Purification by flash chromatography was performed using Merck silica gel 60. The compounds were visualized under UV light. All the bacterial cultures used were purchased from MTCC, Institute of Microbial Technology and Chandigarh, India. An *Artemia cyst was* purchased from local aquarium store. GenElute mini Pre Kit for pUC19 DNA isolation was purchased from Sigma Aldrich (India). MilliQ™ (18.2 m℧, Millipore) was used for the preparation of all deionized water. HPLC grade DMSO was used to dissolve the platinum compounds.

Micro elemental analysis (C, H, N and S) of the synthesized compounds was performed with a *EuroEA* elemental analyser. Room temperature magnetic measurement for the complexes was made using Gouy's magnetic balance. Melting points were determined on Buchi 540 melting point apparatus.

^{1}H NMR and ^{13}C NMR spectra were obtained on a 400 MHz and 100 MHz Bruker avance nuclear magnetic resonance spectrometer, either in DMSO-d_6 (35 °C), referenced internally to the solvent. The attached proton test in a ^{13}C APT (Attached Proton Test) characterisation showed CH, CH_2 and CH_3 signals unattached to protons. The APT experiment yields methine (CH) and methyl (CH_3) signals negative and quaternary (C) and methylene (CH_2) signals positive. The chemical shift of each resonance was quoted as an approximate midpoint of its multiplicity.

The electronic spectra were recorded on a UV-160A UV-Vis spectrophotometer, Shimadzu, Kyoto (Japan). Infrared spectra were recorded on a FT-IR ABB Bomen MB-3000 spectrophotometer (Canada) in the range of 4,000 to 400 cm^{-1}. The magnetic moments were measured by Gouy's method using mercury tetrathiocyanatocobaltate(II) as the calibrate (χ_g=16.44 × 10^{-6} cgs units at 20 °C). The LC-MS spectra were recorded using thermo mass spectrophotometer (USA). MIC study was carried out using laminar air flow cabinet, Toshiba, Delhi, (India). Fluorescence spectroscopy was carried out by FluoroMax-4, spectrofluorometer, HORIBA (Scientific). Photo quantization of the gel after electrophoresis was done using AlphaDigiDoc™ RT. Version V.4.0.0 PC–Image software, CA (USA). Hydrodynamic chain length study was carried out by viscometric bath.

2.2 General synthesis of the ligands (L^{1-6})

Synthesis was achieved by using an adaptation of the published method.(Hodges & Rund, 1975) For synthesis of ligands **(L^{1-3})**, thiophene-2-carbonyl chloride (0.015 mol) in chloroform ($CHCl_3$) was reacted with substituted aniline (0.015 mol) derivatives. The reaction mixture was stirred for 2 h at 0 °C. Pyridine was used as a catalyst to promote the quick synthesis of ligands. After stirring, aq. HCl was added (3 - 4 drops) and the mixture was extracted with chloroform using brine solution

as demulsifier. Extracted organic layer was dried over $MgSO_4$ and evaporated to obtain the precipitate. The residue obtained was purified by column chromatography on silica using (hexane: ethyl acetate = 4:1) system. Solid obtained as a fine crystalline product was filtered and dried in vacuum. For the synthesis of ligands **(L^{4-6})**, ligands **(L^{1-3})** (0.015 mol) and Lawesson's reagents (0.015 mol) were refluxed in toluene for 3 h. After refluxing, water was added to the reaction mixture. Obtained precipitate was extracted with chloroform using brine as demulsifier, dried over $MgSO_4$ and evaporated to dryness. The residue was then purified by column chromatography on silica gel using (hexane: ethyl acetate = 4:1) system, and the finally ligands (L^{4-6}) were obtained as yellow crystalline product, which were filtered and dried in vacuum.

*2.2.1 N-Phenylthiophene-2-carboxamide (**L^1**)*

The ligand (**L^1**) was synthesized using thiophene-2-carbonyl chloride and aniline following the general process described in experimental section. **Colour:** white crystal, **Yield:** 66 %, **mol. wt.** 203.26 g/mol, **m.p.** 251 °C; **Anal. Calc. (%) For $C_{11}H_9NOS$:** C, 65.00; H, 4.46; N, 6.89; S, 15.77. **Found (%):** C, 64.98; H, 4.40; N, 6.86; S, 15.20. **UV-Vis: λ (nm) (ε, M^{-1} cm^{-1}):** 301 (13,850), 357 (4,275). **^{1}H NMR (400 MHz, DMSO-d_6) δ/ppm:** 8.036 (d, 1H, J = 3.6 Hz, $H_{2''}$), 7.862 (d, 1H, J = 4.8 Hz, $H_{4''}$), 7.729 (d, 2H, J = 8.4 Hz, $H_{2,6}$), 7.361 (t, 2H, J = 7.6 Hz, $H_{3,5}$), 7.228 (dd, 1H, J = 4.8 Hz, J = 4.4 Hz, $H_{3''}$), 7.112 (t, 1H, J = 7.2 Hz, H_4), 10.220 (s, 1H, $H_{1'}$). **^{13}C NMR (100 MHz, DMSO-d_6) δ/ppm:** 137.0 (C_1), 121.6 ($C_{2,6}$), 128.9 ($C_{3,5}$), 128.0 (C_4), 130.3 ($C_{2'}$), 129.0 ($C_{3'}$), 131.9 ($C_{4'}$), 139.4 ($C_{5'}$), 161.8 ($C_{2''}$). [Signal observed = 9: Ar-CH = 3, Ar-C = 1 carbonyl = 1, thiophene-C = 1, thiophene-CH = 3]. **Mass (m/z):** 202.26 $[M]^+$.

*2.2.2 N-(4-Chlorophenyl) thiophene-2-carboxamide (**L^2**)*

The ligand **(L^2)** was synthesized using thiophene-2-carbonyl chloride and 4-chloroaniline. **Colour:** white crystal, **Yield:** 70 %, **mol. wt.** 237.71 g/mol, **m.p.** 163 °C; **Anal. Calc. (%) For $C_{11}H_8ClNOS$:** C, 55.58; H, 3.39; N, 5.89; S, 13.49. **Found (%):** C, 55.30; H, 3.20; N, 5.69; 13.10. **UV-Vis: λ (nm) (ε, M^{-1} cm^{-1}):** 300 (13,950), 359 (4,295). **^{1}H NMR (400 MHz, DMSO-d_6) δ/ppm:** 8.368 (d, 2H, J = 7.2 Hz, $H_{3,5}$), 8.274 (dd, 1H, J = 4.0 Hz, J = 4.4 Hz, $H_{3''}$), 7.926 (d, 2H, J = 7.6 Hz, $H_{2,6}$), 7.361 (d, 1H, J = 3.6 Hz, $H_{2''}$), 7.030 (d, 1H, J = 4.4 Hz, $H_{4''}$), 10.765 (s, 1H, $H_{1'}$). **^{13}C NMR (100 MHz, DMSO-d_6) δ/ppm:** 136.0 (C_1), 121.6 ($C_{2,6}$), 129.0 ($C_{3,5}$), 133.3 (C_4), 130.3 ($C_{2'}$), 129.0 ($C_{3'}$), 131.9 ($C_{4'}$), 139.4 ($C_{5'}$), 161.8 (C2"); [Signal observed = 9: Ar-CH = 2, Ar-C = 2, carbonyl = 1, thiophene-C = 1, thiophene-CH = 3]. **Mass m/z(%):** 236.70 $[M]^+$, 238.70 [M + 2].

*2.2.3 N-(4-Nitrophenyl) thiophene-2-carboxamide (**L^3**)*

The ligand **(L^3)** was synthesized using thiophene-2-carbonyl chloride and 4-nitroaniline as described in general process. **Colour:** light yellow crystal, **Yield:** 82 %, mol. wt. 248.26 g/mol, **m.p.** 253 °C**; Anal. Calc. (%) For $C_{11}H_8N_2O_3S$:** C, 53.22; H, 3.25; N, 11.28; S, 12.91. **Found (%):** C, 53.01; H, 3.12; N, 11.08; S, 12.36. **UV-Vis: λ (nm) (ε, M^{-1} cm^{-1}):** 298 (13,600), 360 (4,290). **^{1}H NMR (400 MHz, DMSO-d_6) δ/ppm:** 8.270 (d, 2H, J = 8.0 Hz, $H_{3,5}$), 8.171 (d, 2H, J = 8.0 Hz, $H_{2,6}$), 8.052 (d, 1H, J = 4.0 Hz, $H_{2''}$), 7.939 (d, 1H, J = 4.0 Hz, $H_{4''}$), 7.260 (dd, 1H, J = 4.0 Hz, J= 4.0 Hz, $H_{3''}$), 10.442 (s, 1H, $H_{1'}$).**^{13}C NMR (100 MHz, DMSO-d_6) δ/ppm:** 144.0 (C_1), 119.9 ($C_{2,6}$), 124.1 ($C_{3,5}$), 143.5 (C_4), 130.3 ($C_{2'}$), 129.0 ($C_{3'}$), 131.9 ($C_{4'}$), 139.4 ($C_{5'}$), 161.8 ($C_{2''}$); [Signal observed = 9: Ar-CH = 2, Ar-C = 2, carbonyl = 1, thiophene-C = 1, thiophene-CH = 3]. **Mass m/z:** 247.26 $[M]^+$.

*2.2.4 N-Phenylthiophene-2-carbothioamide (**L^4**)*

The ligand **(L^4)** was synthesized, using ligand **(L^1)** and Lowsson's reagent, according to the general process described in experimental section. **Colour:** light yellow crystal, **Yield:** 87 %, **mol. wt.** 219.33 g/mol, **m.p.** 167 °C; **Anal. Calc. (%) For $C_{11}H_9NS_2$:** C, 60.24; H, 4.14; N, 6.39; S, 29.24. **Found (%):** C, 60.01; H, 4.08; N, 6.15; S, 28.94. **UV-Vis: λ (nm) (ε, M^{-1} cm^{-1}):** 280 (13,700), 388 (4,285). **^{1}H NMR (400 MHz, DMSO-d_6) δ/ppm:** 8.036 (d, 1H, J = 3.6 Hz, $H_{2''}$), 7.862 (d, 1H, J = 4.8 Hz, $H_{4''}$), 7.719 (d, 2H, J = 8.0 Hz, $H_{2,6}$), 7.323 (t, 1H, J = 6.8, H_4), 7.248 (dd, 1H, J = 4.0 Hz, J = 4.8 Hz, $H_{3''}$), 7.112 (t, 2H, J = 7.2 Hz, $H_{3,5}$), 10.232 (s, 1H, $H_{1'}$). **^{13}C NMR (100 MHz, DMSO-d_6) δ/ppm:** 139.0 (C_1), 123.8 ($C_{2,6}$), 129.1 ($C_{3,5}$), 128.4 (C_4), 129.1 ($C_{2'}$), 127.2 ($C_{3'}$), 126.3 ($C_{4'}$), 144.0 ($C_{5'}$), 197.0 ($C_{2''}$); [Signal observed = 9: Ar-CH = 3, Ar-C = 1, thiocarbonyl = 1, thiophene-C = 1, thiophene-CH = 3]. **Mass m/z:** 218.32 $[M]^+$.

2.2.5 N-(4-Chlorophenyl) thiophene-2-carbothioamide (L^5)

The ligand **(L^5)** was synthesized using ligand **(L^2)** and Lowsson's reagent. **Colour:** dark yellow crystal, **Yield:** 85 %, **mol. wt.** 253.35 g/mol, **m.p.** 240 °C; **Anal. Calc. (%) For $C_{11}H_8ClNS_2$:** C, 52.06; H, 3.18; N, 5.52; S, 25.27. **Found (%):** C, 51.77; H, 3.12; N, 5.12; S, 25.07. **UV-Vis: λ (nm) (ε, M^{-1} cm^{-1}):** 278 (13,935), 387 (9,085). **^{1}H NMR (400 MHz, DMSO-d_6) δ/ppm:** 7.882 (d, 2H, J = 7.6 Hz, $H_{3,5}$), 7.733 (d, 2H, J = 7.2 Hz, $H_{2,6}$), 7.520 (d, 1H, J = 3.6 Hz, $H_{2''}$), 7.506 (d, 1H, J = 4.4 Hz, $H_{4''}$), 7.280 (dd, 1H, J = 4.4 Hz, J = 4.4 Hz, $H_{3''}$), 11.565 (s, 1H, $H_{1'}$). **^{13}C NMR (100 MHz, DMSO-d_6) δ/ppm:** 137.1 (C_1), 125.0 ($C_{2,6}$), 125.4 ($C_{3,5}$), 133.7 (C_4), 129.1 ($C_{2'}$), 127.2 ($C_{3'}$), 126.3 ($C_{4'}$), 144.0 ($C_{5'}$), 197.0 ($C_{2''}$); [Signal observed = 9: Ar-CH = 2, Ar-C = 2, thiocarbonyl = 1, thiophene-C = 1, thiophene-CH = 3]. **Mass m/z:** 252.76 $[M]^+$, 254.95 [M + 2].

2.2.6 *N-(4-Nitrophenyl) thiophene-2-carboxamide (L^6)*

The ligand **(L^6)** was synthesized using ligand **(L^3)** and Lowsson's reagent. **Colour:** brown powder, **Yield:** 88 %, **mol. wt.** 264.32 g/mol, **m.p.** 270 °C; **Anal. Calc. (%) For $C_{11}H_8ClNS_2$:** C, 49.99; H, 3.05; N, 10.60; S, 24.26. **Found (%):** C, 51.17; H, 3.02; N, 9.13; S, 25.97. **UV-Vis: λ (nm) (ε, M^{-1} cm^{-1}):** 281 (13,935), 389 (9,000). **^{1}H NMR (400 MHz, DMSO-d_6) δ/ppm:** 8.023 (d, 1H, J = 4.0 Hz, $H_{2''}$), 7.870 (d, 1H, J = 4.0 Hz, $H_{4''}$), 7.779 (d, 2H, J = 7.6 Hz, $H_{3,5}$), 7.405 (d, 2H, J = 7.2 Hz, $H_{2,6}$), 7.237 (dd, 1H, J = 3.6 Hz, J = 3.2 Hz, $H_{3''}$), 10.336 (s, 1H, $H_{1'}$). **^{13}C NMR (100 MHz, DMSO-d_6) δ/ppm:** 145.1 (C_1), 124.8 ($C_{2,6}$), 124.2 ($C_{3,5}$), 143.9 (C_4), 129.1 ($C_{2'}$), 127.2 ($C_{3'}$), 126.3 ($C_{4'}$), 144.0 ($C_{5'}$), 197.0 ($C_{2''}$); [Signal observed = 9: Ar-CH = 2, Ar-C = 2, carbonyl = 1, thiophene-C = 1, thiophene-CH = 3]. **Mass m/z:** 263.32 $[M]^+$.

2.3 General synthesis of [Pt(L^{1-6})(Cl_2)] complexes (1a-1f)

Herein, we report six mononuclear Pt(II) complexes **(1a-1f)** with the aromatic bidentate thiophene-2-carboxamide **(L^{1-3})** and thiophene-2-carbothioamide **(L^{4-6})** derivative ligands having -S, O/ -S, S donor atoms. The complexes were synthesized using method proposed by Hodges and Rund.(Wolfe, Shimer, & Meehan, 1987) Complexes [Pt(II)(L^{1-6})Cl_2] were synthesized by refluxing 1:1 ratio of **(L^{1-6})** (0.2 mmol) and K_2PtCl_4 (0.2 mmol) in water-methanol system (50 mL) at 60 °C with 1-2 drops of hydrochloric acid (free acid is to avoid displacement of Cl^- by ^-OH) until the solution became colourless (0.5 - 6 h). Reaction mixture was allowed to cool at room temperature. The obtained product was washed with hot water and dried under vacuum.

*2.3.1 Synthesis of **[Pt(L^1)(Cl_2)] (1a)***

It was synthesized using ligand **(L^1)**. **Colour:** brown powder, **Yield:** 70 %, **mol. wt.** 469.25 g/mol, **m.p.** ≥ 300 °C, **Anal. Calc. (%) For $C_{11}H_9Cl_2NOPtS$:** C,

28.16; H, 1.93; N, 2.99; S, 6.83; Pt, 41.57. **Found (%):** C, 28.01; H, 1.71; N, 2.71; S, 6.54; Pt, 41.04. **Conductance:** 24 Ω^{-1} cm^2 mol^{-1}. **UV-Vis: λ (nm) (ε, M^{-1} cm^{-1}):** 292 (13,460), 387 (6,100), 419 (5,505). **^{1}H NMR (400 MHz, DMSO-d_6) δ/ppm:** 8.025 (d, 1H, J = 3.6 Hz, $H_{2''}$), 7.860 (d, 1H, J = 4.8 Hz, $H_{4''}$), 7.723 (d, 2H, J = 7.6 Hz, $H_{2,6}$), 7.361 (t, 2H, J = 7.6 Hz, $H_{3,5}$), 7.224 (t, 1H, J = 7.6 Hz, H_4), 7.114 (dd, 1H, J = 4.0 Hz, J = 3.6 Hz, $H_{3''}$), 10.204 (s, 1H, $H_{1'}$). **^{13}C NMR (100 MHz, DMSO-d_6) δ/ppm:** 140.0 (C_1), 122.3 ($C_{2,6}$), 129.5 ($C_{3,5}$), 128.2 (C_4), 135.1 ($C_{2'}$), 129.9 ($C_{3'}$), 132.0 ($C_{4'}$), 145.0 ($C_{5'}$), 165.5 ($C_{2''}$); [Signal observed = 9: Ar-CH = 3, Ar-C = 1, carbonyl = 1, thiophene-C = 1, thiophene-CH = 3].

2.3.2 *Synthesis of* ***[Pt(L^2)(Cl_2)] (1b)***

It was synthesized using ligand **(L^2)**. **Colour:** brown powder, **Yield:** 75 %, **mol. wt.** 503.70 g/mol, **m.p.** ≥300 °C, **Anal. Calc. (%) For $C_{11}H_8Cl_3NOPtS$:** C, 26.23; H, 1.60; N, 2.78; S, 6.37; Pt, 38.73. **Found (%):** C, 25.89; H, 1.63; N, 2.67; S, 6.02; Pt, 38.05. **Conductance:** 22 Ω^{-1} cm^2 mol^{-1}. **UV-Vis: λ (nm) (ε, M^{-1} cm^{-1}):** 292 (13,500), 376 (6,000), 418 (5,670). **^{1}H NMR (400 MHz, DMSO-d_6) δ/ppm:** 8.033 (d, 1H, J = 3.6 Hz, $H_{2''}$), 7.974 (dd, 1H, J = 4.4 Hz, J = 4.4 Hz, $H_{3''}$), 7.842 (d, 1H, J = 4.8 Hz, $H_{4''}$), 7.418 (d, 2H, J = 7.2 Hz, $H_{3,5}$), 7.273 (d, 2H, J = 8.0 Hz, $H_{2,6}$), 10.348 (s, 1H, $H_{1'}$). **^{13}C NMR (100 MHz, DMSO-d_6) δ/ppm:** 140.1 (C_1), 123.6 ($C_{2,6}$), 128.0 ($C_{3,5}$), 134.0 (C_4), 138.0 ($C_{2'}$), 129.3 ($C_{3'}$), 135.9 ($C_{4'}$), 142.0 ($C_{5'}$), 164.0 ($C_{2''}$); [Signal observed = 9: Ar-CH = 2, Ar-C = 2, carbonyl = 1, thiophene-C = 1, thiophene-CH = 3].

2.3.3 Synthesis of ***[Pt(L^3)(Cl_2)] (1c)***

It was synthesized using ligand **(L^3)**. **Colour:** brown powder, **Yield:** 82 %, **mol.wt.** 514.25 g/mol, **m.p.** ≥ 300 °C, **Anal. Calc. (%) For $C_{11}H_8C_{l2}N_2O_3PtS$:** C, 27.22; H, 1.87; N, 2.89; S, 6.23; Pt, 40.20. **Found (%):** C, 25.29; H, 1.40; N, 5.40; S,

6.08; Pt, 39.82. **Conductance:** 20 Ω^{-1} cm^2 mol^{-1}. **UV-Vis: λ (nm) (ε, M^{-1} cm^{-1}):** 292 (13,355), 389 (5,950), 417 (5,500). **^{1}H NMR (400 MHz, DMSO-d_6) δ/ppm:** 8.282 (d, 2H, J = 7.2 Hz, $H_{3,5}$), 8.124 (d, 1H, J = 4.0 Hz, $H_{2''}$), 8.034 (d, 2H, J = 9.2 Hz, $H_{2,6}$), 7.953 (d, 1H, J = 4.0 Hz, $H_{4''}$), 7.271 (dd, 1H, J = 3.6 Hz, J = 3.6 Hz, $H_{3''}$), 10.791 (s, 1H. $H_{1'}$).**^{13}C NMR (100 MHz, DMSO-d_6) δ/ppm:** 148.0 (C_1), 121.5 ($C_{2,6}$), 126.3 ($C_{3,5}$), 149.8 (C_4), 131.0 ($C_{2'}$), 129.2 ($C_{3'}$), 123.0 ($C_{4'}$), 145.0 ($C_{5'}$), 167.0 ($C_{2''}$); [Signal observed = 9: Ar-CH = 2, Ar-C = 2, carbonyl = 1, thiophene-C = 1, thiophene-CH = 3].

*2.3.4 Synthesis of **[Pt(L^4)(Cl_2)] (1d)***

It was synthesized using ligand (**L^4**). **Colour:** brown powder, **Yield:** 75 %, **mol.wt.** 485.32 g/mol, **m.p.** ≥ 300 °C, **Anal. Calc. (%) For $C_{11}H_9Cl_2NPtS_2$:** C, 27.22; H, 1.87; N, 2.89; S, 13.21; Pt, 36.89. **Found (%):** C, 27.01; H, 1.67; N, 2.78; S, 13.11; Pt, 38.50. **Conductance:** 25 Ω^{-1} cm^2 mol^{-1}. **UV-Vis: λ (nm) (ε, M^{-1} cm^{-1}):** 292 (10,555), 405 (4,720), 419 (4,955). **^{1}H NMR (400 MHz, DMSO-d_6) δ/ppm:** 8.046 (d, 1H, J = 4.8 Hz, $H_{2''}$), 7.875 (d, 1H, J = 4.0 Hz, $H_{4''}$), 7.739 (d, 2H, J = 7.2 Hz, $H_{2,6}$), 7.361 (t, 1H, J = 8.0 Hz, H_4), 7.166 (dd, 1H, J = 3.6 Hz, J = 3.6 Hz, $H_{3''}$), 7.062 (t, 2H, J = 8.0 Hz, $H_{3,5}$), 10.969 (s, 1H, $H_{1'}$). **^{13}C NMR (100 MHz, DMSO-d_6) δ/ppm:** 143.0 (C_1), 124.0 ($C_{2,6}$), 130.0 ($C_{3,5}$), 128.5 (C_4), 133.5 ($C_{2'}$), 131.4 ($C_{3'}$), 127.8 ($C_{4'}$), 155.2 ($C_{5'}$), 199.0 ($C_{2''}$); [Signal observed = 9: Ar-CH = 3, Ar-C = 1, thiocarbonyl = 1, thiophene-C = 1, thiophene-CH = 3].

*2.3.5 Synthesis of **[Pt(L^5)(Cl_2)] (1e)***

It was synthesized using ligand (**L^5**). Colour: light brown powder, **Yield:** 80 %, **mol.wt.** 519.76 g/mol, **m.p.** ≥ 300 °C, **Anal. Calc. (%) For $C_{11}H_8Cl_3NPtS_2$:** C, 25.42; H, 1.55; N, 2.69; S, 12.34, Pt, 37.53. **Found (%):** C, 25.40; H, 1.51; N, 2.58; S, 12.25; Pt, 37.17. **Conductance:** 19 Ω^{-1} cm^2 mol^{-1}. **UV-Vis: λ (nm) (ε, M^{-1} cm^{-1}):** 294

(10,570), 405 (4,740), 422 (4,970). **^{1}H NMR (400 MHz, DMSO-d$_6$) δ/ppm:** 7.902 (d, 2H, J = 7.2 Hz, $H_{3,5}$), 7.881 (d, 2H, J = 7.6 Hz, $H_{2,6}$), 7.739 (d, 1H J = 4.0 Hz, $H_{2''}$), 7.598 (d, 1H, J = 4.0 Hz, $H_{4''}$), 7.224 (dd, 1H, J = 4.8 Hz, J = 3.6 Hz, $H_{3''}$), 11.590 (s, 1H, $H_{1'}$). **^{13}C NMR (100 MHz, DMSO-d$_6$) δ/ppm:** 140.2 (C_1), 128.1 ($C_{2,6}$), 130.3 ($C_{3,5}$), 136.4 (C_4), 133.5 ($C_{2'}$), 128.0 ($C_{3'}$), 127.1 ($C_{4'}$), 148.0 ($C_{5'}$), 198.3 ($C_{2''}$); [Signal observed = 9: Ar-CH = 2, Ar-C = 2, thiocarbonyl = 1, thiophene-C = 1, thiophene-CH = 3].

2.3.6 Synthesis of ***[Pt(L^6)(Cl$_2$)] (1f)***

It was synthesized using ligand (**L^6**). Colour: brown powder, **Yield:** 78 %, **mol.wt.** 530.31 g/mol, **m.p.** ≥ 300 °C**, Anal. Calc. (%) For $C_{11}H_8Cl_2N_2O_2PtS_2$:** C, 24.91; H, 1.52; N, 5.28; S, 12.09; Pt, 36.79. **Found (%):** C, 24.92; H, 1.50; N, 5.29; S, 12.01; Pt, 35.30. **Conductance:** 20 Ω^{-1} cm^2 mol^{-1}. **UV-Vis: λ (nm) (ε, M^{-1} cm^{-1}):** 292 (10,550), 404 (4,710), 421 (4,995). **^{1}H NMR (400 MHz, DMSO-d$_6$) δ/ppm:** 8.030 (d, 2H, J = 7.2 Hz, $H_{3,5}$), 7.860 (d, 1H, J = 4.8 Hz, $H_{2''}$), 7.723 (d, 2H, J = 7.6 Hz, $H_{2,6}$), 7.374 (d, 1H, J = 4.4 Hz, $H_{4''}$), 7.203 (dd, 1H, J = 4.8 Hz, J = 4.4 Hz, $H_{3''}$), 10.204 (s, 1H, $H_{1'}$). **^{13}C NMR (100 MHz, DMSO-d$_6$) δ/ppm:** 148.3 (C_1), 126.0 ($C_{2,6}$), 125.2 ($C_{3,5}$), 145.2 (C_4), 130.2 ($C_{2'}$), 128.2 ($C_{3'}$), 127.9 ($C_{4'}$), 149.0 ($C_{5'}$), 197.8 ($C_{2''}$); [Signal observed = 9: Ar-CH = 2, Ar-C = 2, thiocarbonyl = 1, thiophene-C = 1, thiophene-CH = 3,]. **LC-MS m/z(%):** 530.31 [M], 532.42 [M + 2], 534.16 [M + 4].

2.4 Biological screening of synthesized compounds

2.4.1 In vitro antibacterial activity

The MIC informs about the degree of resistance of certain bacterial species towards the test compounds. MIC value was performed by serially two fold dilution of the test compound added to three gram$^{(-ve)}$ microorganisms namely *Escherichia coli* (MTCC 433), *Pseudomonas aeruginosa* (MTCC P-09), *Serratia marcescens* (MTCC 7103) and two

gram$^{(+ve)}$ bacteria namely *Bacillus subtilis* (MTCC 7193), *Staphylococcus aureus* (MTCC 3160). The lowest compound concentration inhibiting visible bacterial growth is reported as MIC. (Patra et al., 2015), (Sadana, Mirza, Aneja, & Prakash, 2003)

2.4.2 Nucleotide binding experiments

All the experiments involving the interaction of the Pt(II) complexes **(1a-1f)** with CT DNA were used for nucleotide binding study. The stock solution was prepared by dissolving CT-DNA in a Tris-HCl buffer (pH 7.2) containing 5% DMSO at 4 °C for complete dissolution and used within 4 days. Ratio of UV absorbance kept at 260 and 280 nm was about 1.89:1 for CT DNA in the buffer, suggesting the CT DNA sufficiently free from protein.(Reichmann, Rice, Thomas, & Doty, 1954) The nucleotide binding experiments were completed at room temperature. All experiments were carried out by keeping the concentration of platinum complexes constant (400 µM) while Concentrations of CT-DNA were determined spectrophotometrically by assuming $\boldsymbol{\varepsilon}_{260}$= 6600 M^{-1} cm^{-1}.(Marmur, 1961) (H. Paul, 2012; Ramakrishnan, Suresh, Riyasdeen, Akbarsha, & Palaniandavar, 2011; Y. Li, 2010).

2.4.3 Hydrodynamic chain length study

Viscosity experiments were carried out using reported method (Gajera, Mehta, & Patel, 2015). The flow time of solutions in a Tris-HCl buffer (pH 7.2) was recorded in triplicate for each sample with a digital stopwatch, and the average flow time was calculated. Data are presented as $(\eta/\eta^{\circ})^{1/3}$ versus the binding ratio.

2.4.4 Molecular modelling study

The rigid molecular modelling study was performed by using HEX 8.0 software (Mustard & Ritchie, 2005) and the most stable configuration was chosen as input for investigation. Pt(II) complexes were .mol format converted to (Protein Data Bank) .pdb format using CHIMERA 1.5.1 software. CT-DNA used in the experimental work was too

large for current computational resources to dock, therefore, the structure of the DNA of sequence (5'-D(CPGPCPGPAPAPTPTPCPGPCPG)-3') (1BNA) for groove binding and an octamer (5'-D(CPGPCPGPAPAPTPTPCPGPCPG)-3') (1BNA) for intercalation(Ricci & Netz, 2009) (PDB ID: 1BNA, a familiar sequence used in oligodeoxynucleotide study) obtained from the Protein Data Bank (http://www.rcsb.org/pdb). All calculations were using on an Intel CORE i5, 2.5 GHz based machine running MS Windows 8, 64 bit as the operating system. The by default parameters were used for the docking calculation with correlation type shape only, FFT mode at 3D level, grid dimension of 6 with receptor range 180 and ligand range 180 with twist range 360 and distance range 40.

2.4.5 Quenching of DNA–ethidium bromide fluorescence by the Pt(II) complexes.

In the emission quenching experiment, ethidium bromide (EB) was used as a common fluorescent probe for the DNA in order to examine the mode and process of metal complex binding to the DNA.(C. V. Kumar, Barton, & Turro, 1985) A 33.3 µM of the EB and 10 µM of DNA solution added to 1 M Tris-HCl buffer (pH 7.2) solution. Before measurements, the system was shaken and incubated at ambient temperature for 10 min. The emission was recorded at 500–800 nm. The fluorescence spectra of EB bound to DNA were recorded (with excitation wavelength of 510 nm), emission at 610 nm (λ_{max}) and slit wavelength 1.45 nm in the FluoroMax-4, HORIBA (Scientific) spectrofluorometer. Then the solution of each of the Pt(II) complexes was titrated into the CT-DNA EB system and diluted in 1 M Tris-HCl buffer to 3.0 mL to get the solution with the [complex]/[DNA] (r = 0 to 3.33) mole ratio. All measurements were performed at room temperature.

2.4.6 DNA mobility shift assay

In gel-electrophoresis method, DNA cleavage assay was carried out which works on the principle that migration of DNA takes place under the influence of electric potential, which is negatively charged at neutral pH, and migrates toward the positively charged anode.

The sample were incubated for 30 min at 37 °C and the samples were analysed by 1 % agarose gel electrophoresis containing 0.5 mg/mL ethidium bromide, [Tris-acetate-ethylene diaminetetraacetic acid (EDTA) (TAE) buffer, pH 8.0] for 3 h at 100 mV. The oxidative cleavage of pUC19 plasmid DNA was monitored using agarose gel electrophoresis. The gel was visualized by UV light and photographed on UV transilluminator. The extent of cleavage of the SC DNA was determined by measuring the intensities of the bands using AlphaDigiDoc^{TM} RT.

2.4.7 In vitro cytotoxicity against brine shrimp lethality bioassay (BSLB)

The cytotoxicity assay was performed on brine shrimp nauplii by Meyer method.(Ferrigni, 1982) The lethal concentrations of compounds resulting in 50% mortality (LC_{50}) of the brine shrimp from the 24 h and the dose–response data were transformed into a straight line by means of a trend line fit linear regression analysis; the LC_{50} was determine from the best-fit line, a graph of mortality vs. concentration of nauplii.(M.R. Islam, 2007) The LC_{50} value is obtained the antilogarithm of log [complex] vs. 50% mortality (LC_{50}). All data has been collected from three independent experiments and the LC_{50} determined using OriginPro 8 software.

2.4.9 In vitro cell proliferation assay

Determination of half maximal inhibitory concentration (IC_{50}) value of complexes (1a-1f) was determined by MTT (3-(4,5-dimethylthiazol-2-yl)-2,5-diphenyltetrazolium bromide) assay. Briefly, HCT 116 cells were treated with a series of concentrations (control, DMSO, 1, 10, 50, 100, 500, 1000 µg/mL) of complexes **(1a-1f)** for 24 h. The cells were washed twice with DPBS and incubated with 0.5 mg/ml MTT solution for 4 h at 37 °C. Thereafter, 0.1 ml of SDS-HCl (10 % SDS in 0.01 M HCl) was added to each well, mixed thoroughly and allowed for incubation in the dark for 20 min at 37 °C. Finally, the absorbance of each well was recorded at 570 nm with a reference wavelength of 650 nm using a multimode micro plate reader (Spectra Max M2e, Molecular devices, USA). The results are represented in terms of percentage inhibition of cell proliferation compared to that of vehicle control. Cell

viability was evaluated by trypan blue exclusion assay. HCT 116 cells were treated with 1, 10, 50, 100, 500, 1000 µg/ml of complexes (1a-1f) conjugate for 24 h. After completion of incubation, cells were harvested and washed once with DPBS. Equal amount of cell suspension was mixed with trypan blue. Subsequently, live and dead cells were counted and percentage of cell death was determined by the following formula (Percentage of cell death = Number of dead cells/Total number of cells x 100. In addition, cell proliferation of Human colorectal carcinoma (HCT 116) was examined by MTT assay. The results are represented as percentage of cell proliferation in different treatment group.

3. Results and discussion

3.1 Synthesis of substituted ligands (L^{1-6}) and complexes (1a-1f)

The synthesized ligands and complexes schemes are represented in supplymetry material 1 and 2, we focused upon the effect of change in hetero atom of ligands **(L^{1-6})** i.e. oxygen atom in ligands **(L^{1-3})** is replaced by sulphur atom in ligands **(L^{4-6})**. Ligands and complexes have been fully characterized by ^{13}C and ^{1}H NMR spectroscopy as well as by mass spectrometry.

3.2 ^{1}H NMR spectrum

^{1}H NMR spectra of free ligands **(L^{1-6})** and Pt(II) complexes **(1a-1f)** were recorded in DMSO-d_6 solution. ^{1}H NMR data are shown in the experimental section and spectra are represented in supplementary material 3 and 4. In the ^{1}H NMR spectra of compounds, the doublet (d), doublet of doublet (dd), triplet (t) are observed in the range of 7.12 - 8.50 ppm, which are correspond to the aromatic protons of the phenyl and thiophene rings. The signal appears between 10.00 - 12.00 ppm corresponds to the amide and thioamide hydrogen of ligands (L^{1-6}) and Pt(II) complexes (1a-1f).

3.3 ^{13}C NMR spectrum

^{13}C NMR spectra of ligands (L^{1-6}) and Pt(II) complexes **(1a-1f)** are shown in supplementary material 5. ^{13}C NMR data are reported in the experimental section. Peak of Pt(II) complexes **(1a-1c)** shifted to downfield from 161.8 ppm to 164.0 - 167.0 ppm than their respective ligands **(L^{1-3})** due to presence of carbonyl group and peaks of Pt(II) complexes **(1d-1f)** shifted to downfield from 197.0 ppm to 197.8 - 199.0 ppm than their respective ligands **(L^{4-6})** due to presence of thiocarbonyl group. Thiocarbonyl group containing compounds have been shifted to more downfield than the carbonyl group containing compounds.

3.4 LC - MS spectrum

The mass fragments and mass spectra of bidentate ligands **(L^{1-6})** are represented in supplementary material 6. The mass spectra of complexes showed a single molecular peak in the LC-MS spectrum indicating stability of the complexes. The isotopic pattern confirmed the presence of platinum metal ion. The representative LC-MS spectrum and probable mass fragmentation pattern of complex **(1f)** $[C_{11}H_8Cl_2N_2O_2PtS_2]$ (mol.wt. = 530.31 g/mol) are shown in figure 1. The mass spectrum of the complex **(1f)** shows molecular ion peak at $[C_{11}H_8Cl_2N_2O_2PtS_2]$ [M] 530.31, [M+2] 532.42, [M+4] 534.16 m/z. Peak at 459.41 m/z is due to bidentate ligand attached with platinum metal. The fragment of bidentate ligand give peak at 264.32 m/z due to loss of platinum metal ion.

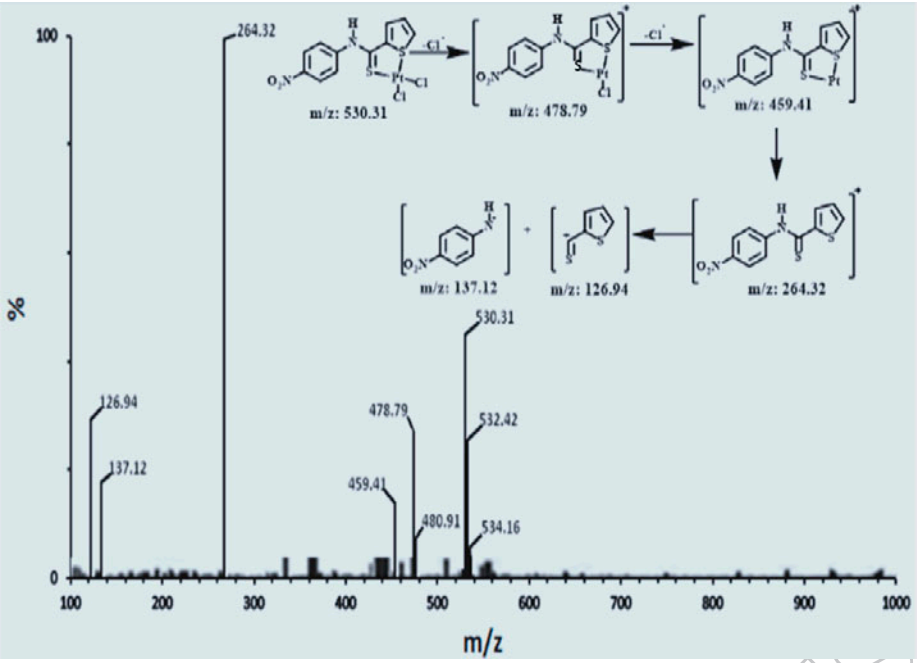

Fig. 1. LC-MS spectrum of complex (1f)

3.5 Electronic spectra and conductance measurements

The electronic spectra of the ligands **(L^{1-6})** and complexes **(1a-1f)** were recorded in the UV-visible region using DMSO solution at room temperature. The appropriate data of complexes (1a-1f) and ligands **(L^{1-6})** are shown in experimental section. Absorption spectrum obeys the Lambert-Beer's law and are taken in the range of 100-150 µM concentration of Pt(II) complexes. UV –Visible absorption and reflectance spectra of platinum(II) complexes are taken in solution state and solid state.(supplymetry material 7) We observed that the wavelength of Pt(II) complexes in solid state and in solution remain same, which indicate that platinum(II) complexes are stable in solid state as well as in solution state. This observation ruled out the possibility of hydrolysis of complexes in plasma. The electronic spectra of the mononuclear Pt(II) complexes show three different high-energy absorption bands with varied intense peaks at wavelengths 280-300 nm is consigned to the π-π^* typically parallels to a intra ligand charge transfer (ILCT) transition.(A. B. P. Lever, 1984.) In

addition, the peak observed with broad bands at lower frequency (310-395 nm) is assigned metal to ligand charge transfer (MLCT) transitions.(Shiju, Arish, Bhuvanesh, & Kumaresan, 2015) Further addition, the peak observed with broad bands at very lower frequency (397-420 nm) is consigned to d-d transition. Pt(II) complexes having *p*-substituted -NO_2 ligands (1c, 1f) show large red-shift than the Pt(II) complexes having *p*-substituted -Cl ligands **(1b, 1e)**, which can be attributed to the stronger electron-pushing ability of the substituent -NO_2 on Pt(II) complexes **(1c, 1f)** resulting in the energy of the MLCT transition being higher than -Cl on Pt(II) complexes **(1b, 1e)**.

All complexes are soluble in DMSO and non-electrolytes ($\Lambda \leq 19 - 25$ $\Omega^{-1}cm^2mol^{-1}$).

3.6 Thermogravimetric analysis (TGA)

The content of particular components in a complex changes in weight loss and extent of conversion patterns with increasing temperature. In order to determine such thermal stability and decomposition mechanism of the solid complexes examined via thermogravimetric analyse technique. The objective of this analysis is to analyse weather the water molecule is present in the lattice space or coordinated to the metal in complex. TGA was carried out for Pt(II) complex **(1d)** at a heating rate of 10 °C per minute in the range of 20-800 °C under N_2 atmosphere.

The TGA graph representing loss in mass of complex **(1d)** with respect to temperature is shown in supplementary material 8, which indicates that complex decomposes in two main well define steps. There is no loss in weight up to 110 °C, suggesting the absence of water molecule in the lattice. Further increment of the temperature causes decomposition of complex in two steps. First mass loss occurring between 120 °C to 310 °C (14%) corresponds to two chlorine molecules, second mass loss occurring in

the temperature range of 310-557 °C (45%) is attributed to loss of bidentate ligand and leaving behind the platinum as residue. A similar type of thermal degradation trend was observed in the literature for platinum metal complexes.(Abdel Ghani & Mansour, 2011; Li et al., 2011)

3.7 Infrared spectra

The characterization of FT-IR spectra recorded for the free ligands (**L^{1-6}**) are vary from their respective complexes **(1a-1f)** and provided significant indications of the bonding sites of amide and thioamide ligands (L^{1-6}) to the platinum metal ion. The main bands with assignments are listed in supplementary material 9 (Table 1). The band of $\nu_{(-NHC=O)}$ in ligands (L^{1-3}) is observed at (1642 - 1649) cm^{-1} (Abdel Ghani & Mansour, 2011), which is disappear in ligands (L^{4-6}). A new peak is observed in ligands (L^{4-6}) in the range of (1250-1270) cm^{-1}, which clearly indicate presence of thiocarbonyl group in ligands (L^{4-6}).(Abdel Ghani & Mansour, 2011) The $\nu_{(N-H)}$ of amide functional group of the ligands (L^{1-3}) is observed in the range of (3200-3363) cm^{-1}, while $\nu_{(N-H)}$ band of thioamide functional group of the ligands (L^{4-6}) is observed in the range of (3273-3364) cm^{-1}. The band $\nu_{(-C-S-C)}$ is observed in the range of (1100-1300) cm^{-1} in ligands (L^{1-6}). The band of $\nu_{(-NHC=O)}$ in complexes (1a-1c) is observed at 1630 - 1639 cm^{-1} (Li et al., 2011; Zhang et al., 2009) frequencies indicate that the oxygen atom of carbonyl group coordinated with platinum metal ion . The band of $\nu_{(-NHC=S)}$ is observed in the range of (1300-1380) cm^{-1} in complexes (1d-1f), it indicate that sulphur atom of thiocarbonyl group are coordinated with platinum metal ion. These are further confirmed by the presence of $\nu_{(-C=O-Pt)}$ band in the range of (460-500) cm^{-1} and the band of $\nu_{(-C=S-Pt)}$ in the range of (530-550) cm^{-1}, in the far IR frequency region.(Zhang et al., 2009) The $\nu_{(N-H)}$ of amide functional group of the complexes (1a-1c) is observed in the range of (3296 - 3315) cm^{-1}, while $\nu_{(N-H)}$ of thioamide functional

group of the complexes (1d-1f) is observed in the range of (3080-3213) cm^{-1}. The coordination of chelating group (>C=O) of ligand in complexes (1a-1c), (>C=S) group in complexes (1d-1f) and sulphur atom of thiophene ring of ligand (L^{1-6}) coordinate to platinum metal ion and form the five membered chelate ring. The sulphur atom of thiophene ring coordinated to platinum metal is further confirmed by appearance of new peak in the range of 415-450 cm^{-1}.(Veysel T. Yilmaza, 2014)

3.8 Biological screening of synthesized compounds

3.8.1 Antimicrobial activity

Antibacterial activity of the Pt(II) complexes against various bacterial strains estimated by the MIC (μM) are given in supplementary material 10 and shown in figure 2. In this study five pathogen bacterial species are considered some of the most virulent microorganisms for the human population. Effect of the solvent used in the antibacterial tests is tested and found that the solvent has no effect on bacterial growth. The MIC values of the Pt(II) complexes (1a-1f) are in the range of 35 μM to 125 μM for all bacterial strains tested. The highest antibacterial activity is observed for complexes (1d-1f) against $Gram^{(-ve)}$ and $Gram^{(+ve)}$ bacteria having MIC value of in the range of 30-45 μM concentration. The MIC's of complexes (1c-1d) are generally higher than those for complexes (1a-1c). The significant antibacterial activities of complexes (1d-1f) may be correlated with their DNA binding affinities. The antimicrobial activity of the platinum complexes are greater than those of the respective free ligand, this indicates that the complexation to metal enhances the activity of the ligands (Shiju et al., 2015; Tysoe, Morgan, Baker, & Strekas, 1993).

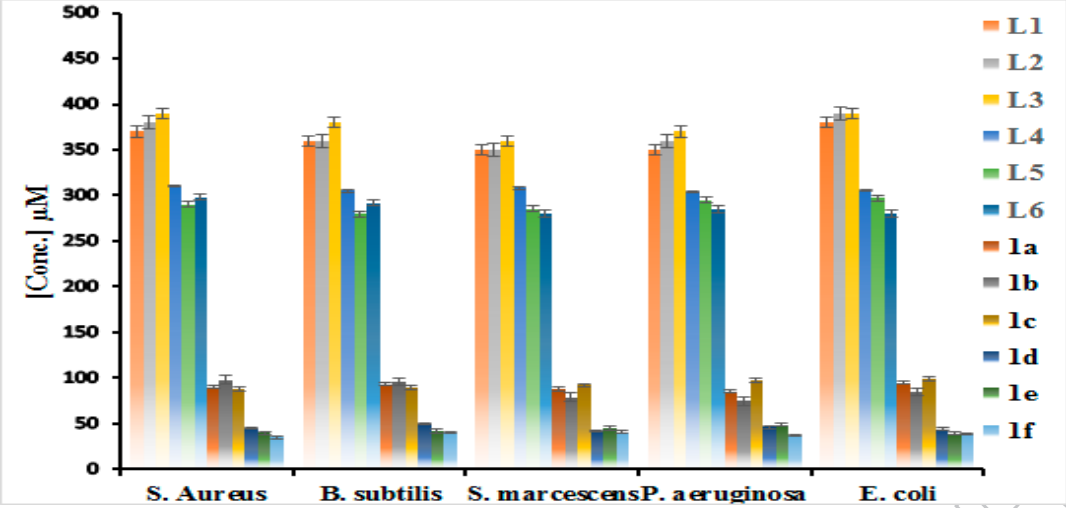

Fig. 2. Effect of different concentration of ligands (L^{1-6}) and synthesized Pt(II) complexes (1a-1f) on gram$^{(+ve)}$ and gram$^{(-ve)}$ bacteria.

3.8.2 Nucleotide binding experiments

The study of change in electronic state of a molecule by the action of UV-Visible light is a significant tool to determine the interactions of complexes with CT-DNA. Figure 3 shows the absorption spectra of complex (1f) in the presence and absence of CT-DNA at different concentrations. The figure shows that complex has a very strong absorption band at 315 nm. As the CT-DNA concentration is increased, the absorption spectrum of complex (1f) shows clear hypochromism and bathochromic shift at the maximum peak. Hypochromism with red shift (2-8) nm are observed at 315 nm, indicating that the complexes (1a-1f) bind to CT-DNA via partial intercalation mode of binding. This could be attributed to the strong stacking interaction between the planar aromatic chromophore and the base pairs of DNA. Also, the degree of the hypochromism is in agreement with the strength of partial intercalative action(Ameta, Singh, & Kale, 2013; Mansouri-Torshizi, Moghaddam, Divsalar, & Saboury, 2009; Millar, Ho, & Aroney, 1988; "NCCLS, National Committee for Clinical Laboratory Standards, Performance Standards for Antimicrobial Disk Susceptibility Test," 1997; Temple, McFadyen, Holmes, Denny, & Murray, 2000). The binding constant value of the complexes is measured using the following eqn (1):(Pyle et al., 1989)

$$\frac{[DNA]}{\varepsilon_a - \varepsilon_b} = \frac{[DNA]}{\varepsilon_a - \varepsilon_b} + \frac{1}{K_b}\left(\varepsilon_b - \varepsilon_f\right) \quad (1)$$

where, [DNA] is the concentration of DNA, ε_a ε_f and ε_b correspond to A_{obsd}/[complex], the extinction coefficient for the free complex, and the extinction coefficient for the complex in the fully bound form, respectively. Complexes (1a-1f), however, show significant hypochromicity when treated with CT-DNA. The intrinsic nucleotide binding constant (K_b) values of all the complexes are found in the range of 0.768 – 1.611 × 10^5 M^{-1} and through an increasing concentration of CT-DNA, significant hypochromicity (H%) ranging from 16.66% to 21.13% were observed in the bands of compounds, (Table 1) these indicate the partial intercalating mode. Complex (1f) has the highest binding constant value, which is attributed to the different positions of the substituents of -NO_2 functional group on the phenyl ring.(Křikavová, Vančo, Šilha, Marek, & Trávníček, 2016; Özel, Barut, Demirbaş, & Biyiklioglu, 2016) The interactions of complex (1f) with DNA have shown, that the complexes are electron-acceptors, while the DNA molecule is an electron donor. Since, -NO_2 functional group is a powerful electron-withdrawing group, which can accept electrons from DNA, complex (1f) shows strong binding affinity towards CT-DNA compared to other synthesized complexes, binding constant values are found in the order of 1f > 1e > 1c > 1d > 1b > 1a. The K_b value of synthesized complexes (1a-1f) are found higher binding affinity than the oxaliplatin (5.3 × 10^3 M^{-1}) and carboplatin (0.33 × 10^3 M^{-1}) (Soori H1, 2015 Jan 7) and lower than the intercalator ethidium bromide (EB) (5.52 × 10^6 M^{-1}).(Meenongwa et al., 2016)

From the values of the binding constant (K_b), ΔG is free energy changes for the binding process have been calculated using equation (2):

$$\Delta G = -RT \ln K_b \quad (2)$$

Binding constants are the measure of the complex stability while the free energy indicates the spontaneity/non-spontaneity of compound–DNA binding. The free energy of the complexes

(1a-1f) were calculated and observed in the range of -27.87 to -29.70 kJmol^{-1} showing the spontaneity of compound–DNA interaction. ΔG and K_b values are represented in Table 1.

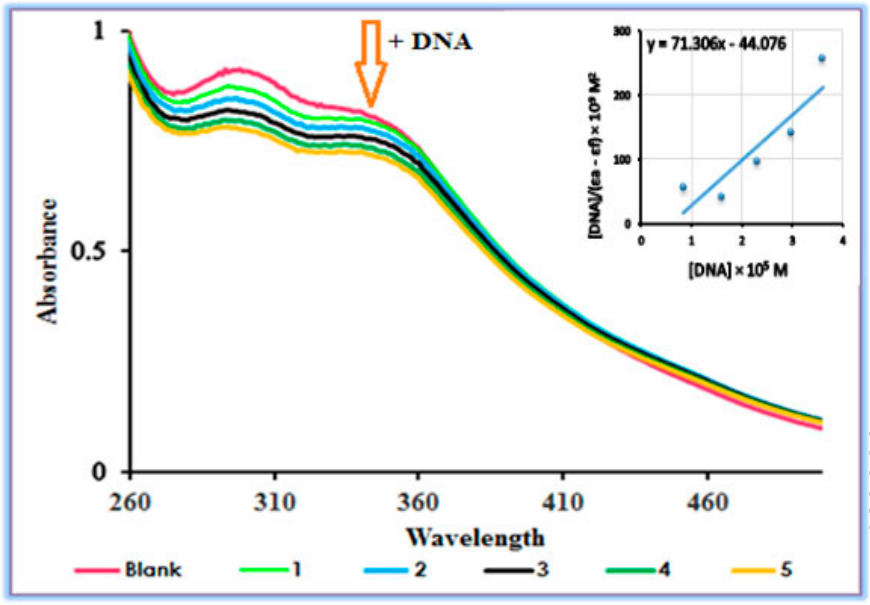

Fig. 3. Absorption spectral changes on addition of CT-DNA to the solution of complex (1f) after incubating it for 10 min at room temperature in phosphate buffer (Tris-HCl, pH=7.2). Inset: plot of [DNA]/(ε_a-ε_b) vs. [DNA]. (Arrow shows the change in absorption with increase in concentration of DNA).

Table 1. Binding constant (K_b), % hypochromicity and standard free energy changes (ΔG) values of synthesized Pt(II) complexes.

Complexes	**[a]*H%***	**[b]K_b (M^{-1})**	**ΔG(J mol^{-1})**
1a	19.23 ± 0.78	0.768 ± 0.05 × 10^5	-27873.0
1b	16.66 ± 0.69	0.875 ± 0.10 × 10^5	-28193.3
1c	20.70 ± 0.91	1.463 ± 0.08 × 10^5	-29466.8
1d	16.77 ± 0.73	0.939 ± 0.12 × 10^5	-28368.7
1e	20.92 ± 0.08	1.540 ± 0.05 × 10^5	-29593.9
1f	21.13 ± 0.57	1.611 ± 0.06 × 10^5	-29705.6

[a] $H\% = [(A_{free} - A_{bound})/A_{free}] \times 100\%$.
[b] K_b = Intrinsic DNA binding constant determined from the UV-Visible absorption spectral titration.

3.8.3 Hydrodynamic chain length study

It is well known that viscosity measurement is an effective tool to study such binding models in solution, in the absence of crystallographic structure data, visual or photo physical probes generally provide necessary but not sufficient information to support a partial intercalative binding model. Ethidium bromide interact to DNA via classical intercalation, increases the axial chain length of the DNA and it becomes more rigid, resulting in an increase in the relative hydrodynamic volume. When the DNA helix is partially intercalated by small planar molecules, base pairs separate to accommodate the binding molecules, resulting in the increase of viscosity of the DNA sample solution. On the other hand, a decrease in viscosity will be observed with groove binding of the compound due to the tightening of the CT-DNA helix, and no significant changes on viscosity via hydrogen bonding.(Colmenarejo et al., 1995; Rajput, Rutkaite, Swanson, Haq, & Thomas, 2006)

As complex to DNA concentration ratio increase, the viscosity of the solution increase significantly. Values of $(\eta/\eta^{\circ})^{1/3}$ for complex (1f) show in figure 4. These results are agree with those of the spectral analyses, suggesting that complex (1f) has a sensible partial intercalating ability to DNA. Results suggest that among these complex (1f) is the most powerful intercalation(Davis et al., 2012) to CT-DNA concluded from the viscosity test, which is in agreement with the spectral analysis.

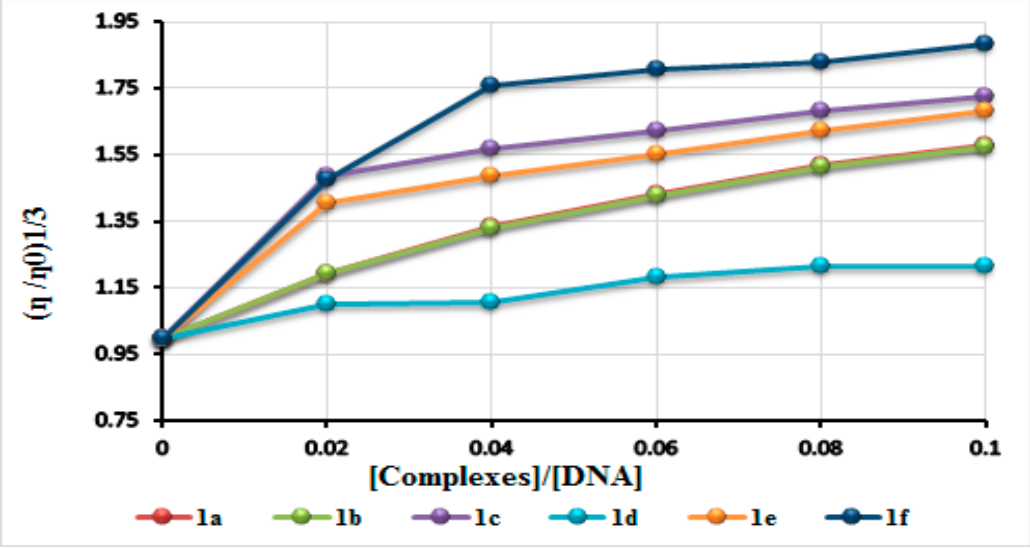

Fig. 4. Viscosity measurements of the complexes (1a-1f)

3.8.4 Molecular modelling study

Molecular modelling study has played important roles both in the molecular recognition of nucleic acid as well as in the rational design of new chemotherapeutic drugs,(Rohs, Bloch, Sklenar, & Shakked, 2005; Zhu et al., 2015) discovery as well as in the mechanistic study by placing a small molecule into the binding site of the target specific area of DNA. The molecular docking studies of complexes with DNA duplex of sequence (5'-D(CPGPCPGPAPAPTPTPCPGPCPG)-3') dodecamer were performed in order to predict the binding site along with preferred orientation of the molecules inside the DNA. Complex **(1f)** is illustrate in Figure 5 and other complexes are shown in supplementary material 11. The study shown that the complexes under investigation interact with DNA via an intercalation mode involving outside edge stacking interaction with oxygen atom of the phosphate backbone. From the resultant molecular docked structures, it is clear that the planarity of ligand core is comfortable for strong π-π stacking interactions and the complexes fit well into the intercalative mode of the targeted DNA and A–T rich region stabilized by van der Waal's interaction and hydrophobic contacts.(Mehta, Gajera, & Patel, 2016; Pettersen et al., 2004; Tabassum, Zaki, Afzal, & Arjmand, 2013) The resulting binding energies of docked complexes **(1a-1f)** are found to be -224.33 **(1a)**, -251.87 **(1b)**, -349.31**(1c)**, -219.63 **(1d)**, -231.37**(1e)**, -238.47 **(1f)** kJ mol^{-1}, respectively. The more negative the relative binding values, the more potent is the binding between DNA and target molecules. Thus, we can conclude that there is a mutual complement between spectroscopic techniques and molecular docked model, which substantiate our spectroscopic results, and provide further evidence of intercalative binding. Therefore, molecular docking together with absorption spectral and viscosity studies indicate that

the complex interacts with the DNA through the partial intercalation mode mainly inside the DNA helix.

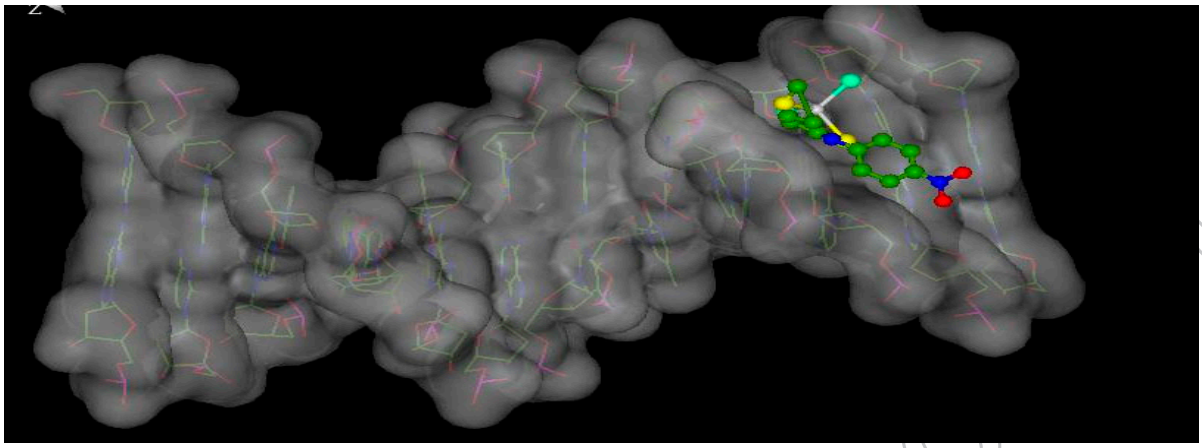

Fig. 5. Molecular docking of the complexes 1f (ball and stick) with the DNA duplex (VDW spheres with solid surface) of sequence DNA (5'-D(CPGPCPGPAPAPTPTPCPGPCPG)-3'). The complex is docked in to the DNA showing partial intercalation between the DNA base pairs.

3.8.5 Quenching of DNA–ethidium bromide fluorescence by the Pt(II) complexes.

Fluorescence spectroscopy is an effective method used to explore the small molecules bind independently to a set of equivalent sites on a biomacromolecules. The binding tendency of platinum complexes to CT-DNA has been examined by the steady state quenching probes with the emission intensity of ethidium bromide (EB).(Lakowicz, 2006) It is well known that ethidium bromide (3,8-diamino-5-ethyl-6-phenyl-phenanthridinium bromide) is typical indicator of intercalation, establishing soluble complexes with nucleic acids, causing a emitting intense fluorescence at about 610 nm presence of DNA, due to its intercalation of the planar Pt(II) complexes among adjacent DNA base pairs on the double helix. (Arjmand & Aziz, 2009) Addition of a second molecule, which may bind to DNA more strongly than EB, two mechanisms have been suggested to account for this reduction in the emission intensity: the replacement of EB and/or electron

transfer.(Pasternack et al., 1991) Compounds competing with EB to intercalation in DNA will induce displacement of bound EB and in a decrease in the fluorescence intensity of the CT-DNA EB system. The extent of decrease in the fluorescence intensity of CT-DNA EB reflects the extent of interaction of the complex with CT-DNA.(Lepecq & Paoletti, 1967) In the present study, the fluorescence intensity of the CT-DNA EB system (with excitation wavelength of 510 nm) is partial replaced by the increasing concentration of the complexes and caused by EB migration from a hydrophobic to an aqueous environment.(Zeng, Yang, Liu, & Tang, 2003) The observed changes clearly indicate partial intercalation mode of binding with CT-DNA. Quenching of an EB-DNA can arise due to inner-filter effect. The mechanism of quenching is obtained from the emission intensity of EB. To rule out the influence of an inner filter effect, a correction factor was carried out to all the fluorescence data, using equation :(1) (J.R. Lakowicz, 2006)

$$I_{coor.} = I_{obs.} \times e^{(Aexi + Aemi)/2} \quad (1)$$

I_{obs} and I_{corr} are the observed and corrected emission intensities, and A_{exi} and A_{emi} are the solution absorption at the excitation and emission wavelengths. Although overall inner-filter effects were negligible, corrected values were used in all the data treatment and analysis.

The quenching of EB bound to DNA by Pt(II) complexes (1a-1f) is in good agreement ([complex]/[DNA] = 3.33) with the linear Stern–Volmer equation (2):(Eftink & Ghiron, 1981; Mahendiran, Kumar, Viswanathan, Velmurugan, & Rahiman, 2016)

$$I_0/I = 1 + K_q [Q] \quad (2)$$

where, I_0 and I represent the fluorescence intensities in the absence and presence of quencher (complexes), respectively. K_q is a linear Stern–Volmer quenching constant,

Q is the concentration of the quencher (complexes). In the quenching plot for complex (1b) (insets of Figure 6.) of I_0/I vs. [complex], indicating that complex (1b) reveals the highest binding tendency. K_q is given by the ratio of the slope to the intercept. The quenching abilities of Pt(II) complexes, evaluated by the linearity Stern–Volmer quenching constant (K_q) are found in the range of $2.6 \times 10^3 - 9.0 \times 10^4\ M^{-1}$. These values show that the partial replacements of EB bound to DNA base pairs by the complexes result in a decrease of the fluorescence intensity, which is corresponding with the K_b values (Table 1).

The titration data found from the fluorescence quenching experiment is helpful for the calculation of number of binding sites (n) and the associative binding constant (K_a) using the following equation (3):(Kathiravan & Renganathan, 2009)

$$log\ \frac{(I_0-I)}{I} = \log Ka\ + nlog[Q] \quad (3)$$

where, n and K_a are represent the number of binding sites and associative binding constant of Pt(II) complexes, respectively. The number of binding sites n, per nucleotide is obtained from the slope of $\log[(I_0 - I)/I]$ vs. log [Q] (Figure 6). The associative binding constant (K_a) values of Pt(II) complexes are found in the range of $0.34 \times 10^2 - 3.1 \times 10^4\ M^{-1}$ and the results of all complexes (1a -1f) are represented in supplementary material 12. The value of n is nearly 1, suggesting that the complex bond to CT-DNA base pair according to the molar ratio of 1:1. Thus, the fluorescence study lead us to a conclusion that the complexes can bind to DNA via partial intercalative mode.

In order to evaluation the interaction force of CT DNA with complexes, the standard free energy changes (ΔG) for the binding process have been calculated using the van't Hoff equation (4):(Hong, Chang, Li, & Niu, 2016)

$$\Delta G = -RT \ln K_a \quad (4)$$

where, T is the temperature (25 ^{0}C, 298 K here), K_a is associative binding constant and R is gas constant 8.314 Jmol^{-1} K^{-1}. The ΔG value for the Pt(II) complexes are obtained in the range of the -08.72 to -25.67 kJmol^{-1}. The results are summarized in supplementary material 12 and Table 2. The negative sign for ΔG means that the binding process is spontaneous.

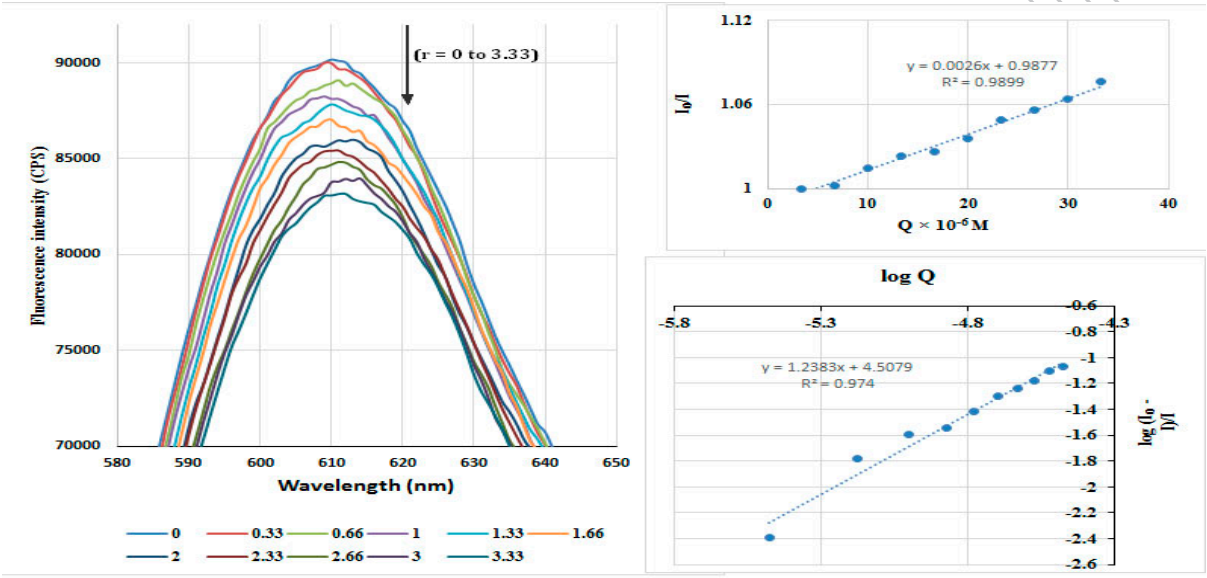

Fig. 6. Emission spectra of EB bound to DNA in the presence of Pt(II) complex **(1b)**. ([DNA] = 1.00 × 10^{-5} M, [EB] = 33.3 µM, [Quencher] (µM): 0 - 3.33 µM. The arrow shows the intensity changes upon gradual increasing the complex concentration. Inset: plot of I_0/I vs. [Quencher] and comparative plot of log[I_0-I/I] vs. log[Q] for the titration of CT-DNA EB system with Pt(II) complex (1b) in 1 M Tris-HCl buffer (pH 7.2) medium.

Table. 1. Linear Stern-Volmer quenching constant (K_q), binding sites (n) and association binding constant (K_a) from competitive.

Complexes	**K_q (M^{-1})**	**K_a (M^{-1})**	**n**	**ΔG(J mol^{-1})**
1a	9.0 × 10^4	1.62 × 10^2	0.8558	-12,607.65
1b	2.6 × 10^3	3.10 × 10^4	1.2383	-25,671.60
1c	2.9 ×10^3	1.73 × 10^3	0.9510	-18,482.00

1d	3.8×10^3	2.65×10^3	0.9648	-19,510.00
1e	3.1×10^3	0.69×10^4	1.0830	-21,929.32
1f	4.0×10^4	0.34×10^2	0.7543	-8,757.46

3.8.6 DNA mobility shift assay

The degree to which Pt(II) complexes **(1a-1f)** could function as DNA cleavage agents examined using supercoiled pUC19 plasmid DNA as a target. The efficiency of cleavage in the presence of the complexes is probed by DNA mobility shift assay (ethidium bromide staining). The DNA cleavage can occur by hydrolytic and oxidative pathways, Hydrolytic DNA cleavage involves cleavage of phosphodiester bond to generate fragments which can be subsequently relegated, in which started in a modest way of converting supercoil (SC) conformation (Form I) form of plasmid pUC19 DNA to the open-circular (OC) of the nicked circular (Form II) form, it is now being used for identifying the percentage of cleavage as a function of concentration of nuclease. Oxidative DNA cleavage involves either oxidation of the deoxyribose moiety by abstraction of sugar hydrogen or oxidation of nucleases.

Results are shown in figure 7 the line 1 is the control corresponding to a zero concentration of a metal salt. DNA cleavage is controlled by relaxation of the supercoiled circular conformation (Form I) of plasmid pUC19 DNA to the nicked circular (Form II). In gel electrophoresis experiments effected on the supercoiled circular conformation, the fastest migration was observed for DNA of supper coil (SC) Form I and whereas the slowest moving was open circular (OC) Form II. Following the cleavage of one strand, the supercoil will relax to produce the slower moving nicked conformation. As anticipated, no distinct DNA nuclease is observed for the control. All the complexes show the efficient cleavage ability in figure 8 The degree of interaction of complex to DNA represents in % cleavage of DNA by complexes (1a-1f) in the order of 1f > 1d > 1a > 1b > 1c > 1e > K_2PtCl_4. Percentage of conversion of the SC-DNA to OC-DNA according to the following equation are describe in

literature, which determines the degree of DNA nuclease assay.(Colmenarejo et al., 1995; J. Yang, 2000,)

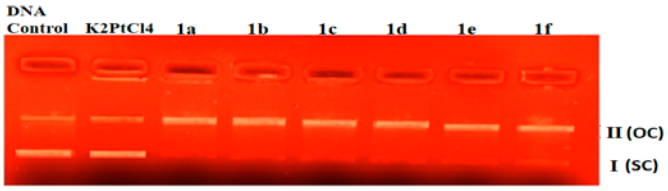

Fig. 7. Photogenic view of cleavage of pUC19 DNA (300 µg/cm^3) with series of Pt(II) complexes (200 µM) using 1 % agarose gel containing 0.5 µg/cm^3 EtBr. Reactions were incubated in TE buffer solution (pH 8) at a final volume of 15 mm^3 for time period of 3 h at 37 ^{0}C. Lane 1. DNA control, lane 2. K_2PtCl_4, lane 3. (1a), lane 4. (1b), lane 5. (1c), lane 6. (1d), lane 7. (1e), lane 8. (1f).

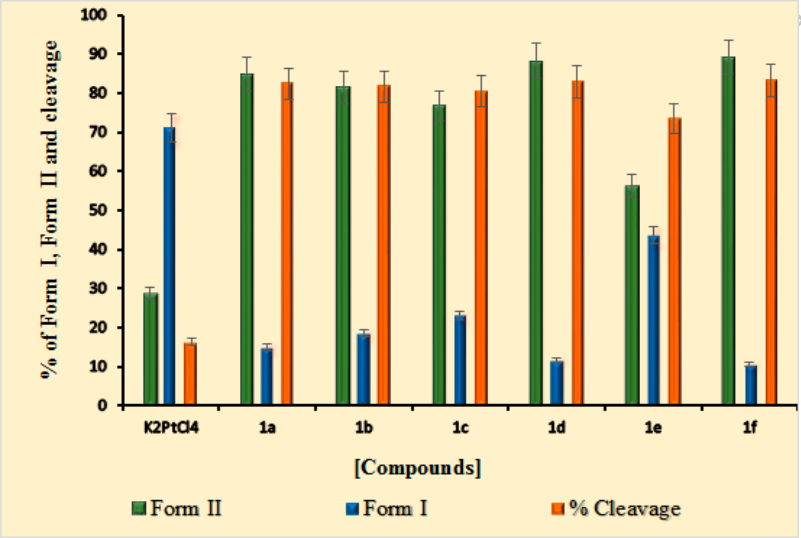

Fig. 8. Plot of nuclease cleavage (% of form I, form II and DNA cleavage) assay of the complexes (1a-1f). Error bars represent standard deviation of three replicates.

3.8.7 In vitro cytotoxicity against brine shrimp lethality bioassay

A graph of % mortality against log of concentration is plotted and LC_{50} is calculated from the log of concentration required to cause fatality of 50 % nauplii. Antilog of the obtained value at 50 % fatality gives the value of LC_{50}. The data obtained are represented in

the figure 9. Form the result it is inferred that the complexes show significant cytotoxicity against brine shrimp and can be further studied *in vitro* for their anticancer property.

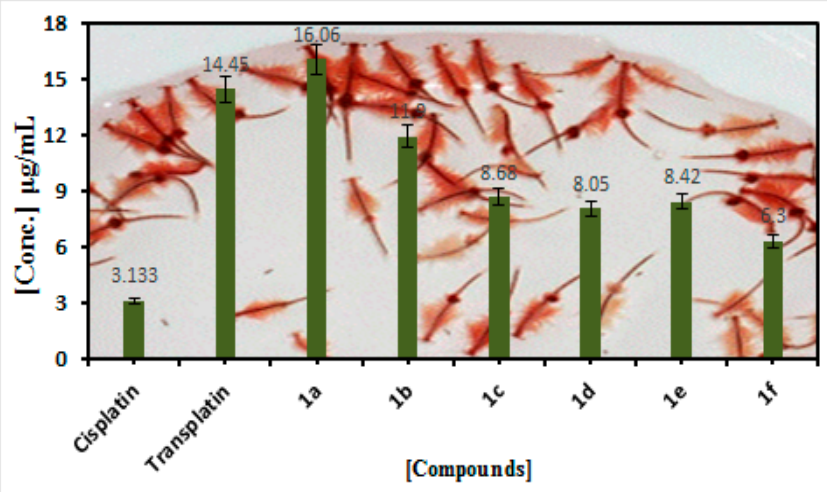

Fig. 9. Pot of LC_{50} values (from *in vitro* cytotoxic activity) of synthesized Pt(II) complexes (1a-1f) in µg/mL. Error bars represent standard deviation of three replicates

3.8.8 In vitro cell proliferation assay

The MTT (3-(4,5-dimethylthiazol-2-yl)-2,5-diphenyltetrazolium bromide) assay is used to determine the half inhibitory concentration (IC_{50}) values for the metallointercalators with cell proliferation of the HCT 116 (human colorectal cancer cell line) from the plot represented in the figure 10. The toxicity of the complex decreases in the order, 1c > 1b > 1f > 1e > 1d > 1a this behaviour could be attributed to a decrease in lipophilicity of complexes as there is an decrease in electronegative power of the substituent on the ligand as we go from L^3 to L^1 and L^6 to L^4. The half inhibitory concentration value for complex (1c) is 121.87 µg/mL which is approximately 1.5 times more potent than complex (1b) (IC_{50}= 181.17 µg/mL), 4.2 times more potent than complex (1f) (IC_{50}= 515.39 µg/mL), 4.5 times more potent than complex (1e) (IC_{50}=542.34 µg/mL), 5.9 times more potent than complex (1d) (IC_{50}=725.62 µg/mL) and complex (1a) (IC_{50}> 1000 µg/mL). IC_{50} values for cisplatin, oxaliplatin and carboplatin towards cell proliferation of the HCT 116 are 15.49±12 µg/mL,

(mol.wt.=300.05 g/mol), 22.64±2.22 µg/mL, (mol.wt.=397.29 g/mol) and 101.36±4.56 µg/mL (mol.wt. 371.25 g/mol), respectively.(Volarevic, 2013; Zhao, Gou, Sun, Fang, & Wang, 2012) Complex (1c) exhibited nearly equal cytotoxic efficacy compared to that of carboplatin.(Ceyda Icsel, 2015) All compounds are considerably less active than oxaliplatin 22.64±2.22 µg/mL, (mol.wt.=397.29 g/mol).(Zhao et al., 2012) Next, Trypan blue and MTT (3-(4,5-dimethylthiazol-2-yl)-2,5-diphenyltetrazolium bromide) assay concluded that cells were damaged. As shown in figure 11 in cell death analysis, complexes (1a-1f) efficiently induce cell death in HCT 116 cells within time period of 24 h. Thus, these results indicate that complexes (1a-1f) improve inhibition of cell proliferation in cancer selectively.

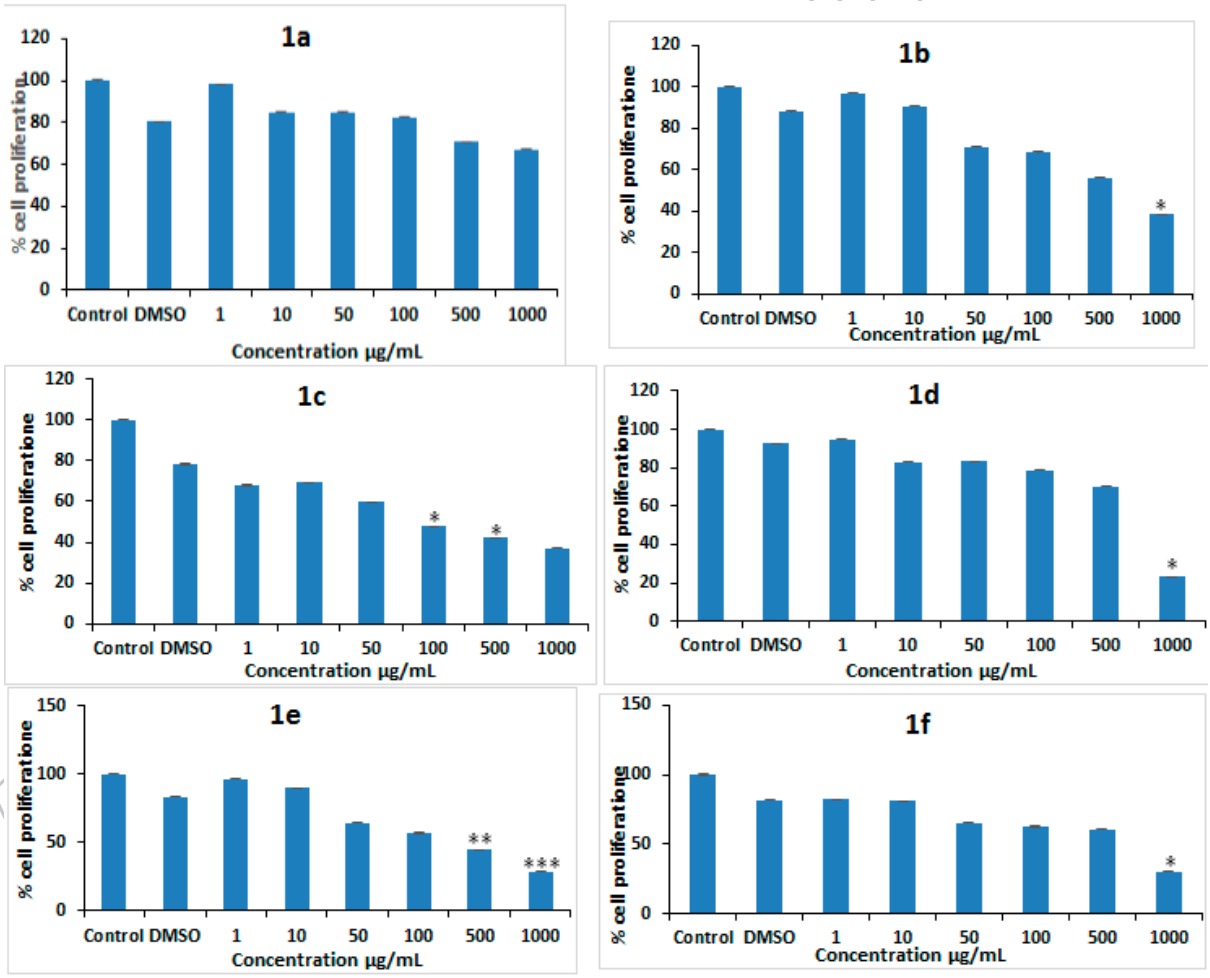

Fig. 10. Effect of synthesized Pt(II) complexes conjugate on cell proliferation. Determination of IC_{50} values of Pt(II) complexes (1a-1f) conjugate in HCT 116 cells. HCT 116 cells were

treated with the various concentrations (control (100 % DMSO), 1% DMSO, 1, 10, 50, 100, 500, 1000 µg/mL) of Pt(II) complexes (1a-1f) conjugate for 24 h. 1 % DMSO was used as a vehicle control. MTT assay determined Inhibition of HCT 116 cells. The obtained values were plotted and the IC_{50} values were analysed the data with t-test using Sigmaplot 12.0. Error bars represent standard deviation of three replicates.

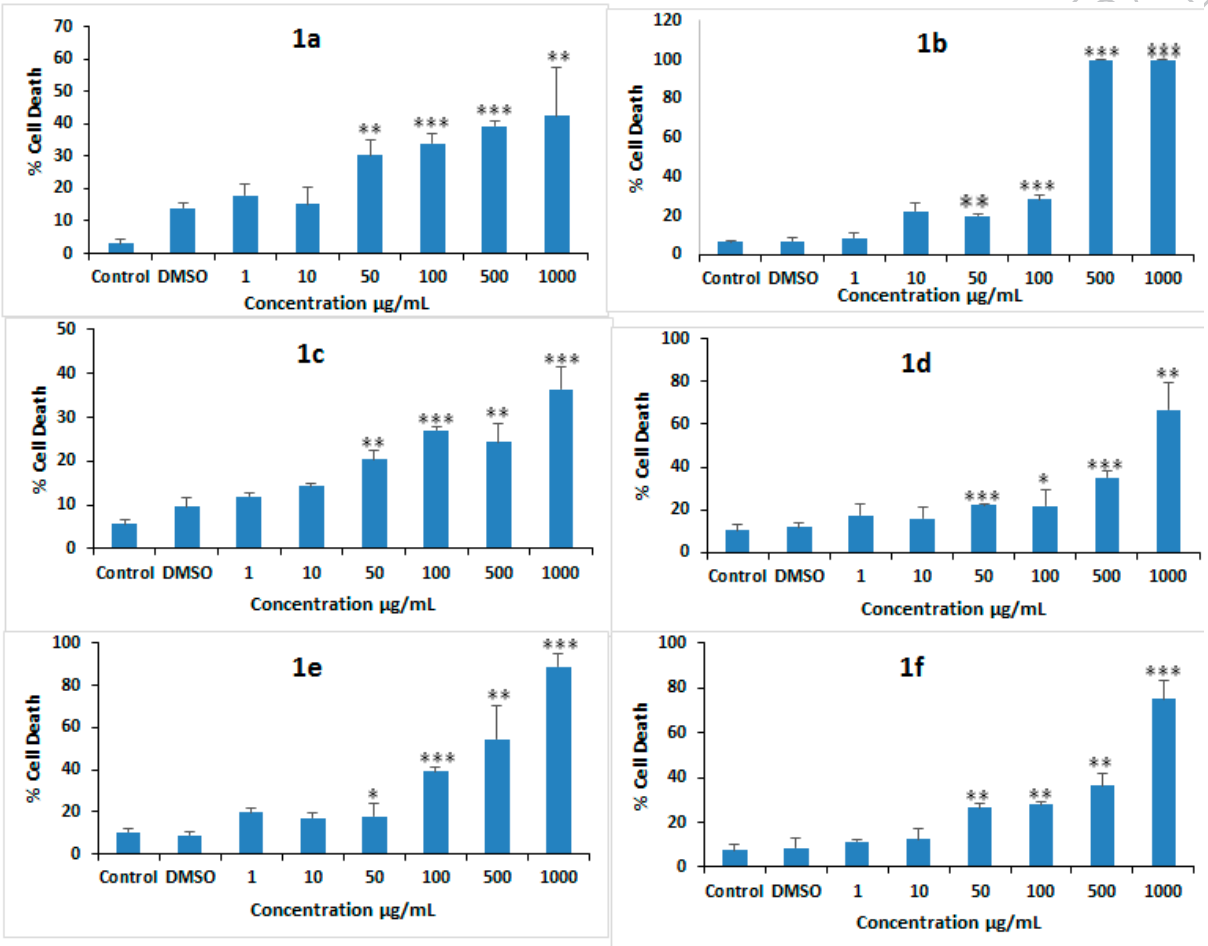

Fig. 11. Evaluation of cell death by trypan blue exclusion assay. HCT 116 cells were treated with (control(100 % DMSO), 1% DMSO, 1, 10, 50, 100, 500, 1000 µg/mL) of Pt(II) complexes (1a-1f) conjugate for 24 h. Similarly, 1 % DMSO was used as a vehicle control. During analysis, the cells were harvested, washed and subjected to trypan blue exclusion assay. Graphs represent the cell death in mentioned concentration of Pt(II) complexes (1a-1f). Error bars represent mean ± SEM of three independent experiments. Significant difference

indicated as *p ≤ 0.05 between untreated and complexes treated cells; **p ≤ 0.01, ***p ≤ 0.001. Error bars represent standard deviation of three replicates.

4. Conclusions

Pt(II) complexes (1d-1f) containing -S, S donor ligands are more persuasive than Pt(II) complexes (1a-1c) containing -S, O donor ligands. The antimicrobial test results disclose that all Pt(II) complexes (1a-1f) have good MIC's value against both $Gram^{(-ve)}$ and $Gram^{(+ve)}$ bacterial species compared the ligands (L^{1-6}) and K_2PtCl_4. Pt(II) complexes display a partial intercalative mode proved by the absorption titration, viscosity experiments and fluorescence quenching analysis of EB-binding competitive studies. Complex (1f) is bound more strongly than the other complexes due to presence of nitro ($-NO_2$) group. Presence of nitro ($-NO_2$) group act as not only chemical isosteres for the oxygen atoms in the nitro group, but also participate in ''strong'' NH bonding as a result it shows better antibacterial and DNA interaction activity as well as *in vitro* cytotoxic activity. Docking studies of the complexes with the DNA helix of sequence (5'-D(CPGPCPGPAPAPTPTPCPGPCPG)-3') were performed to predict the chosen binding site, which suggests partial intercalation between complex and DNA base pairs. The DNA cleavage study of pUC19 shows that all the complexes have a high cleavage ability compared to the K_2PtCl_4.

In consideration of the complexity of the cellular system, the synergic action of -S, O / -S, S donor and platinum-based moieties was studied in this paper. However, the newly synthesized compounds exhibited good stability and -S, O / -S, S donor releasing properties and showed considerable anticancer activity against HCT-116 cells *in vitro* cell proliferation assay. Besides, the interaction of complexes with DNA, which formed platinum/DNA adducts, played the leading role in the anticancer

effects of complexes (1a-1f), while the thiophene species were important for the cytotoxic activity on the HCT-116 colon cancer cell line. Thus, these compounds are promising anticancer agents and deliver a new view for the design of anticancer drugs beyond those currently in use.

Conflict of interest

The authors report no conflicts of interest. The authors alone are responsible for the content and writing of the paper.

Acknowledgements

We thanks Head of the Department of Chemistry, Sardar Patel University, Vallabh Vidyanagar, Gujarat, India, for providing the research laboratory facilities, C.S.M.C.R.I (Central Salts & Marine Chemical Research Institute), Bhavanagar for LC-MS analysis, DST-PURSE, Sardar Patel University, Vallabh Vidyanagar for LC-MS analysis, U.G.C., New Delhi for providing financial assistance of UGC BSR Fellowship Grant No. C/2013/BSR/Chemistry/7489 and UGC CAS and "UGC BSR One Time Grant", vide UGC letter No. F.19-119/2014(BSR).

Notes and references

A. B. P. Lever. (1984.). Electronic Spectroscopy, Elsevier Publishing Co., . *Amsterdam,*

Abdel Ghani, N. T., & Mansour, A. M. (2011). Novel Pd(II) and Pt(II) complexes of N,N-donor benzimidazole ligand: Synthesis, spectral, electrochemical, DFT studies and evaluation of biological activity. *Inorganica Chimica Acta, 373*(1), 249-258. doi: http://dx.doi.org/10.1016/j.ica.2011.04.036

Ameta, R. K., Singh, M., & Kale, R. K. (2013). Synthesis and structure-activity relationship of benzylamine supported platinum(iv) complexes. *New Journal of Chemistry, 37*(5), 1501-1508. doi: 10.1039/C3NJ41141A

Arjmand, F., & Aziz, M. (2009). Synthesis and characterization of dinuclear macrocyclic cobalt(II), copper(II) and zinc(II) complexes derived from 2,2,2′,2′-S,S[bis(bis-N,N-2-thiobenzimidazolyloxalato-1,2-ethane)]: DNA binding and cleavage studies. *European Journal of Medicinal Chemistry, 44*(2), 834-844. doi: http://dx.doi.org/10.1016/j.ejmech.2008.05.006

Aslanoglu, M., Isaac, C. J., Houlton, A., & Horrocks, B. R. (2000). Voltammetric measurements of the interaction of metal complexes with nucleic acids. *Analyst, 125*(10), 1791-1798. doi: 10.1039/B005440M

Boulikas, T. (2003). *M.Oncol. Rep., 10*, 1663

Ceyda Icsel, V. T. Y. (2015). New palladium(II) and platinum(II)

5,5-diethylbarbiturate complexes with

2-phenylpyridine, 2,2'-bipyridine and

2,2'-dipyridylamine: synthesis, structures, DNA

binding, molecular docking, cellular uptake,

antioxidant activity and cytotoxicity. *Dalton Trans.,*. doi: 10.1039/c5dt00728c

Colmenarejo, G., Gutiérrez-Alonso, M. C., Bárcena, M., Kelly, J. M., Montero, F., & Orellana, G. (1995). Interaction with DNA of Photoactive Viologens Based on the 6-(2-Pyridinium)phenanthridinium Structure. *Journal of Biomolecular Structure and Dynamics, 12*(4), 827-846. doi: 10.1080/07391102.1995.10508779

Davis, K. J., Carrall, J. A., Lai, B., Aldrich-Wright, J. R., Ralph, S. F., & Dillon, C. T. (2012). Does cytotoxicity of metallointercalators correlate with cellular uptake or DNA affinity? *Dalton Transactions, 41*(31), 9417-9426. doi: 10.1039/C2DT30217A

Eftink, M. R., & Ghiron, C. A. (1981). Fluorescence quenching studies with proteins. *Analytical Biochemistry, 114*(2), 199-227. doi: http://dx.doi.org/10.1016/0003-2697(81)90474-7

Ferrigni, B. N. M. N. R. (1982). *Journal of Medicinal Plant Research, 45*, 31-35

Florea, A.-M., & Büsselberg, D. (2011). Cisplatin as an Anti-Tumor Drug: Cellular Mechanisms of Activity, Drug Resistance and Induced Side Effects. *Cancers, 3*(1), 1351

Gajera, S. B., Mehta, J. V., & Patel, M. N. (2015). DNA interaction, cytotoxicity, antibacterial and antituberculosis activity of oxovanadium(iv) complexes derived from fluoroquinolones and 4-hydroxy-5-((4-hydroxyphenyl)diazenyl)thiazole-2(3H)-thione. *RSC Advances, 5*(28), 21710-21719. doi: 10.1039/C5RA01222H

Guo, Z., & Sadler, P. J. (1999). Metals in Medicine. *Angewandte Chemie International Edition, 38*(11), 1512-1531. doi: 10.1002/(SICI)1521-3773(19990601)38:11<1512::AID-ANIE1512>3.0.CO;2-Y

H. Paul, T. M., M.G.B. Drew, P. Chattopadhya. (2012). *J. Coord. Chem., 65*(8), 1289

Hodges, K. D., & Rund, J. V. (1975). Oxidative addition of halogens and pseudohalogens to dihalo(1,10-phenanthroline)platinum(II). *Inorganic Chemistry, 14*(3), 525-528. doi: 10.1021/ic50145a015

Hong, M., Chang, G., Li, R., & Niu, M. (2016). Anti-proliferative activity and DNA/BSA interactions of five mono- or di-organotin(iv) compounds derived from 2-hydroxy-N[prime or minute]-[(2-hydroxy-3-methoxyphenyl)methylidene]-benzohydrazone. *New Journal of Chemistry, 40*(9), 7889-7900. doi: 10.1039/C6NJ00525J

I.H.Krakoff. (1988,). inPlatinum and Other Metal Coordination Compounds in Cancer Chemotherapy: . *ed.M. Nicolini, Martinus Nijhoff Publishing, Boston,* , 351

J. Yang, R. N. S. W., M. S. Yang, . (2000,). *Chem. Biol. Interact., 125*, 221

J.R. Lakowicz. (2006). *Principles of Fluorescence Spectroscopy,*(third ed., Springer, US)

Ji, S., Shigeta, M., Niko, Y., Watanabe, J., & Konishi, G.-i. (2013). Synthesis of highly soluble fluorescent π-extended 2-(2-thienyl)benzothiazole derivatives via oxidative cyclization of 2-thienylthioanilide as the key step. *Tetrahedron Letters, 54*(52), 7103-7106. doi: http://dx.doi.org/10.1016/j.tetlet.2013.10.071

Kathiravan, A., & Renganathan, R. (2009). Photoinduced interactions between colloidal TiO2 nanoparticles and calf thymus-DNA. *Polyhedron, 28*(7), 1374-1378. doi: http://dx.doi.org/10.1016/j.poly.2009.02.040

Kelland, L. (2007). The resurgence of platinum-based cancer chemotherapy. *Nat Rev Cancer, 7*(8), 573-584

Kostova, I. (2006). Platinum Complexes as Anticancer Agents. *Recent Patents on Anti-Cancer Drug Discovery, 1*(1), 1-22. doi: 10.2174/157489206775246458

Křikavová, R., Vančo, J., Šilha, T., Marek, J., & Trávníček, Z. (2016). Synthesis, characterization, DNA binding studies and in vitro cytotoxicity of platinum(II)-dihalogenido complexes containing bidentate chelating N-donor ligands. *Journal of Coordination Chemistry, 69*(16), 2422-2436. doi: 10.1080/00958972.2016.1199862

Kumar, C. V., Barton, J. K., & Turro, N. J. (1985). Photophysics of ruthenium complexes bound to double helical DNA. *Journal of the American Chemical Society, 107*(19), 5518-5523. doi: 10.1021/ja00305a032

Kumar, S. B., Mahendrasinh, Z., Ankita, S., Mohammedayaz, R., Pragna, P., & Suresh, E. (2012). A binuclear chloride bridged copper(II) complex with a modified ligand structure and different coordination environment and mononuclear cobalt(II) complexes with a pyridylpyrazole ligand: Synthesis, structure and cytotoxic activity. *Polyhedron, 36*(1), 15-20. doi: http://dx.doi.org/10.1016/j.poly.2012.01.019

Lakowicz, J. R. (2006). *Principles of Fluorescence Spectroscopy, 3rd edn*(Plenum Press, New York,), 277–286

Lepecq, J. B., & Paoletti, C. (1967). Fed Eration of European Biochemical Societies 3rd MeetingA fluorescent complex between ethidium bromide and nucleic acids. *Journal of Molecular Biology, 27*(1), 87-106. doi: http://dx.doi.org/10.1016/0022-2836(67)90353-1

Li, X., Zha, M.-Q., Gao, S.-Y., Low, P. J., Wu, Y.-Z., Gan, N., & Cao, R. (2011). Synthesis, photoluminescence, catalysis and multilayer film assembly of an ethynylpyridine platinum compound. *CrystEngComm, 13*(3), 920-926. doi: 10.1039/C0CE00382D

Loehrer, P. J., Williams, S. D., & Einhorn, L. H. (1988). Testicular Cancer: The Quest Continues. *Journal of the National Cancer Institute, 80*(17), 1373-1382. doi: 10.1093/jnci/80.17.1373

M. Zala, E. S. (2011). *J. Coord. Chem. , 64*, 438

M.R. Islam, S. M. R. I., A.S.M. Noman, J.A. Khanam, S.M.M. Ali, M.W. Lee, . (2007). *Mycobiology 35* 25

Mahendiran, D., Kumar, R. S., Viswanathan, V., Velmurugan, D., & Rahiman, A. K. (2016). Targeting of DNA molecules, BSA/c-Met tyrosine kinase receptors and anti-proliferative activity of bis(terpyridine)copper(ii) complexes. *Dalton Transactions, 45*(18), 7794-7814. doi: 10.1039/C5DT03831F

Mansouri-Torshizi, H., Moghaddam, M. I., Divsalar, A., & Saboury, A. A. (2009). Diimine Platinum(II) and Palladium(II) Complexes of Dithiocarbamate Derivative as Potential Antitumor Agents: Synthesis, Characterization, Cytotoxicity, and Detail DNA-Binding Studies. *Journal of Biomolecular Structure and Dynamics, 26*(5), 575-586. doi: 10.1080/07391102.2009.10507273

Marmur, J. (1961). A procedure for the isolation of deoxyribonucleic acid from micro-organisms. *Journal of Molecular Biology, 3*(2), 208-IN201. doi: http://dx.doi.org/10.1016/S0022-2836(61)80047-8

Meenongwa, A., Brissos, R. F., Soikum, C., Chaveerach, P., Gamez, P., Trongpanich, Y., & Chaveerach, U. (2016). Effects of N,N-heterocyclic ligands on the in vitro cytotoxicity and DNA interactions of copper(ii) chloride complexes from amidino-O-

methylurea ligands. *New Journal of Chemistry, 40*(7), 5861-5876. doi: 10.1039/C5NJ03439F

Mehta, J. V., Gajera, S. B., & Patel, M. N. (2016). Biological applications of pyrazoline-based half-sandwich ruthenium(III) coordination compounds. *Journal of Biomolecular Structure and Dynamics*, 1-9. doi: 10.1080/07391102.2016.1189360

Millar, D. P., Ho, K. M., & Aroney, M. J. (1988). Modification of DNA dynamics by platinum drug binding: a time-dependent fluorescence depolarization study of the interaction of cis- and trans-diamminedichloroplatinum(II) with DNA. *Biochemistry, 27*(23), 8599-8606. doi: 10.1021/bi00423a014

Mjos, K. D., & Orvig, C. (2014). Metallodrugs in Medicinal Inorganic Chemistry. *Chemical Reviews, 114*(8), 4540-4563. doi: 10.1021/cr400460s

Mustard, D., & Ritchie, D. W. (2005). Docking essential dynamics eigenstructures. *Proteins: Structure, Function, and Bioinformatics, 60*(2), 269-274. doi: 10.1002/prot.20569

N. Farrell. (2009). *Compr. Coord. Chem. II 9*, 809

N. Farrell (Ed.). (1989). Transition Metal Complexes as Drugs and Chemotherapeutic Agent, Kluwer Academic Publishers, . *the Netherlands*

NCCLS, National Committee for Clinical Laboratory Standards, Performance Standards for Antimicrobial Disk Susceptibility Test. (1997). *6th ed., Approved Standard, Wayne,, PA, M2-A6,*

Neto, J. L., de Lima, G. M., & Beraldo, H. (2006). Platinum and palladium complexes of thiosemicarbazones derived of 2-acetylthiophene: Synthesis and spectral studies. *Spectrochimica Acta Part A: Molecular and Biomolecular Spectroscopy, 63*(3), 669-672. doi: http://dx.doi.org/10.1016/j.saa.2005.06.016

Özel, A., Barut, B., Demirbaş, Ü., & Biyiklioglu, Z. (2016). Investigation of DNA binding, DNA photocleavage, topoisomerase I inhibition and antioxidant activities of water soluble titanium(IV) phthalocyanine compounds. *Journal of Photochemistry and Photobiology B: Biology, 157*, 32-38. doi: http://dx.doi.org/10.1016/j.jphotobiol.2016.02.005

P. Kalyani. (2012). Editorial Board. *Journal of Pharmaceutical and Biomedical Analysis, 70*, CO2. doi: http://dx.doi.org/10.1016/S0731-7085(12)00447-5

Pasternack, R. F., Caccam, M., Keogh, B., Stephenson, T. A., Williams, A. P., & Gibbs, E. J. (1991). Long-range fluorescence quenching of ethidium ion by cationic porphyrins in the presence of DNA. *Journal of the American Chemical Society, 113*(18), 6835-6840. doi: 10.1021/ja00018a019

Patra, M., Wenzel, M., Prochnow, P., Pierroz, V., Gasser, G., Bandow, J. E., & Metzler-Nolte, N. (2015). An organometallic structure-activity relationship study reveals the essential role of a Re(CO)3 moiety in the activity against gram-positive pathogens including MRSA. *Chemical Science, 6*(1), 214-224. doi: 10.1039/C4SC02709D

Pettersen, E. F., Goddard, T. D., Huang, C. C., Couch, G. S., Greenblatt, D. M., Meng, E. C., & Ferrin, T. E. (2004). UCSF Chimera—A visualization system for exploratory research and analysis. *Journal of Computational Chemistry, 25*(13), 1605-1612. doi: 10.1002/jcc.20084

Pyle, A. M., Rehmann, J. P., Meshoyrer, R., Kumar, C. V., Turro, N. J., & Barton, J. K. (1989). Mixed-ligand complexes of ruthenium(II): factors governing binding to DNA. *Journal of the American Chemical Society, 111*(8), 3051-3058. doi: 10.1021/ja00190a046

Rajput, C., Rutkaite, R., Swanson, L., Haq, I., & Thomas, J. A. (2006). Dinuclear Monointercalating RuII Complexes That Display High Affinity Binding to Duplex and Quadruplex DNA. *Chemistry – A European Journal, 12*(17), 4611-4619. doi: 10.1002/chem.200501349

Ramakrishnan, S., Suresh, E., Riyasdeen, A., Akbarsha, M. A., & Palaniandavar, M. (2011). DNA binding, prominent DNA cleavage and efficient anticancer activities of Tris(diimine)iron(ii) complexes. *Dalton Transactions, 40*(14), 3524-3536. doi: 10.1039/C0DT00466A

Reichmann, M. E., Rice, S. A., Thomas, C. A., & Doty, P. (1954). A Further Examination of the Molecular Weight and Size of Desoxypentose Nucleic Acid. *Journal of the American Chemical Society, 76*(11), 3047-3053. doi: 10.1021/ja01640a067

Rohs, R., Bloch, I., Sklenar, H., & Shakked, Z. (2005). Molecular flexibility in ab initio drug docking to DNA: binding-site and binding-mode transitions in all-atom Monte Carlo simulations. *Nucleic Acids Research, 33*(22), 7048-7057. doi: 10.1093/nar/gki1008

Rosenberg, B., Vancamp, L., Trosko, J. E., & Mansour, V. H. (1969). Platinum Compounds: a New Class of Potent Antitumour Agents. *Nature, 222*(5191), 385-386

Sadana, A. K., Mirza, Y., Aneja, K. R., & Prakash, O. (2003). Hypervalent iodine mediated synthesis of 1-aryl/hetryl-1,2,4-triazolo[4,3-a] pyridines and 1-aryl/hetryl 5-methyl-1,2,4-triazolo[4,3-a]quinolines as antibacterial agents. *European Journal of Medicinal Chemistry, 38*(5), 533-536. doi: http://dx.doi.org/10.1016/S0223-5234(03)00061-8

Shiju, C., Arish, D., Bhuvanesh, N., & Kumaresan, S. (2015). Synthesis, characterization, and biological evaluation of Schiff base–platinum(II) complexes. *Spectrochimica Acta Part A: Molecular and Biomolecular Spectroscopy, 145*, 213-222. doi: http://dx.doi.org/10.1016/j.saa.2015.02.030

Soori H1, R.-C. A., Davoodi J1. (2015 Jan 7). *Eur J Med Chem, 89*, 844-850

Tabassum, S., Zaki, M., Afzal, M., & Arjmand, F. (2013). New modulated design and synthesis of quercetin-CuII/ZnII-Sn2IV scaffold as anticancer agents: in vitro DNA binding profile, DNA cleavage pathway and Topo-I activity. *Dalton Transactions, 42*(27), 10029-10041. doi: 10.1039/C3DT50646K

Temple, M. D., McFadyen, W. D., Holmes, R. J., Denny, W. A., & Murray, V. (2000). Interaction of Cisplatin and DNA-Targeted 9-Aminoacridine Platinum Complexes with DNA†. *Biochemistry, 39*(18), 5593-5599. doi: 10.1021/bi9922143

Thompson, K. H., & Orvig, C. (2003). Boon and Bane of Metal Ions in Medicine. *Science, 300*(5621), 936-939. doi: 10.1126/science.1083004

Tysoe, S. A., Morgan, R. J., Baker, A. D., & Strekas, T. C. (1993). Spectroscopic investigation of differential binding modes of .DELTA.- and .LAMBDA.-Ru(bpy)2(ppz)2+ with calf thymus DNA. *The Journal of Physical Chemistry, 97*(8), 1707-1711. doi: 10.1021/j100110a038

Veysel T. Yilmaza. (2014). *Journal of Photochemistry and Photobiology B: Biology 131*, 31

Volarevic, V. (2013). Cytotoxic effects of palladium(II) and platinum(II) complexes with O,O'-dialkyl esters of (S,S)-ethylenediamineN,N'-di-2-(4-methyl) pentanoic acid on human colon cancer cell lines. *J BUON, 18*(1), 131

Wang, D., & Lippard, S. J. (2005). Cellular processing of platinum anticancer drugs. *Nat Rev Drug Discov, 4*(4), 307-320

Wheate, N. J., Walker, S., Craig, G. E., & Oun, R. (2010). The status of platinum anticancer drugs in the clinic and in clinical trials. *Dalton Transactions, 39*(35), 8113-8127. doi: 10.1039/C0DT00292E

Wolfe, A., Shimer, G. H., & Meehan, T. (1987). Polycyclic aromatic hydrocarbons physically intercalate into duplex regions of denatured DNA. *Biochemistry, 26*(20), 6392-6396. doi: 10.1021/bi00394a013

Y. Li, Z. Y. Y., M.F. Wang. (2010). *J. Fluoresc*. (20), 891

Zeng, Y.-B., Yang, N., Liu, W.-S., & Tang, N. (2003). Synthesis, characterization and DNA-binding properties of La(III) complex of chrysin. *Journal of Inorganic Biochemistry, 97*(3), 258-264. doi: http://dx.doi.org/10.1016/S0162-0134(03)00313-1

Zhang, J., Li, Y., Sun, J., Li, W., Gong, Y., Zheng, X., . . . Wu, J. (2009). Synthesis, cytotoxicity and DNA-binding levels of new type binuclear platinum(II) complexes. *European Journal of Medicinal Chemistry, 44*(11), 4772-4777. doi: http://dx.doi.org/10.1016/j.ejmech.2009.06.017

Zhao, J., Gou, S., Sun, Y., Fang, L., & Wang, Z. (2012). Antitumor Platinum(II) Complexes Containing Platinum-Based Moieties of Present Platinum Drugs and Furoxan Groups as Nitric Oxide Donors: Synthesis, DNA Interaction, and Cytotoxicity. *Inorganic Chemistry, 51*(19), 10317-10324. doi: 10.1021/ic301374z

Zhu, M.-C., Cui, X.-T., Zhao, F.-C., Ma, X.-Y., Han, Z.-B., & Gao, E.-J. (2015). Synthesis, characterization, and DNA interaction of novel Pt(ii) complexes and their cytotoxicity, apoptosis and molecular docking. *RSC Advances, 5*(59), 47798-47808. doi: 10.1039/C5RA04972E

Figures and table:

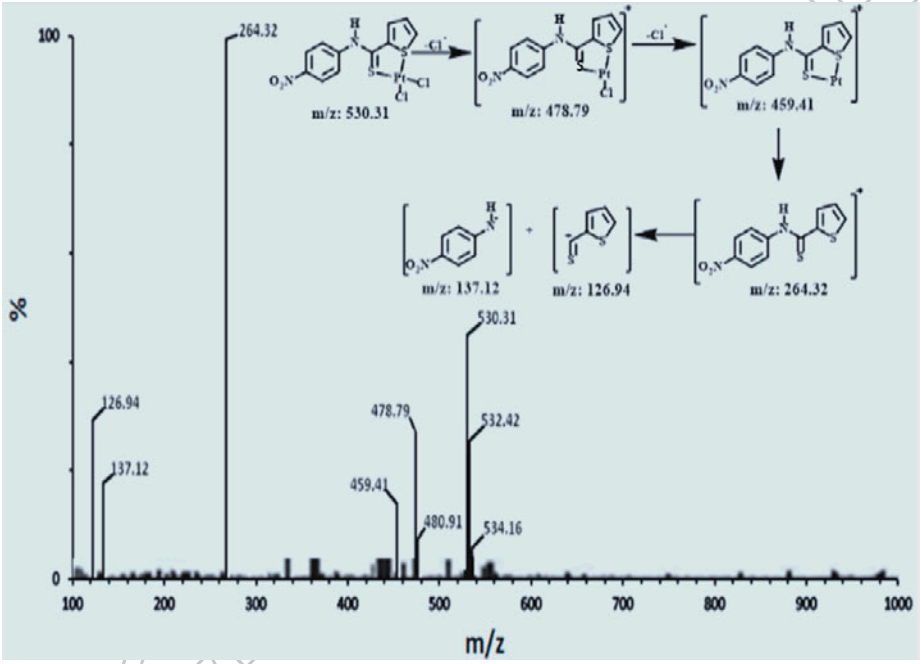

Fig. 1. LC-MS spectrum of complex (1f)

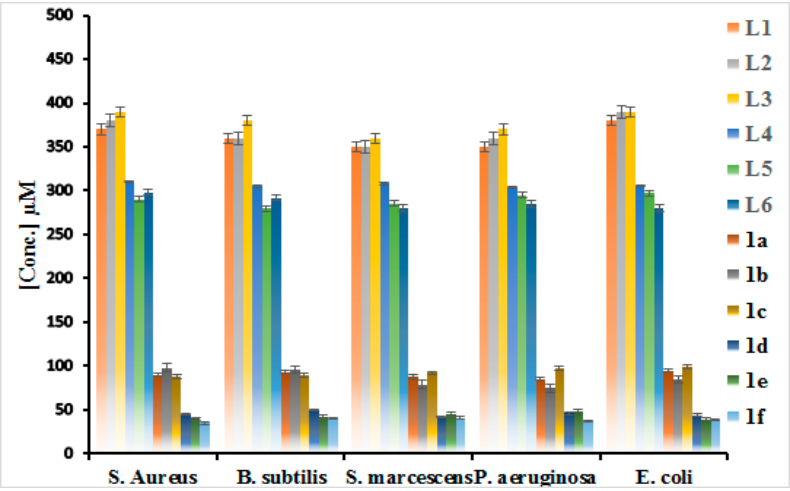

Fig. 2. Effect of different concentration of ligands (L^{1-6}) and synthesized Pt(II) complexes (1a-1f) on Gram$^{(+ve)}$ and Gram$^{(-ve)}$ bacteria.

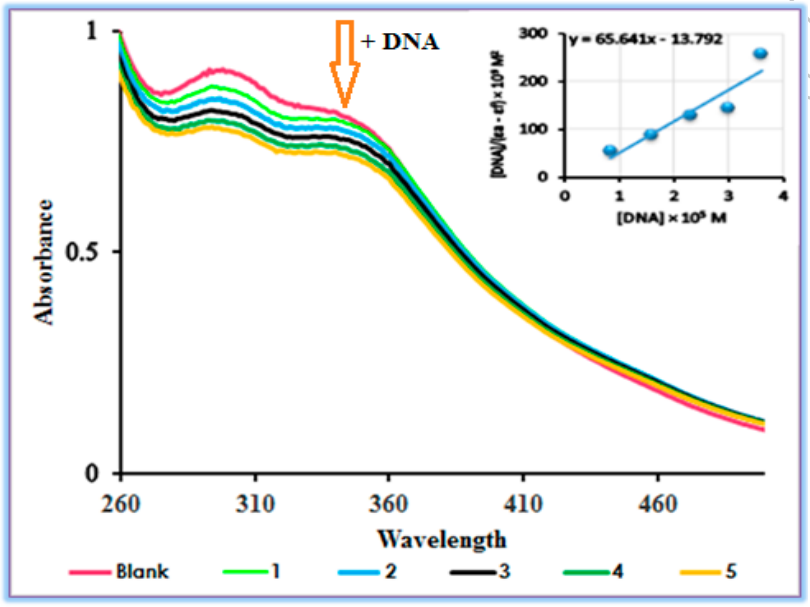

Fig. 3. Absorption spectral changes on addition of CT-DNA to the solution of complex (1f) after incubating it for 10 min at room temperature in phosphate buffer (Tris-HCl, pH=7.2). Inset: plot of [DNA]/ (Ɛa- Ɛb) vs. [DNA]. (Arrow shows the change in absorption with increase in concentration of DNA).

Table 1. Binding constant (K_b), % hypochromicity and standard free energy changes (ΔG) values of synthesized Pt(II) complexes.

Complexes	[a]*H%*	[b]K_b (M^{-1})	ΔG(J mol^{-1})
1a	19.23 ± 0.78	0.768 ± 0.05 × 10^5	-27873.0
1b	16.66 ± 0.69	0.875 ± 0.10 × 10^5	-28193.3
1c	20.70 ± 0.91	1.463 ± 0.08 × 10^5	-29466.8
1d	16.77 ± 0.73	0.939 ± 0.12 × 10^5	-28368.7
1e	20.92 ± 0.08	1.540 ± 0.05 × 10^5	-29593.9
1f	21.13 ± 0.57	1.611 ± 0.06 × 10^5	-29705.6

[a]*H%* = $[(A_{free} - A_{bound})/A_{free}] \times 100\%$.
[b]K_b = Intrinsic DNA binding constant determined from the UV-Visible absorption spectral titration.

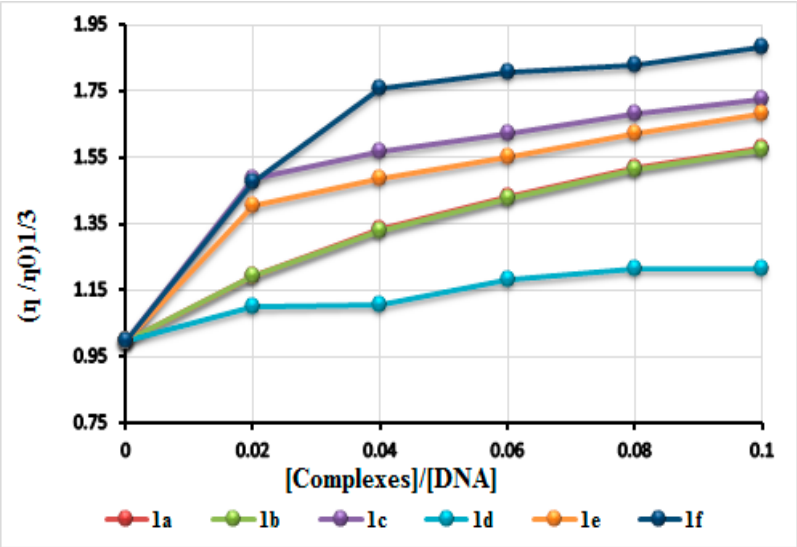

Fig. 4. Viscosity measurements of the complexes (1a-1f)

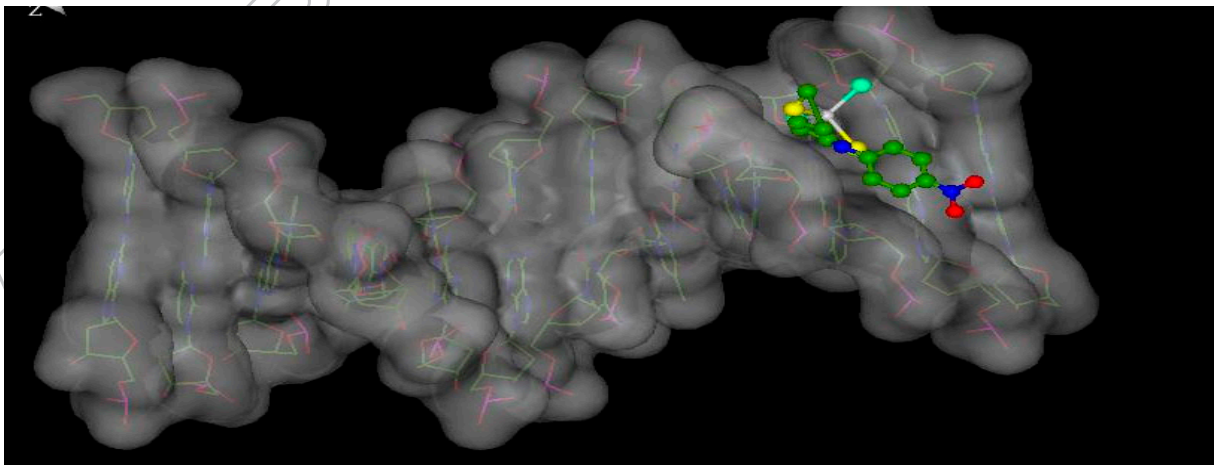

Fig. 5. Molecular docking of the complex (1f) (ball and stick) with the DNA duplex (VDW spheres with solid surface) of sequence (5'-D(CPGPCPGPAPAPTPTPCPGPCPG)-3').

The complex is docked in to the DNA showing partial intercalation between the DNA base pairs.

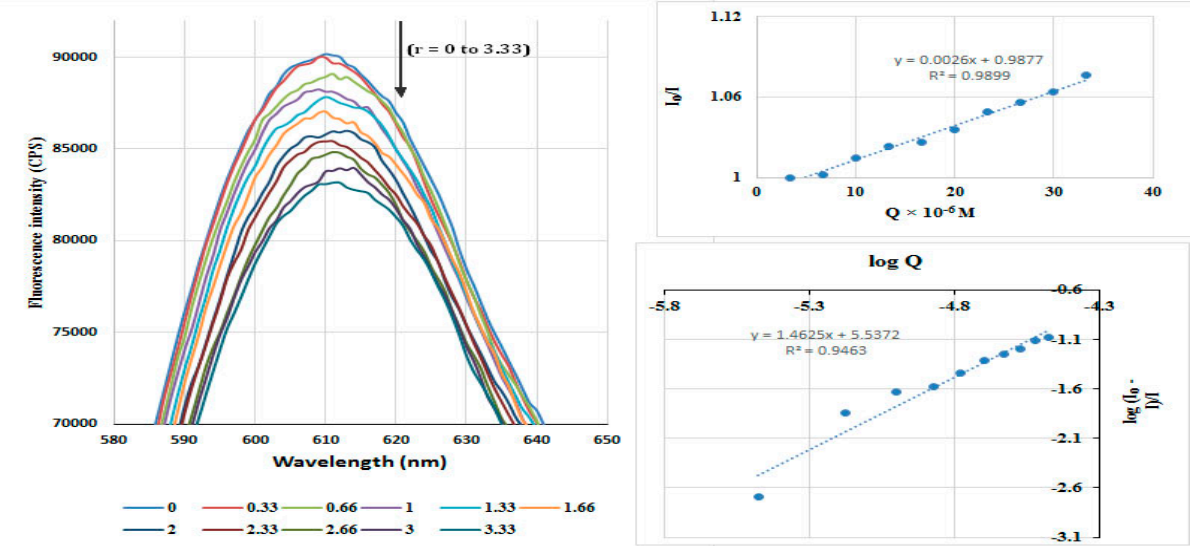

Fig. 6. Emission spectra of EB bound to DNA in the presence of Pt(II) complex (1b). ([DNA] = 1.00 × 10^{-5} M, [EB] = 33.3 µM, [Quencher] (µM): 0 - 3.33 µM. The arrow shows the intensity changes upon gradual increasing the complex concentration. Inset: plot of I_0/I vs. [Quencher] and comparative plot of log[I_0-I/I] vs. log[Q] for the titration of CT-DNA EB system with Pt(II) complex (1b) in 1 M Tris-HCl buffer (pH 7.2) medium.

Table 2. Linear Stern-Volmer quenching constant (K_q), binding sites (n) and association binding constant (K_a) from competitive.

Complexes	K_q (M^{-1})	K_a (M^{-1})	n	ΔG(J mol-1)
1a	9.0 × 10^4	1.62 × 10^2	0.8558	-12,607.65
1b	2.6 × 10^3	3.10 × 10^4	1.2383	-25,671.60
1c	2.9 ×10^3	1.73 × 10^3	0.9510	-18,482.00
1d	3.8 × 10^3	2.65 × 10^3	0.9648	-19,510.00
1e	3.1 × 10^3	0.69 × 10^4	1.0830	-21,929.32
1f	4.0 × 10^4	0.34 × 10^2	0.7543	-8,757.46

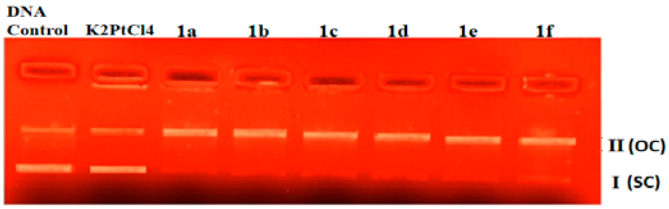

Fig. 7. Photogenic view of cleavage of pUC19 DNA (300 µg/cm^3) with series of Pt(II) complexes (200 µM) using 1 % agarose gel containing 0.5 µg/cm^3 EtBr. Reactions were incubated in TE buffer solution (pH 8) at a final volume of 15 mm^3 for time period of 3 h at 37 ^{0}C. Lane 1. DNA control, lane 2. K_2PtCl_4, lane 3. (1a), lane 4. (1b), lane 5. (1c), lane 6. (1d), lane 7. (1e), lane 8. (1f).

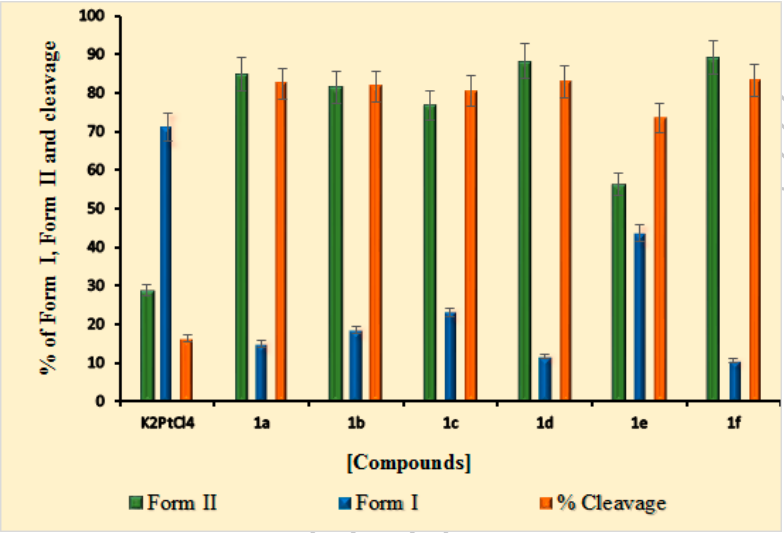

Fig. 8. Plot of nuclease cleavage (% of form I, form II and DNA cleavage) assay of the complexes (1a-1f). Error bars represent standard deviation of three replicates.

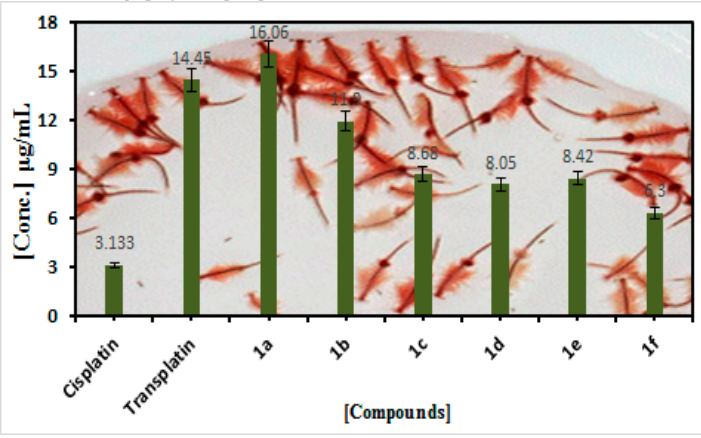

Fig. 9. Plot of LC_{50} values (from *in vitro* cytotoxic activity) of synthesized Pt(II) complexes (1a-1f) in µg/mL. Error bars represent standard deviation of three replicates.

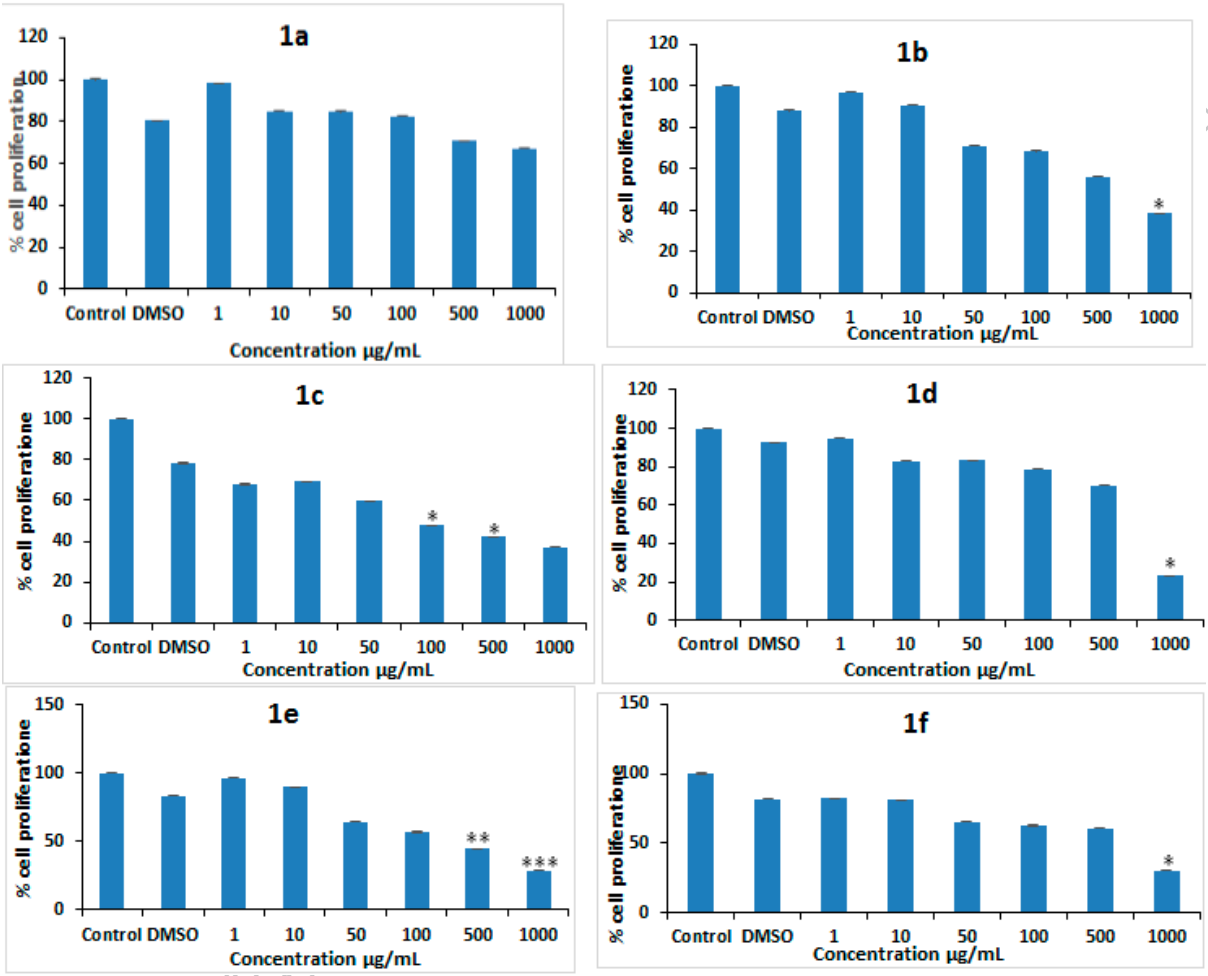

Fig. 10. Effect of synthesized Pt(II) complexes conjugate on cell proliferation. Determination of IC_{50} values of Pt(II) complexes (1a-1f) conjugate in HCT 116 cells. HCT 116 cells were treated with the various concentrations (control (100 % DMSO), 1% DMSO, 1, 10, 50, 100, 500, 1000 µg/mL) of Pt(II) complexes (1a-1f) conjugate for 24 h. 1 % DMSO was used as a vehicle control. MTT assay determined Inhibition of HCT 116 cells. The obtained values were plotted and the IC_{50} values were analysed the data with t-test using Sigmaplot 12.0. Error bars represent standard deviation of three replicates.

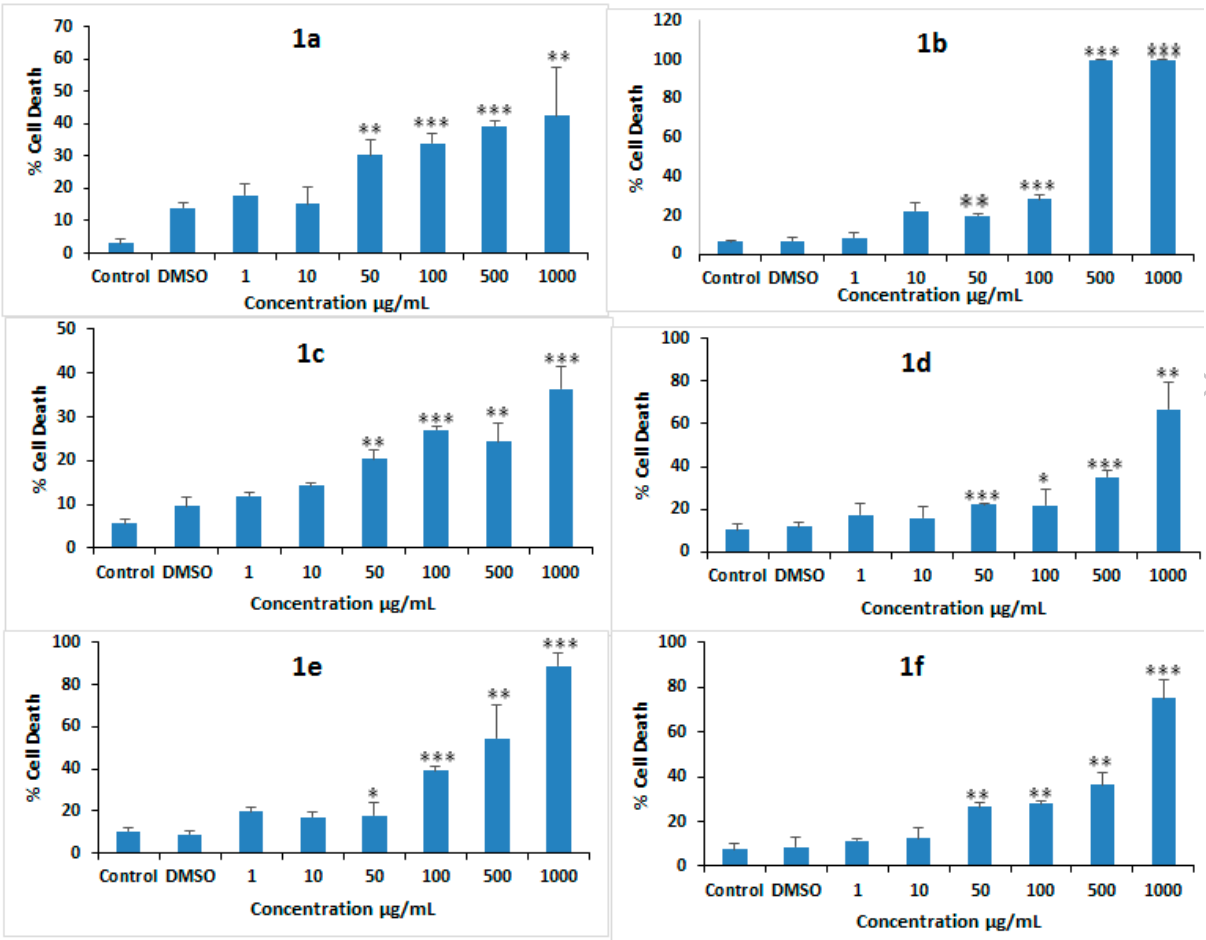

Fig. 11. Evaluation of cell death by trypan blue exclusion assay. HCT 116 cells were treated with (control, DMSO, 1, 10, 50, 100, 500, 1000 µg/mL) of Pt(II) complexes (1a-1f) conjugate for 24 h. Similarly, 1 % DMSO was used as a vehicle control. During analysis, the cells were harvested, washed and subjected to trypan blue exclusion assay. Graphs represent the cell death in mentioned concentration of Pt(II) complexes (1a-1f). Error bars represent mean ± SEM of three independent experiments. Significant difference indicated as *$p \leq 0.05$ between untreated and complexes treated cells; **$p \leq 0.01$, ***$p \leq 0.001$. Error bars represent standard deviation of three replicates.

Design, synthesis, MTT assay, DNA interaction studies of platinum(II) complexes

Miral V. Lunagariya[a], Khyati P. Thakor[a], Bhargav N. Waghela[b],
Foram U. Vaidya[b], Chadramani Pathak[b] and Mohan N. Patel[a]*
Department of Chemistry, Sardar Patel University,

Vallabh Vidyanagar–388 120, Gujarat, India.

Corresponding author. Tel.: +91 2692 226856

E-mail: jeenen@gmail.com

[b]*Department of Cell biology,*

Indian institute of advanced Research,

Gandhinagar, Gujarat, India.

E-mail: cmpathak@iiar.res.in

Supplementary material 1: Synthesis of ligands (L^{1-6})

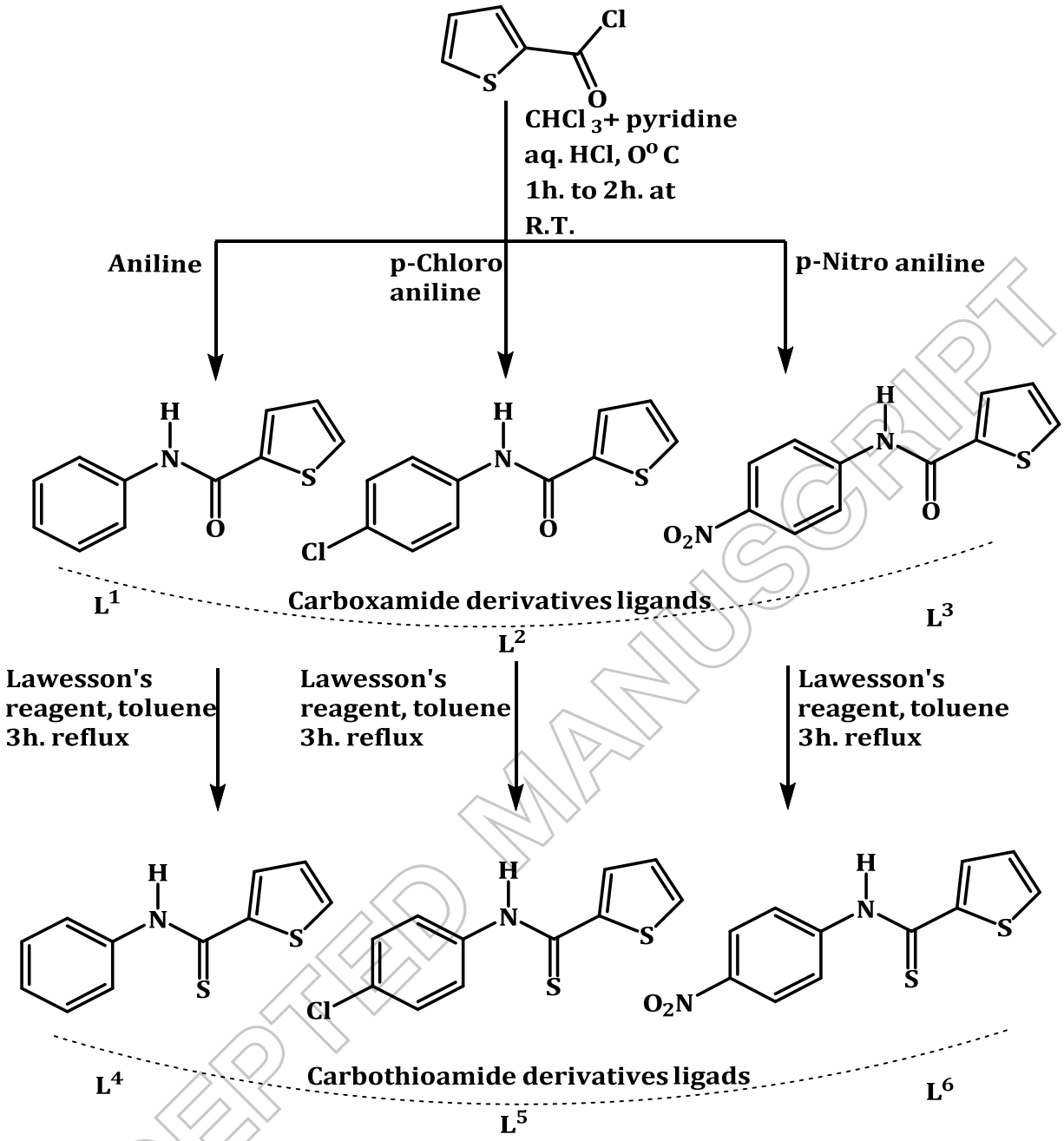

Supplementary material 2: Synthesis of Pt(II) complexes (1a-1f)

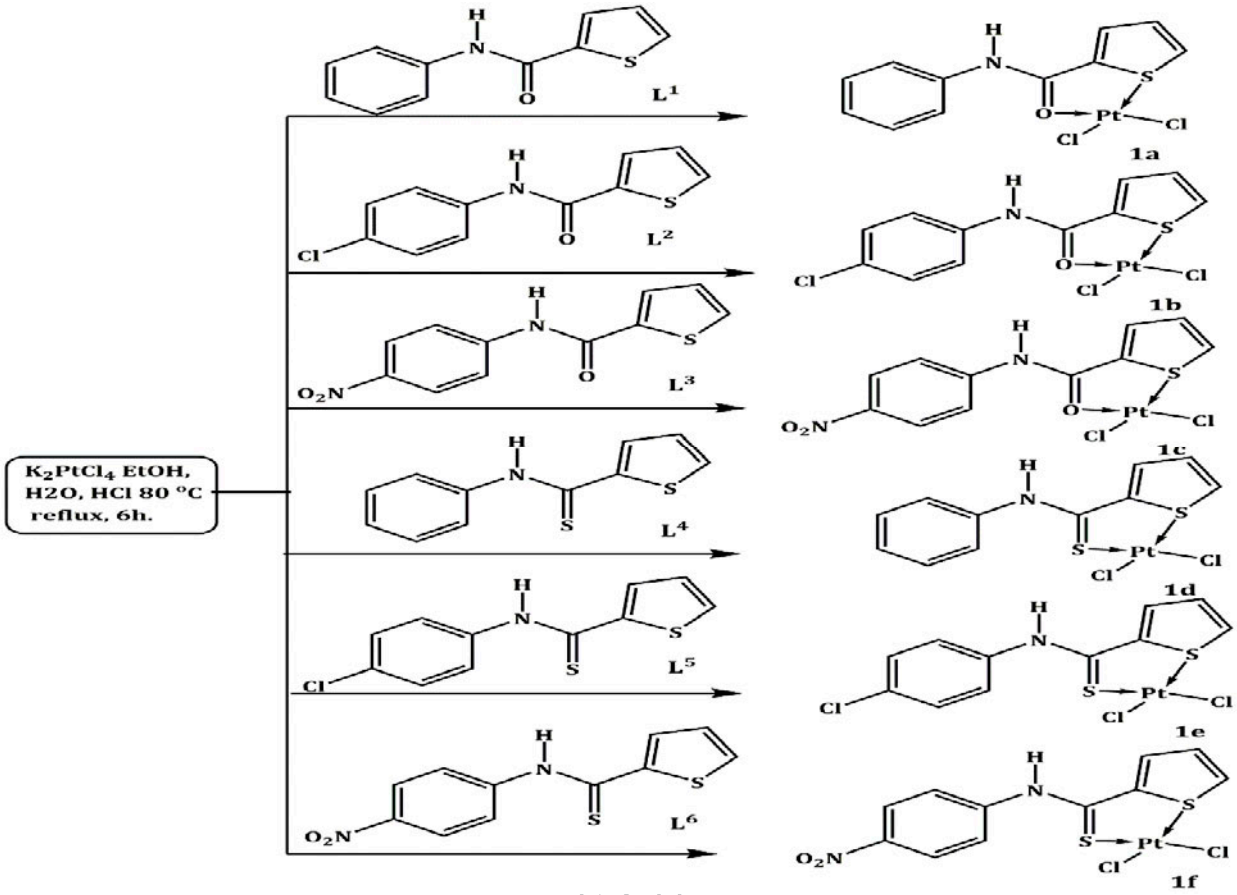

Supplementary material 3: ^{1}H NMR spectra of ligands (L^1 –L^6).

N-Phenylthiophene-2-carboxamide ***(L^1)***

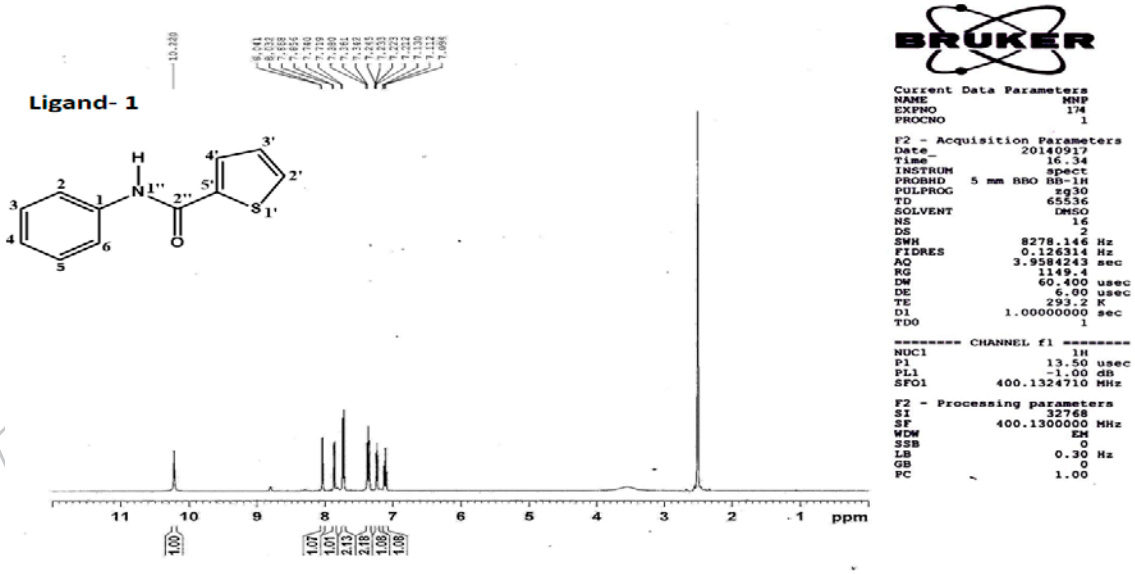

N-(4-Chlorophenyl) thiophene-2-carboxamide ***(L^2)***

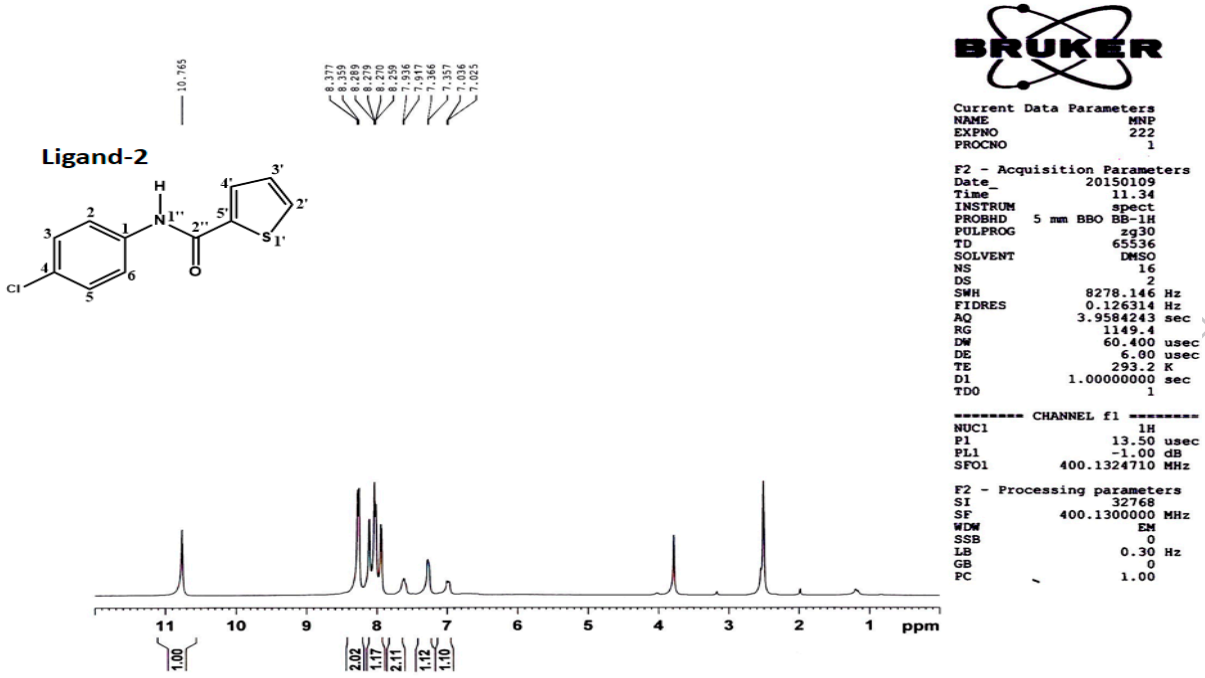

N-(4-Nitrophenyl) thiophene-2-carboxamide (***L*^{3}**)

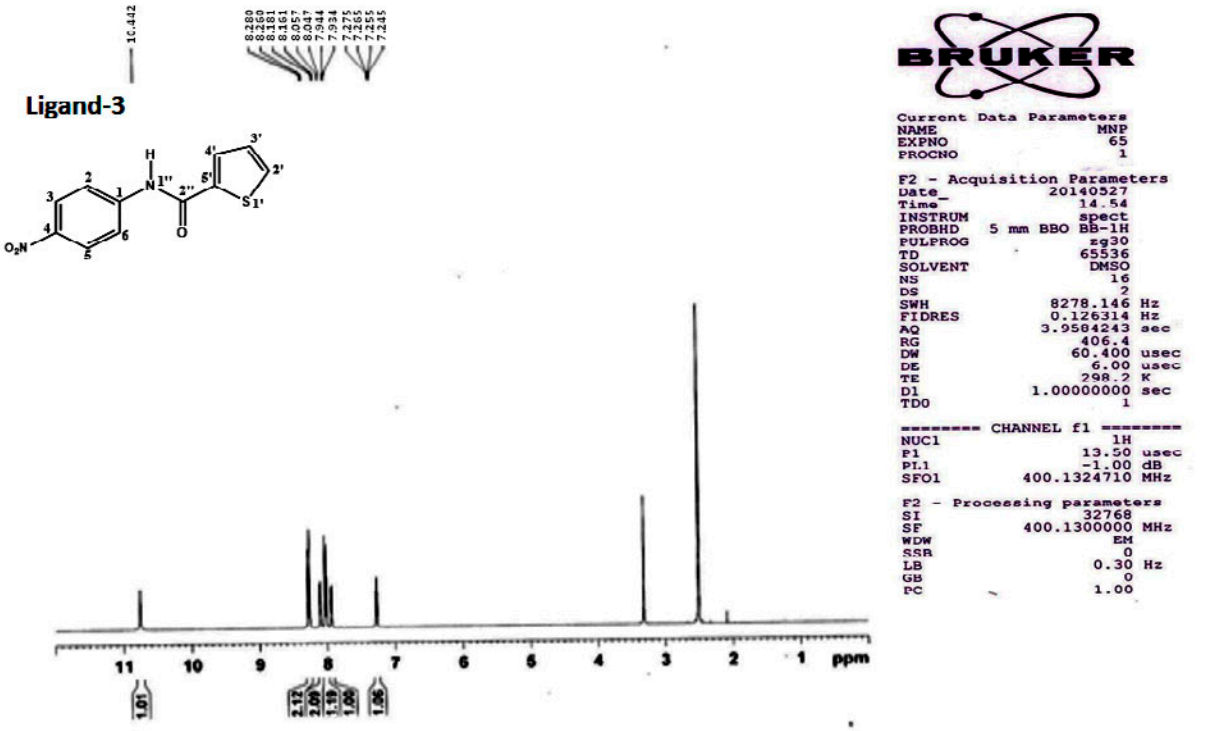

N-Phenylthiophene-2-carbothioamide (***L*^{4}**)

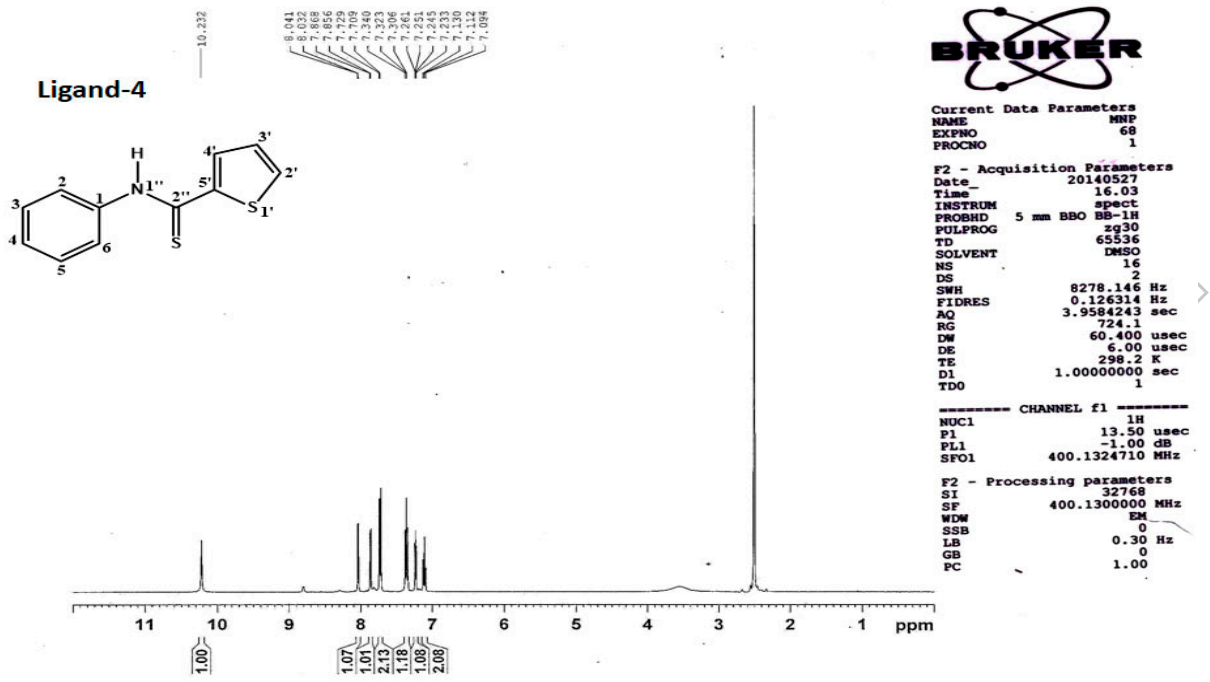

*N-(4-Chlorophenyl) thiophene-2-carbothioamide (**L**^{5})*

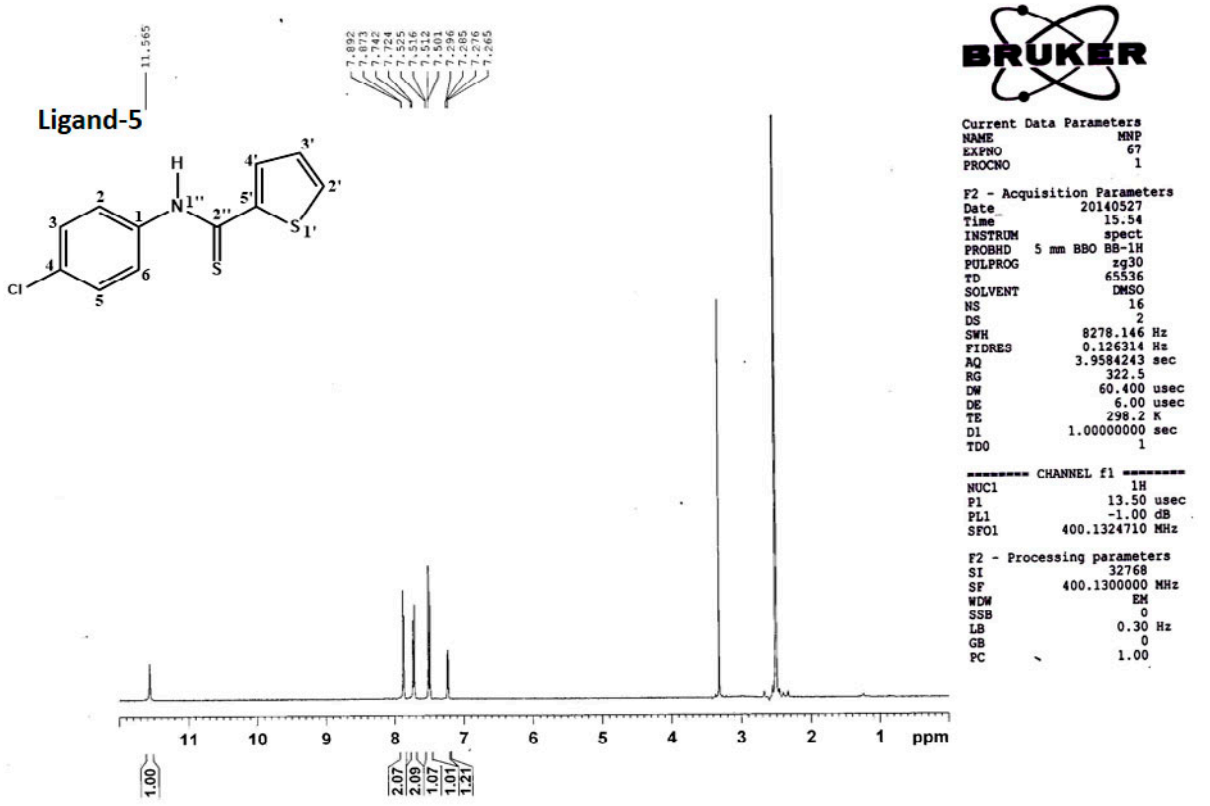

*N-(4-Nitrophenyl) thiophene-2-carboxamide (**L**^{6})*

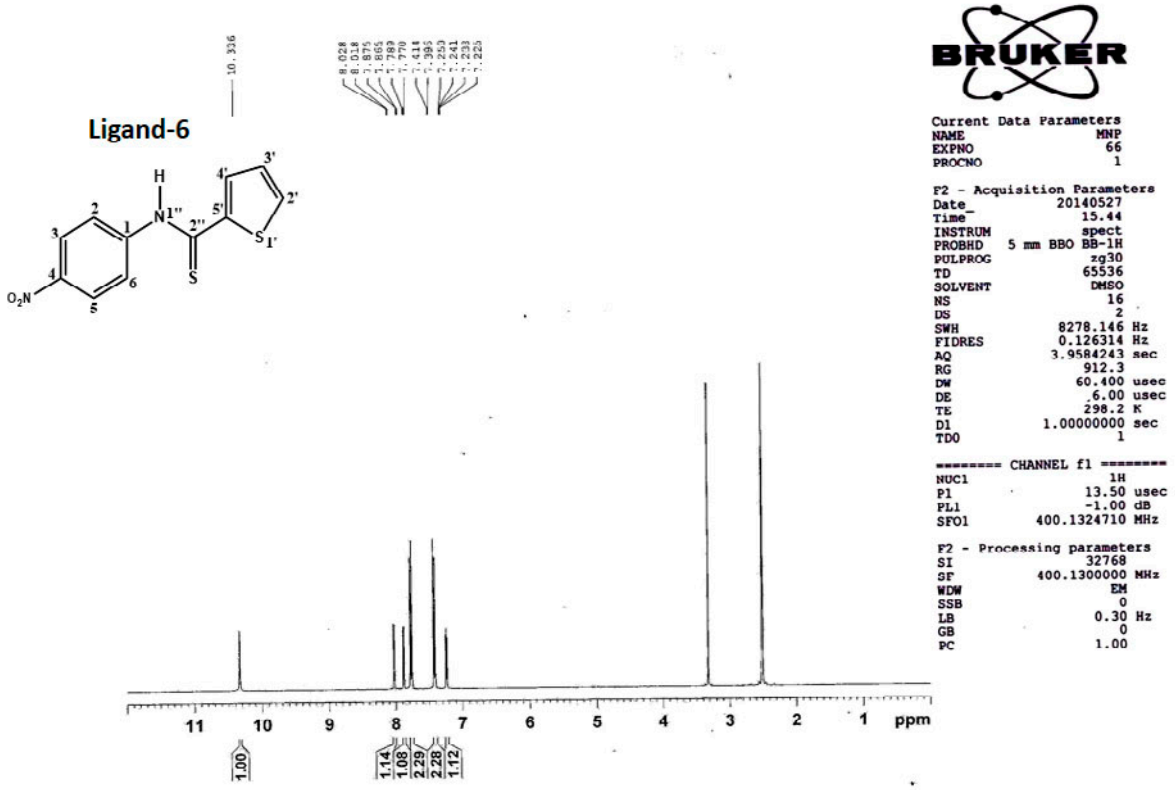

Supplymetry material 4 : ^{1}H NMR spectra of complexes (1a -1f).

[Pt(L^{1})(Cl$_2$)] (1a)

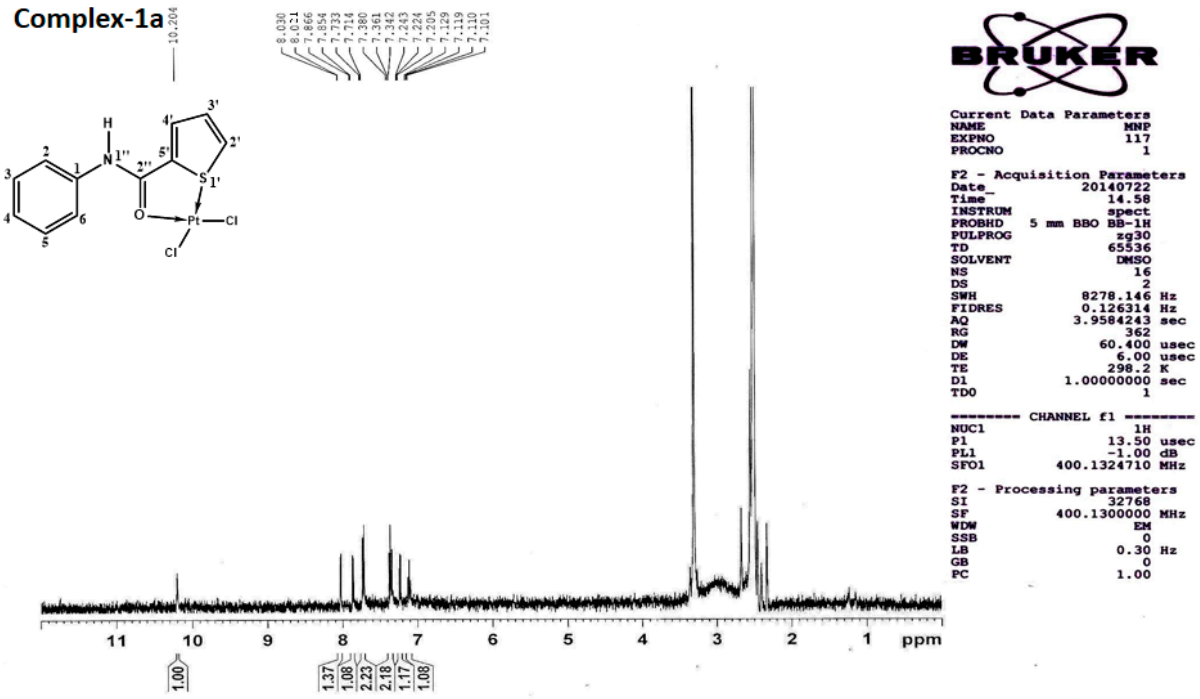

[Pt(L^{2})(Cl$_2$)] (1b)

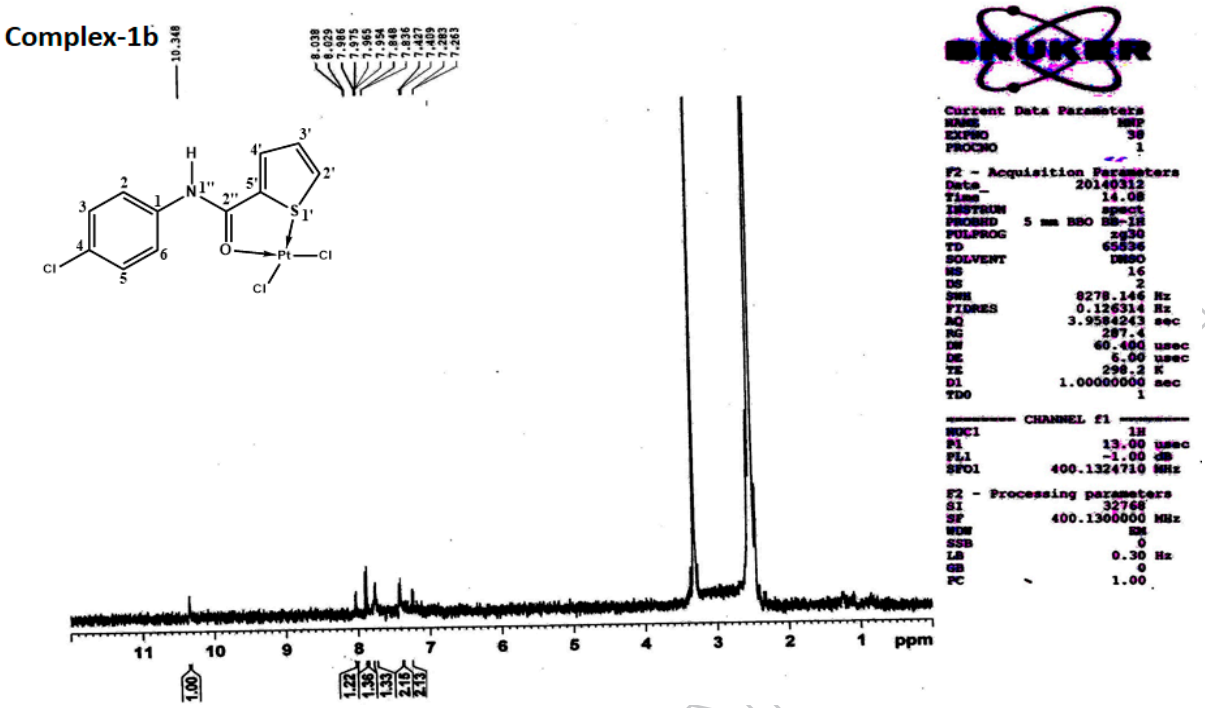

[Pt(L^3)(Cl$_2$)] (1c)

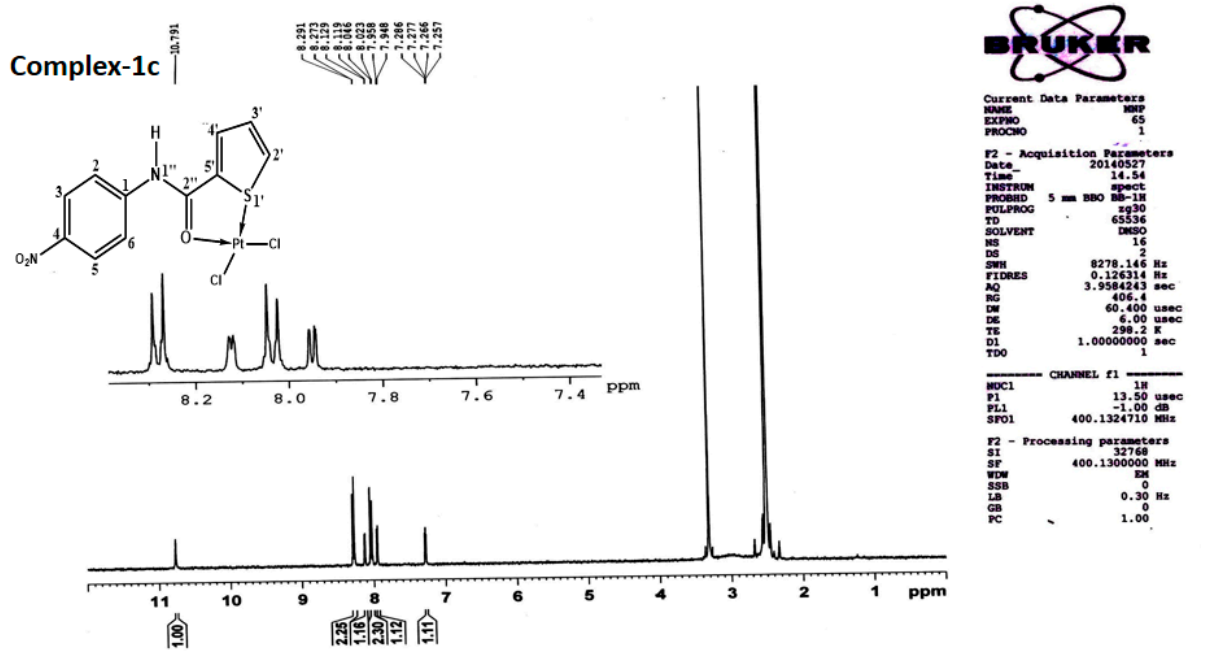

[Pt(L^4)(Cl$_2$)] (1d)

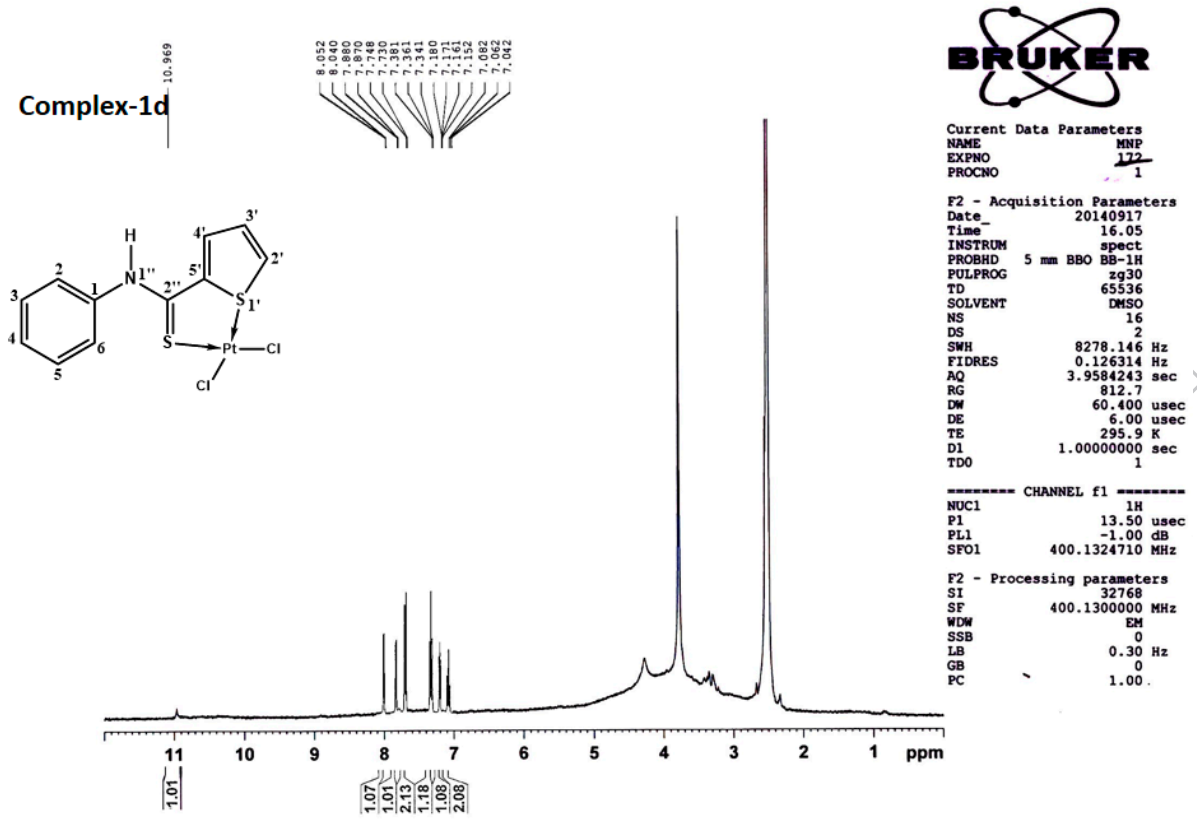
Complex-1d
10.969
8.052
8.040
7.880
7.870
7.748
7.730
7.381
7.361
7.341
7.180
7.171
7.161
7.152
7.062
7.042
H
N1''
2''
3'
4'
5'
2'
S1'
1
2
3
4
5
6
S
Pt
Cl
Cl
11
10
9
8
7
6
5
4
3
2
1
ppm
1.01
1.07
1.01
2.13
1.18
1.08
2.08
BRUKER
Current Data Parameters
NAME MNP
EXPNO 172
PROCNO 1
F2 - Acquisition Parameters
Date_ 20140917
Time 16.05
INSTRUM spect
PROBHD 5 mm BBO BB-1H
PULPROG zg30
TD 65536
SOLVENT DMSO
NS 16
DS 2
SWH 8278.146 Hz
FIDRES 0.126314 Hz
AQ 3.9584243 sec
RG 812.7
DW 60.400 usec
DE 6.00 usec
TE 295.9 K
D1 1.00000000 sec
TD0 1
======== CHANNEL f1 ========
NUC1 1H
P1 13.50 usec
PL1 -1.00 dB
SFO1 400.1324710 MHz
F2 - Processing parameters
SI 32768
SF 400.1300000 MHz
WDW EM
SSB 0
LB 0.30 Hz
GB 0
PC 1.00

[Pt(L^5)(Cl$_2$)] (1e)

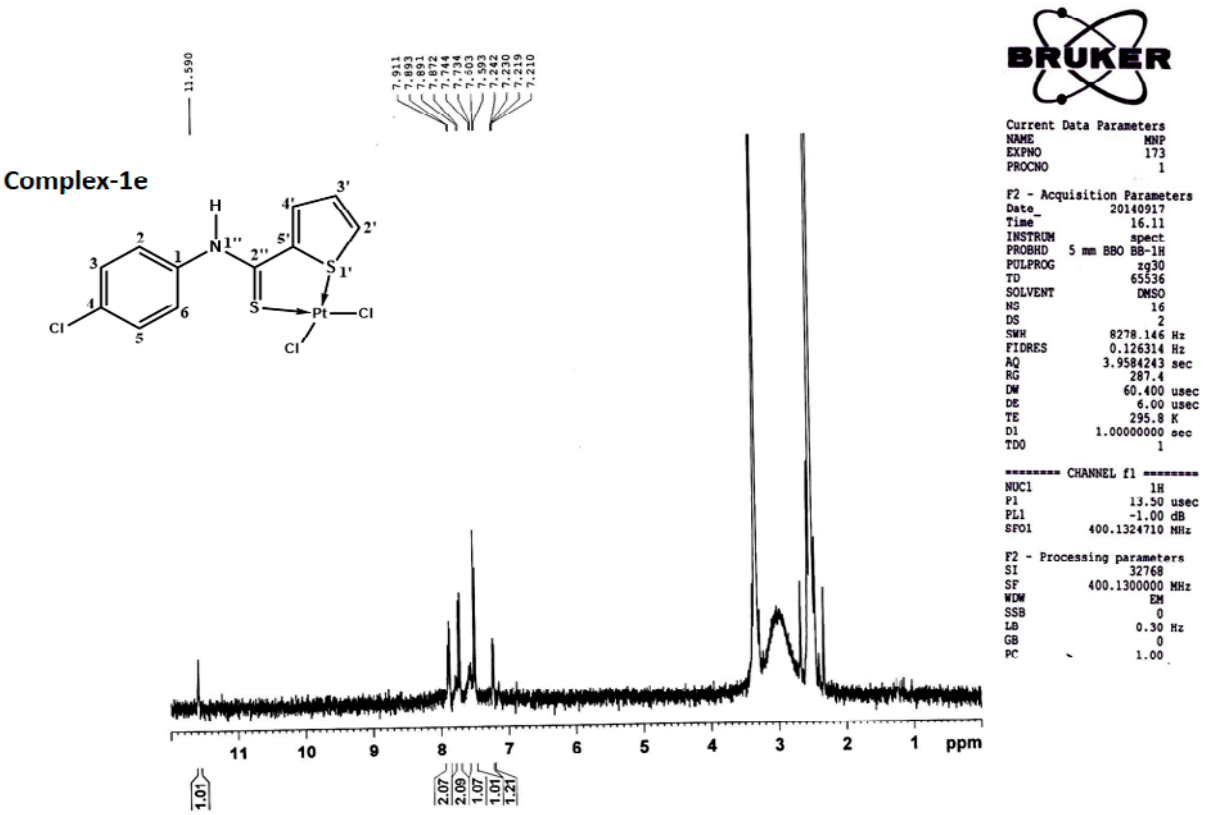
Complex-1e
11.590
7.911
7.893
7.891
7.872
7.744
7.734
7.603
7.593
7.242
7.230
7.219
7.210
H
N1''
2''
3'
4'
5'
2'
S1'
1
2
3
4
5
6
Cl
S
Pt
Cl
Cl
11
10
9
8
7
6
5
4
3
2
1
ppm
1.01
2.07
2.09
1.07
1.01
1.21
BRUKER
Current Data Parameters
NAME MNP
EXPNO 173
PROCNO 1
F2 - Acquisition Parameters
Date_ 20140917
Time 16.11
INSTRUM spect
PROBHD 5 mm BBO BB-1H
PULPROG zg30
TD 65536
SOLVENT DMSO
NS 16
DS 2
SWH 8278.146 Hz
FIDRES 0.126314 Hz
AQ 3.9584243 sec
RG 287.4
DW 60.400 usec
DE 6.00 usec
TE 295.8 K
D1 1.00000000 sec
TD0 1
======== CHANNEL f1 ========
NUC1 1H
P1 13.50 usec
PL1 -1.00 dB
SFO1 400.1324710 MHz
F2 - Processing parameters
SI 32768
SF 400.1300000 MHz
WDW EM
SSB 0
LB 0.30 Hz
GB 0
PC 1.00

[Pt(L^6)(Cl_2)] (1f)

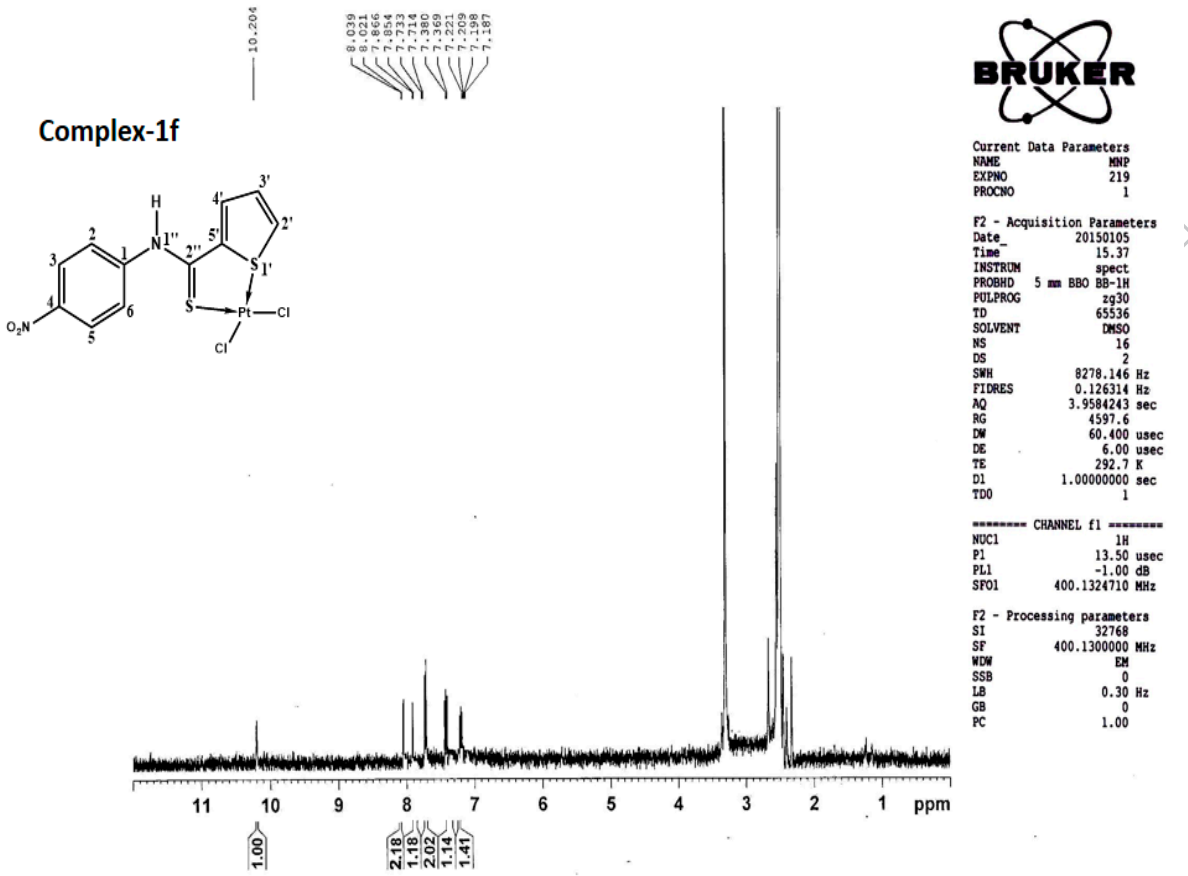

Supplementary material 5: ^{13}C NMR spectra of ligand (L^{1-6}) and Pt(II) complexes (1a-1f)

N-Phenylthiophene-2-carboxamide ***(L^1)***

Ligand-1

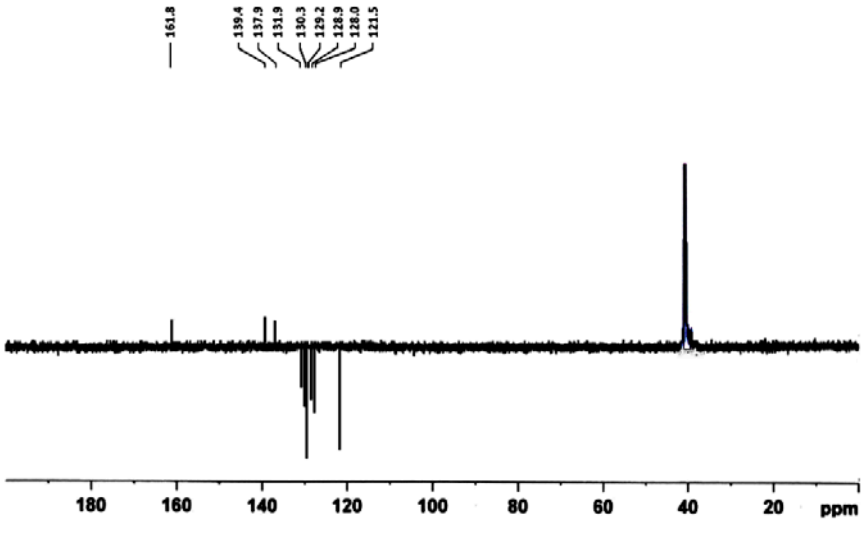

BRUKER

```
Current Data Parameters
NAME                  MNP
EXPNO                 131
PROCNO                  1

F2 - Acquisition Parameters
Date_              20150308
Time                  12.54
INSTRUM               spect
PROBHD   5 mm BBO BB-1H
PULPROG            zgpg30
TD                  65536
SOLVENT              DMSO
NS                    1024
DS                       4
SWH               23980.814 Hz
FIDRES            0.365918 Hz
AQ                1.3664756 sec
RG                   3649.1
DW                  20.850 usec
DE                   6.00 usec
TE                  297.4 K
D1                2.00000000 sec
d11               0.03000000 sec
DELTA             1.89999998 sec
TD0                     1

======== CHANNEL f1 ========
NUC1                   13C
P1                  14.00 usec
PL1                 -4.00 dB
SFO1          100.6228298 MHz

======== CHANNEL f2 ========
CPDPRG2            waltz16
NUC2                    1H
PCPD2               80.00 usec
PL2                 -1.00 dB
PL12                14.46 dB
PL13                15.00 dB
SFO2          400.1316005 MHz

F2 - Processing parameters
SI                     32768
SF            100.6127690 MHz
WDW                       EM
SSB                        0
LB                  1.00 Hz
GB                         0
PC                  1.40
```

N-(4-Chlorophenyl) thiophene-2-carboxamide ***(L^2)***

Ligand-2

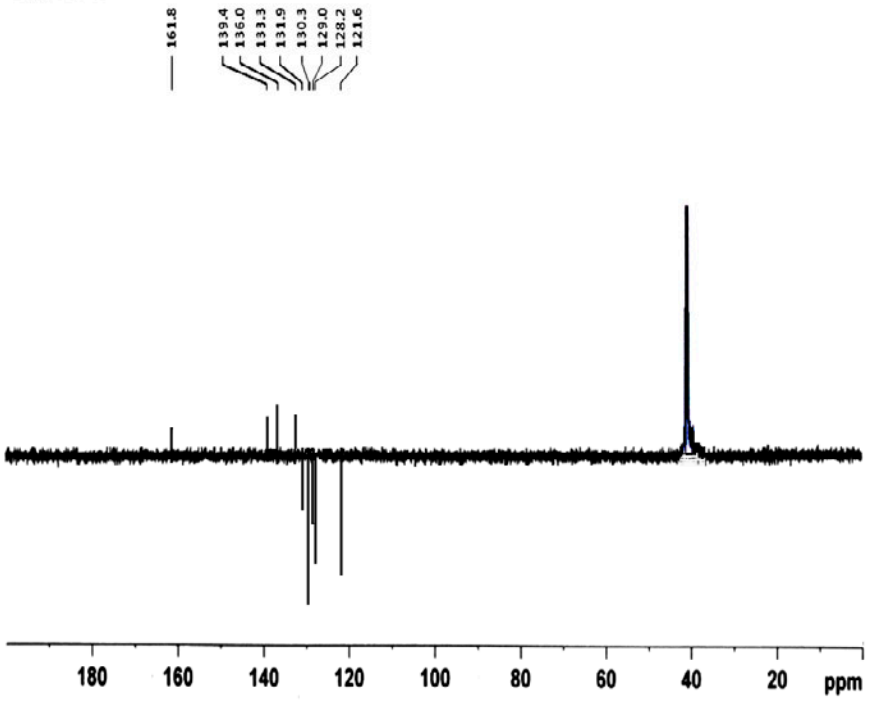

BRUKER

```
Current Data Parameters
NAME                  MNP
EXPNO                 132
PROCNO                  1

F2 - Acquisition Parameters
Date_              20150408
Time                  11.15
INSTRUM               spect
PROBHD   5 mm BBO BB-1H
PULPROG            zgpg30
TD                  65536
SOLVENT              DMSO
NS                    1024
DS                       4
SWH               23980.814 Hz
FIDRES            0.365918 Hz
AQ                1.3664756 sec
RG                   3649.1
DW                  20.850 usec
DE                   6.00 usec
TE                  297.4 K
D1                2.00000000 sec
d11               0.03000000 sec
DELTA             1.89999998 sec
TD0                     1

======== CHANNEL f1 ========
NUC1                   13C
P1                  14.00 usec
PL1                 -4.00 dB
SFO1          100.6228298 MHz

======== CHANNEL f2 ========
CPDPRG2            waltz16
NUC2                    1H
PCPD2               80.00 usec
PL2                 -1.00 dB
PL12                14.46 dB
PL13                15.00 dB
SFO2          400.1316005 MHz

F2 - Processing parameters
SI                     32768
SF            100.6127690 MHz
WDW                       EM
SSB                        0
LB                  1.00 Hz
GB                         0
PC                  1.00
```

*N-(4-Nitrophenyl) thiophene-2-carboxamide (**L**^{3})*

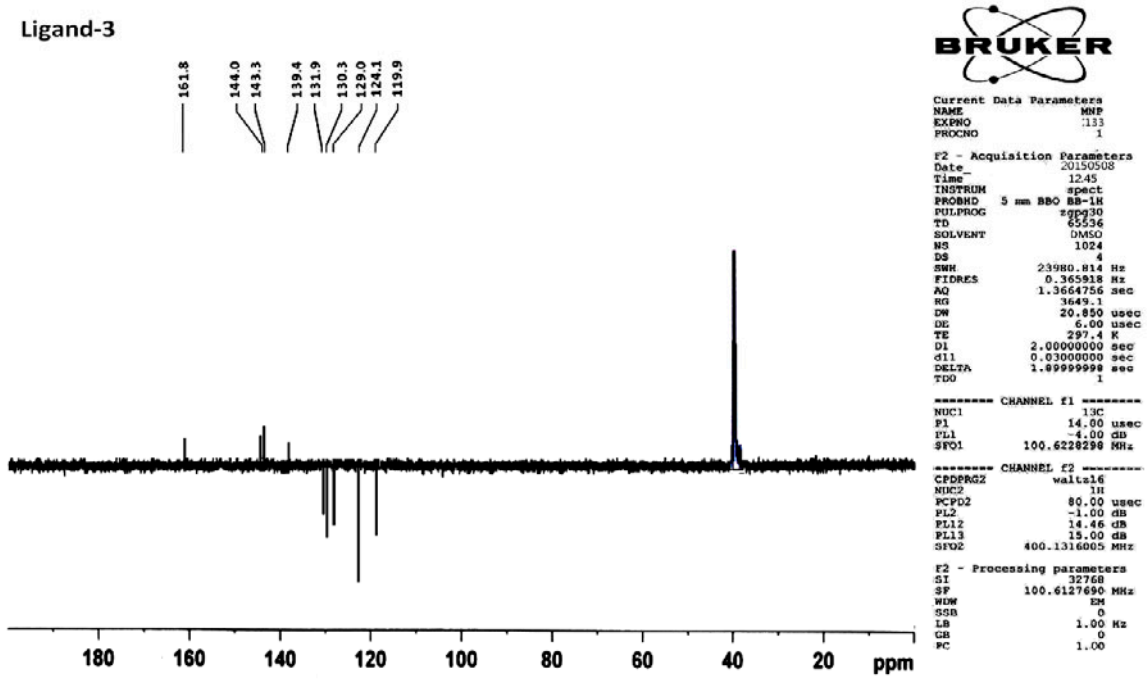

*N-Phenylthiophene-2-carbothioamide (**L**^{4})*

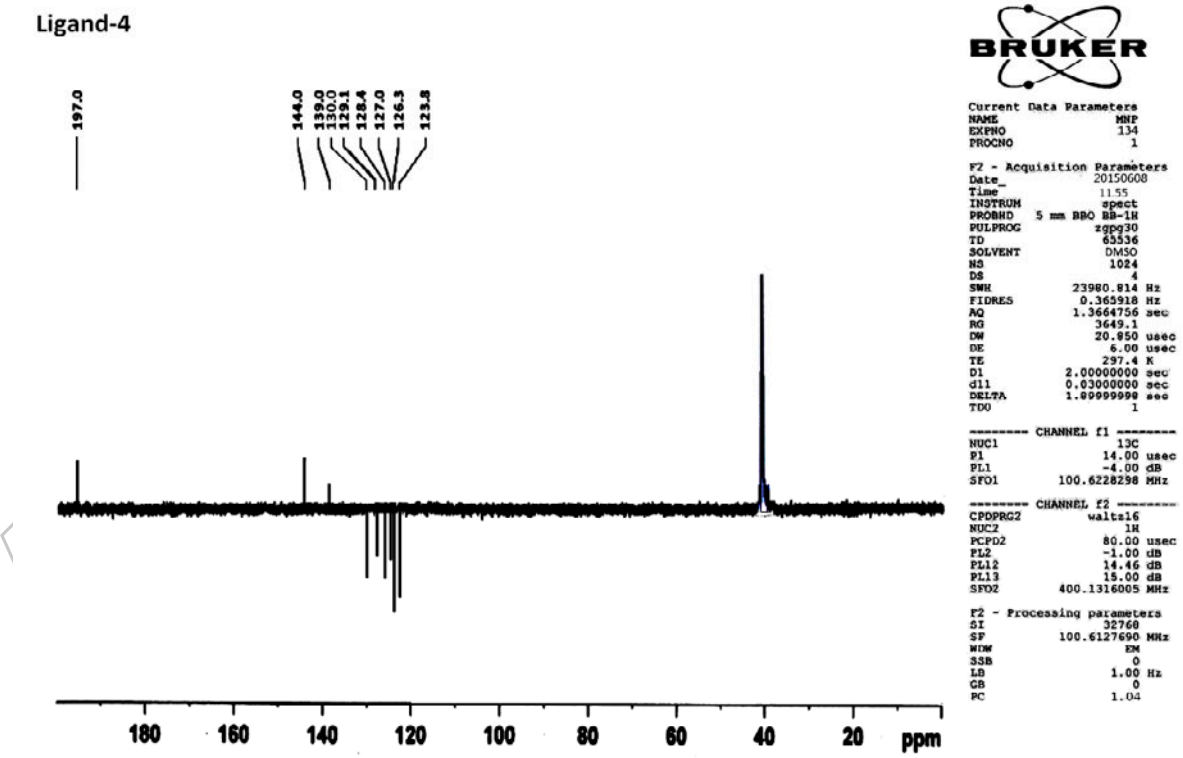

*N-(4-Chlorophenyl) thiophene-2-carbothioamide (**L**^{5})*

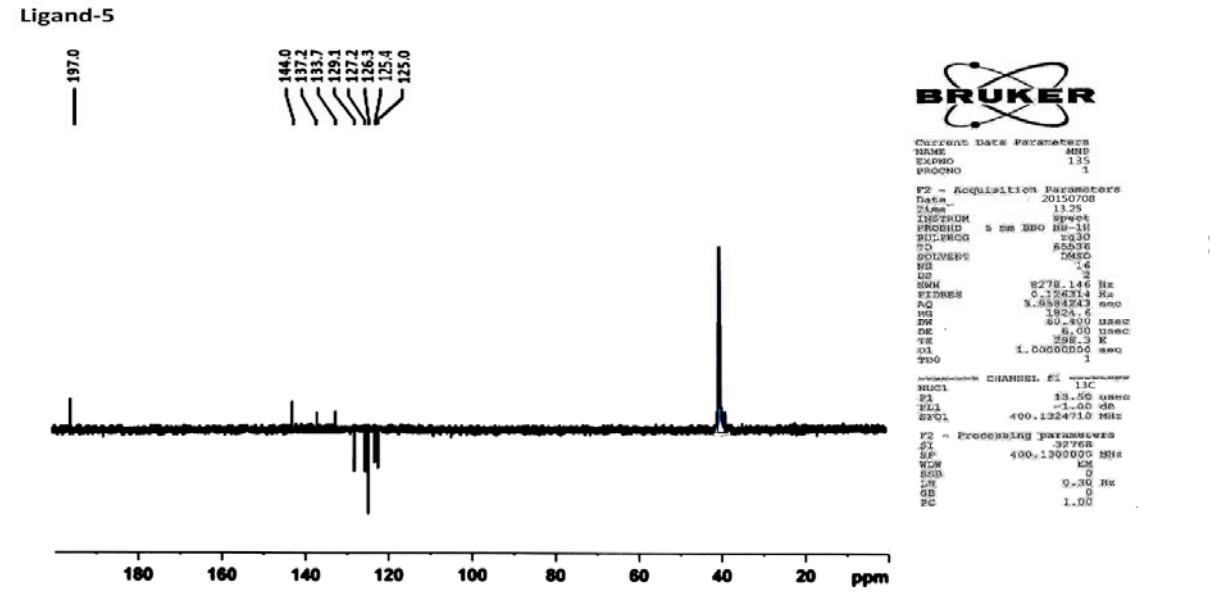

*N-(4-Nitrophenyl) thiophene-2-carboxamide (**L**^{6})*

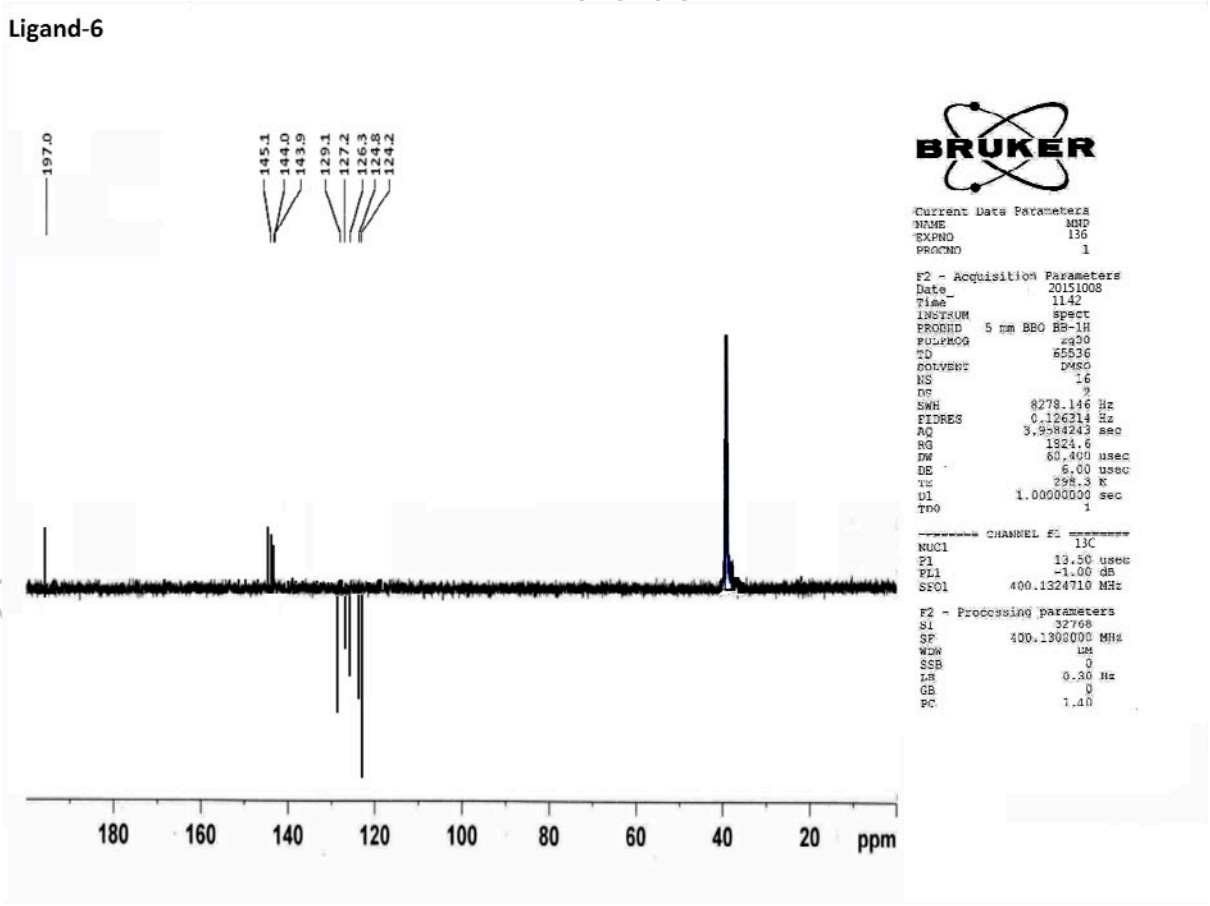

[Pt(L^1)(Cl$_2$)] (1a)

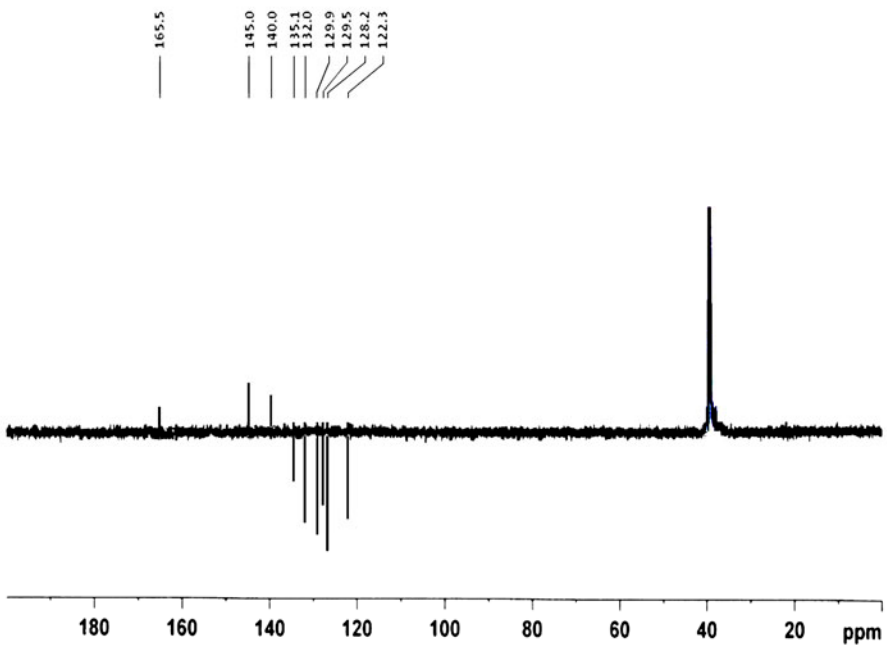

BRUKER

Current Data Parameters
NAME MNP
EXPNO 137
PROCNO 1

F2 - Acquisition Parameters
Date_ 20151108
Time 11.30
INSTRUM spect
PROBHD 5 mm BBO BB-1H
PULPROG zg30
TD 65536
SOLVENT DMSO
NS 16
DS 2
SWH 8278.146 Hz
FIDRES 0.126314 Hz
AQ 3.9584243 sec
RG 1824.6
DW 60.400 usec
DE 6.00 usec
TE 298.3 K
D1 1.00000000 sec
TD0 1

======== CHANNEL f1 ========
NUC1 13C
P1 13.50 usec
PL1 -1.00 dB
SFO1 400.1324710 MHz

F2 - Processing parameters
SI 32768
SF 400.1300000 MHz
WDW EM
SSB 0
LB 0.30 Hz
GB 0
PC 1.00

[Pt(L^2)(Cl$_2$)] (1b)

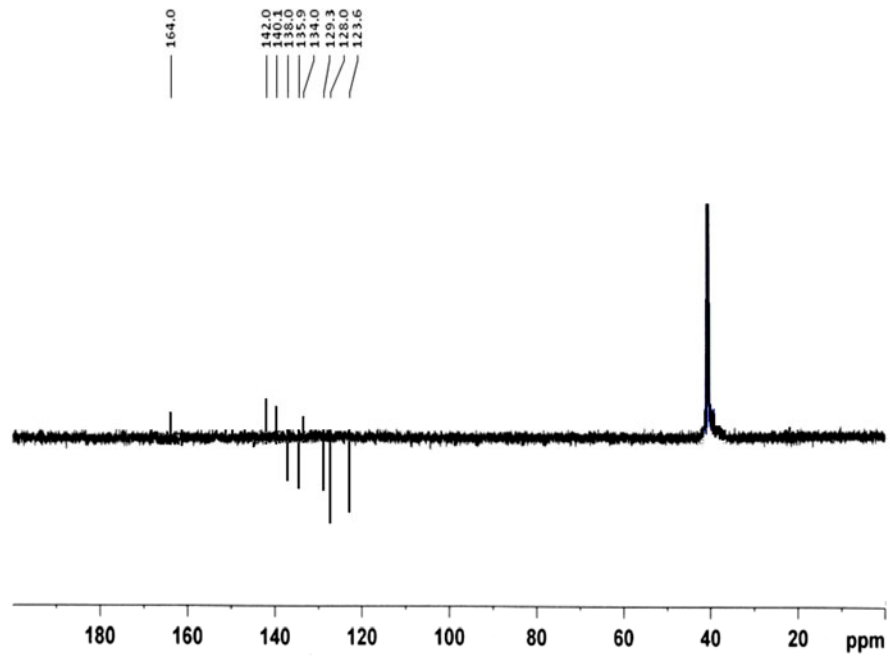

BRUKER

Current Data Parameters
NAME MNP
EXPNO 138
PROCNO 1

F2 - Acquisition Parameters
Date_ 20151208
Time 12.15
INSTRUM spect
PROBHD 5 mm BBO BB-1H
PULPROG zg30
TD 65536
SOLVENT DMSO
NS 16
DS 2
SWH 8278.146 Hz
FIDRES 0.126314 Hz
AQ 3.9584243 sec
RG 1824.6
DW 60.400 usec
DE 6.00 usec
TE 298.3 K
D1 1.00000000 sec
TD0 1

======== CHANNEL f1 ========
NUC1 13C
P1 13.50 usec
PL1 -1.00 dB
SFO1 400.1324710 MHz

F2 - Processing parameters
SI 32768
SF 400.1300000 MHz
WDW EM
SSB 0
LB 0.30 Hz
GB 0
PC 1.40

[Pt(L^3)(Cl$_2$)] (1c)

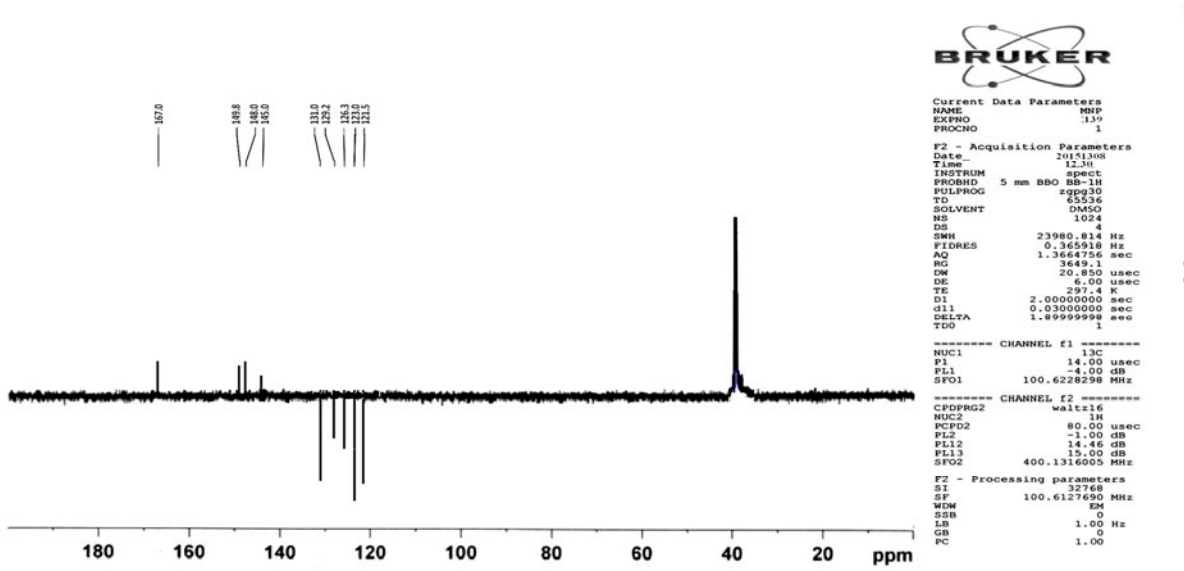

[Pt(L^4)(Cl$_2$)] (1d)

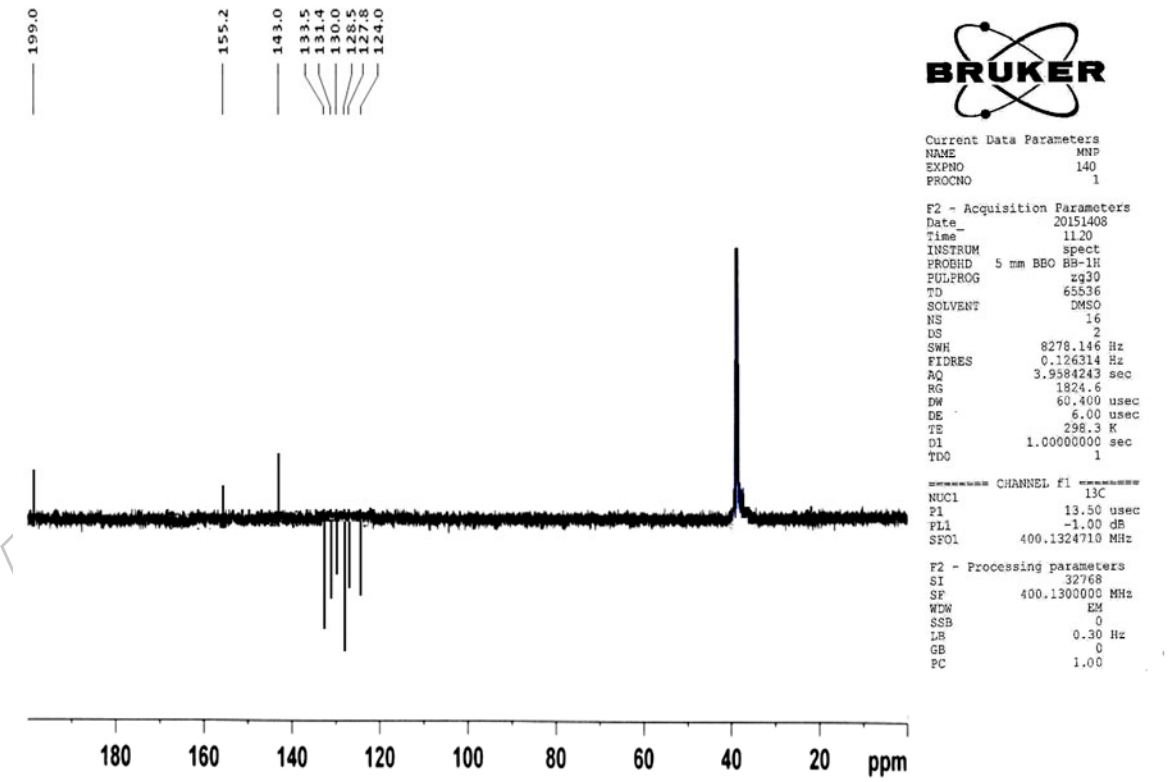

[Pt(L^5)(Cl$_2$)] (1e)

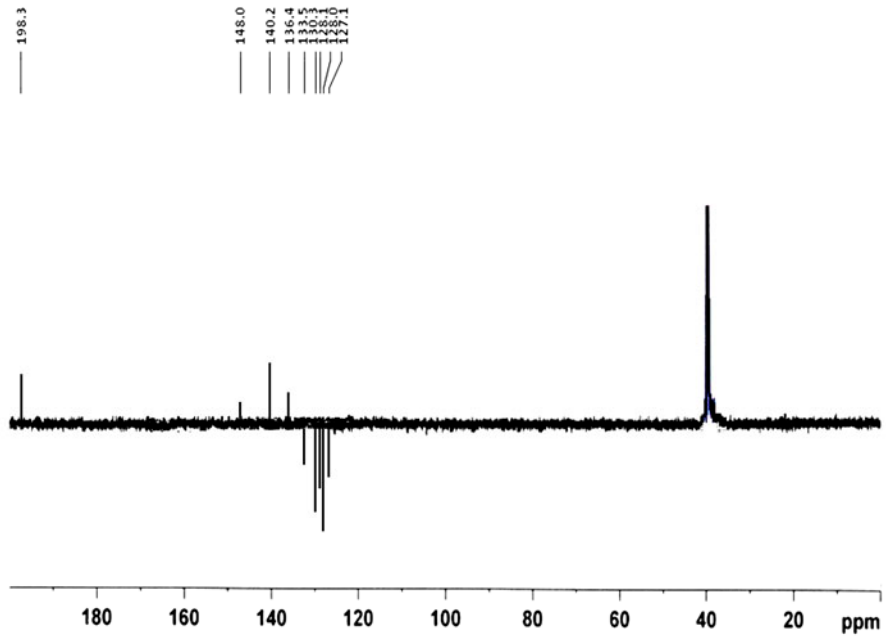

BRUKER

Current Data Parameters
NAME MNP
EXPNO 141
PROCNO 1

F2 - Acquisition Parameters
Date_ 20151808
Time 11.35
INSTRUM spect
PROBHD 5 mm BBO BB-1H
PULPROG zg30
TD 65536
SOLVENT DMSO
NS 16
DS 2
SWH 8278.146 Hz
FIDRES 0.126314 Hz
AQ 3.9584243 sec
RG 1824.6
DW 60.400 usec
DE 6.00 usec
TE 298.3 K
D1 1.00000000 sec
TD0 1

======== CHANNEL f1 ========
NUC1 13C
P1 13.50 usec
PL1 -1.00 dB
SFO1 400.1324710 MHz

F2 - Processing parameters
SI 32768
SF 400.1300000 MHz
WDW EM
SSB 0
LB 0.30 Hz
GB 0
PC 1.00

[Pt(L^6)(Cl$_2$)] (1f)

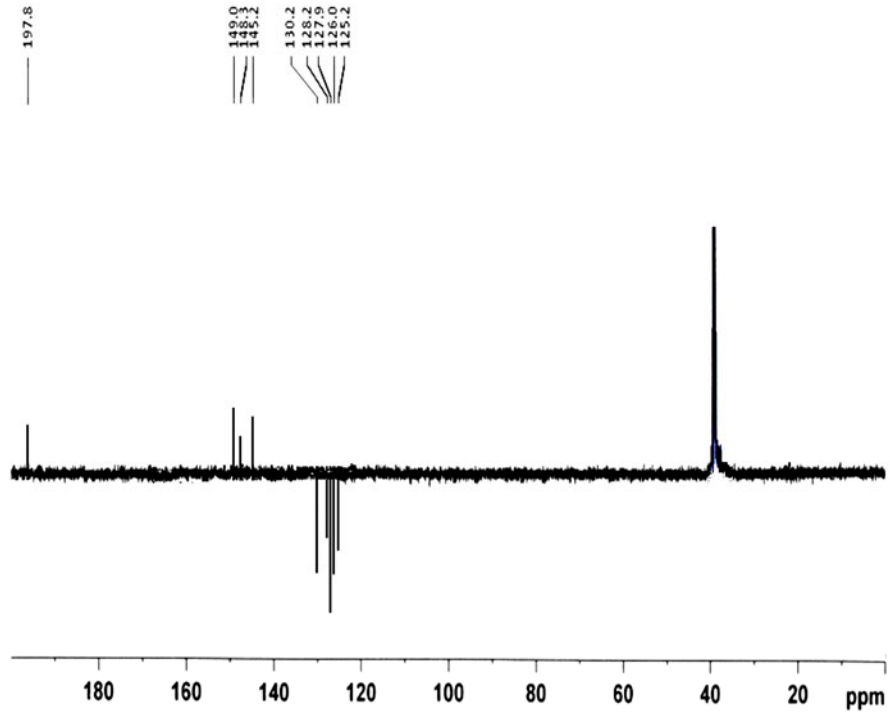

BRUKER

Current Data Parameters
NAME MNP
EXPNO 142
PROCNO 1

F2 - Acquisition Parameters
Date_ 20152008
Time 12.05
INSTRUM spect
PROBHD 5 mm BBO BB-1H
PULPROG zg30
TD 65536
SOLVENT DMSO
NS 16
DS 2
SWH 8278.146 Hz
FIDRES 0.126314 Hz
AQ 3.9584243 sec
RG 1824.6
DW 60.400 usec
DE 6.00 usec
TE 298.3 K
D1 1.00000000 sec
TD0 1

======== CHANNEL f1 ========
NUC1 13C
P1 13.50 usec
PL1 -1.00 dB
SFO1 400.1324710 MHz

F2 - Processing parameters
SI 32768
SF 400.1300000 MHz
WDW EM
SSB 0
LB 0.30 Hz
GB 0
PC 1.00

Supplementary material 6: LC-mass spectra of bidentate ligands (L^{1-6})

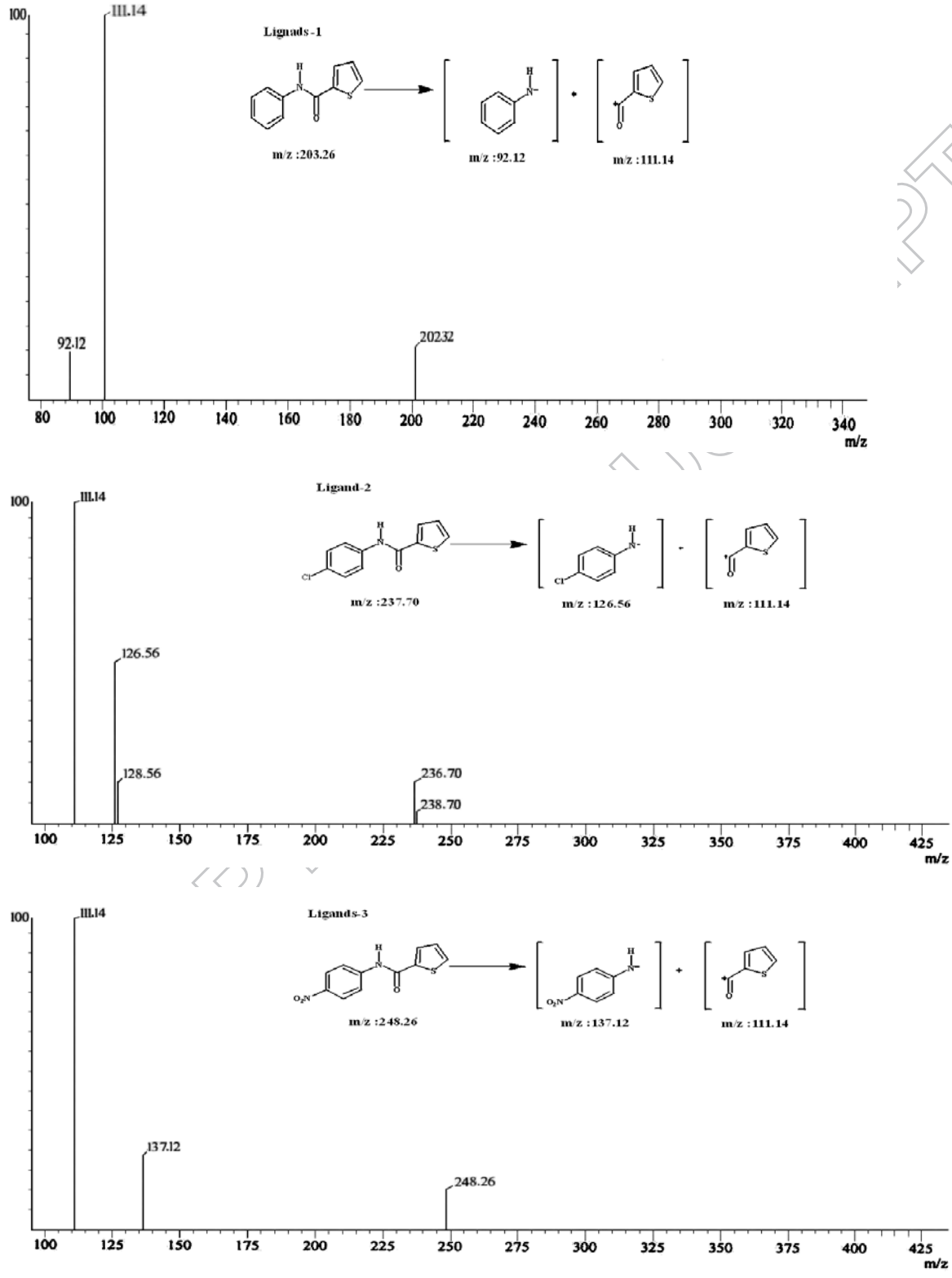

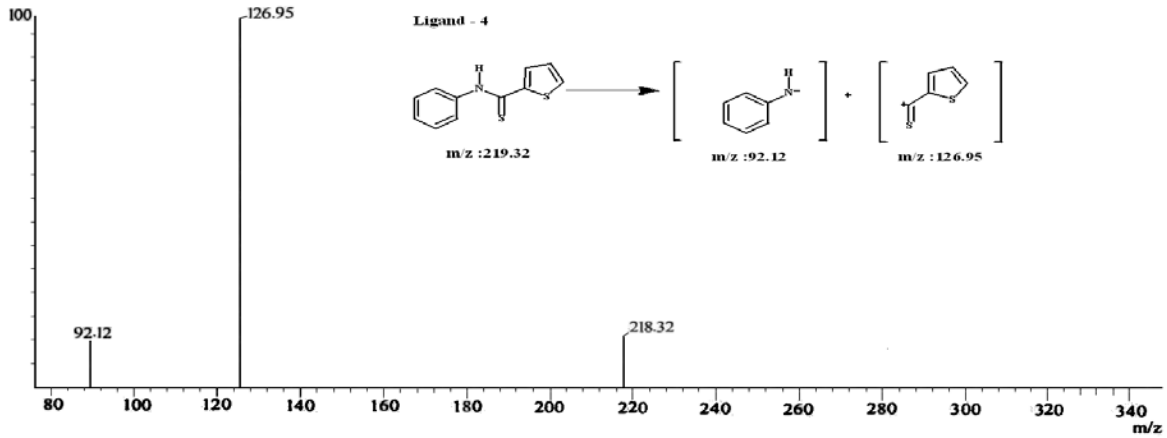
Ligand - 4
126.95
92.12
218.32
m/z :219.32
m/z :92.12
m/z :126.95
100
80 100 120 140 160 180 200 220 240 260 280 300 320 340
m/z

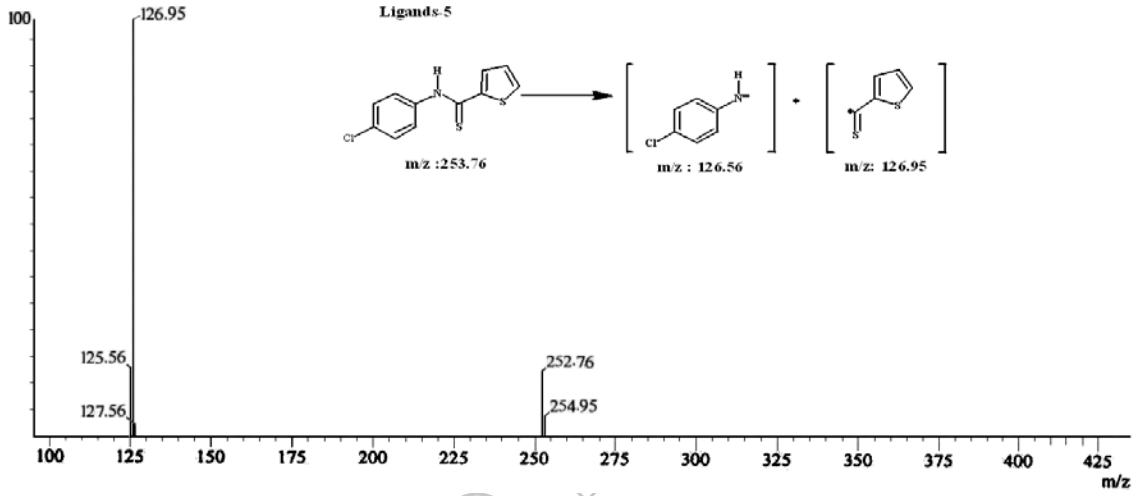
Ligands-5
126.95
125.56
127.56
252.76
254.95
m/z :253.76
m/z : 126.56
m/z: 126.95
100
100 125 150 175 200 225 250 275 300 325 350 375 400 425
m/z

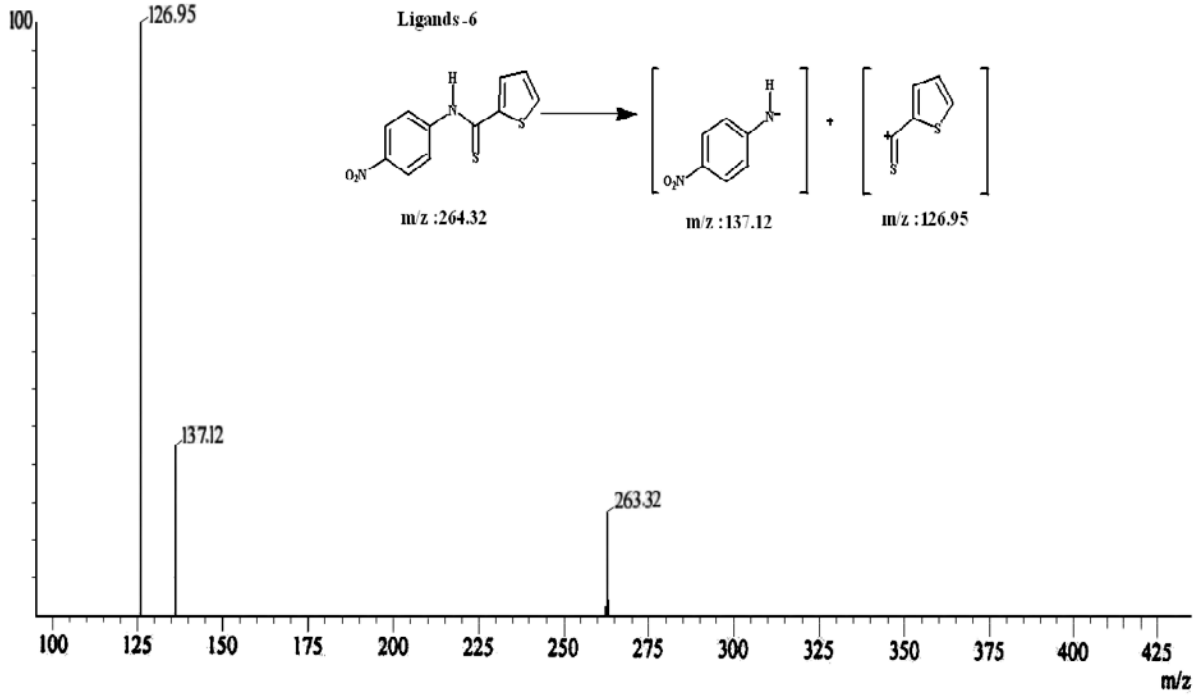
Ligands-6
126.95
137.12
263.32
m/z :264.32
m/z :137.12
m/z :126.95
100
100 125 150 175 200 225 250 275 300 325 350 375 400 425
m/z

Supplementary material 7: UV –Visible absorption and reflectance spectra of platinum(II) complexes **(1a-1f).**

Complexes	λmax (nm)$_{solution}$	λmax (nm)$_{solid}$
1a	292	303
1b	292	291
1c	292	311
1d	292	291
1e	294	305
1f	292	295

Supplementary material 8: Thermogravimetric analysis (TGA) of complex (1d), i.e. [Pt (II)(L^4)(Cl_2)]

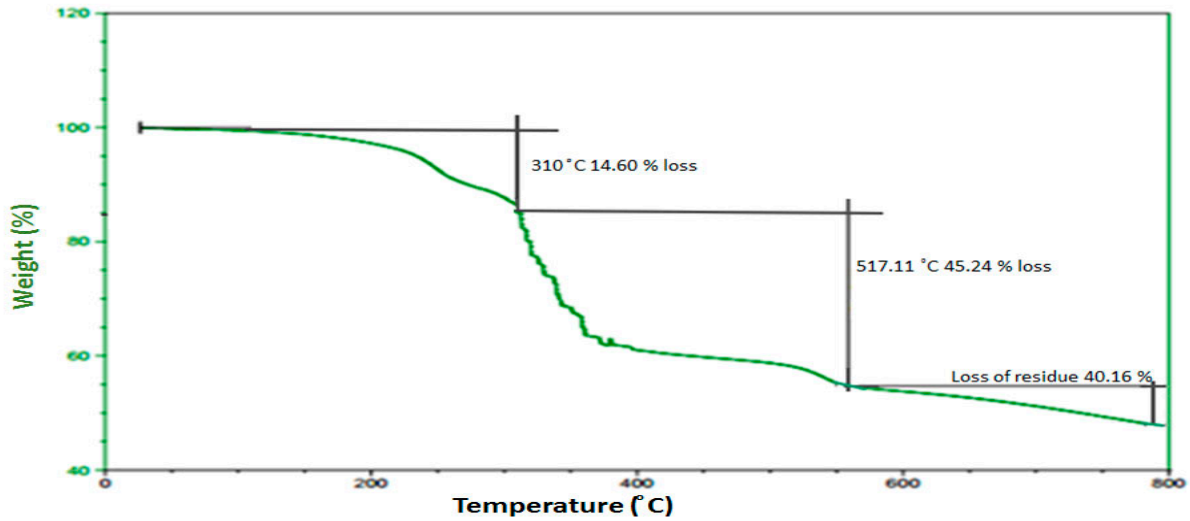

Supplementary material 9: Characteristic absorption bands of IR spectra of the thiophene-2-carboxamide and thiophene-2-carbothioamide derivatives and synthesized complexes in cm^{-1}.

Compounds	$\nu_{(NHC=O)}$ cm^{-1}	$\nu_{(NHC=S)}$ cm^{-1}	$\nu_{(C=C)}$ar(Ar= aromatic)	$\nu_{(C-H)as}$ cm^{-1}	$\nu_{(N-H)}$ cm^{-1}	$\nu_{(-C=O-M)}$$cm^{-1}$	$\nu_{(M-S)}$$cm^{-1}$	$\nu_{(-C=S-M)}$ cm^{-1}
L^1	1642	-	1550	2810	3309	-	-	-
L^2	1645	-	1595	3112	3311	-	-	-
L^3	1649	-	1560	3105	3363	-	-	-
L^4	-	1250	1592	3105	3364	-	-	-
L^5	-	1280	1502	3074	3273	-	-	-
L^6	-	1268	1556	3103	3364	-	-	-

1a	1630	-	1553	3056	3339	485	423	-
1b	1632	-	1530	3105	3315	480	435	-
1c	1639	-	1578	3111	3363	483	413	-
1d	-	1301	1599	3020	3213	-	420	545
1e	-	1363	1570	2966	3080	-	437	556
1f	-	1372	1596	3032	3213	-	425	532

Supplementary material 10: Effect of different concentration of ligands (L^{1-6}) and synthesized Pt(II) complexes on Gram$^{(+ve)}$ and Gram$^{(-ve)}$ bacteria.

Gram$^{(+ve)}$ bacteria			**Gram$^{(-ve)}$ bacteria**		
Compound	***S. Aureus***	***B. Subtilis***	***S. Marcescens***	***P. Aeruginosa***	***E. Coli***
K_2PtCl_4	2792	2688	2756	2956	2996
L^1	370	360	350	350	380
L^2	380	360	350	360	390
L^3	390	380	360	370	390
L^4	310	305	308	304	306
L^5	290	280	285	295	297
L^6	298	292	280	285	280
1a	90	90	88	85	95
1b	98	96	75	75	85
1c	88	89	92	97	99
1d	45	50	42	46	44
1e	40	42	45	41	39
1f	35	40	41	37	39

Supplementary material 11: Molecular docking of the complexes **(1a-1f)** (ball and stick) with the DNA duplex (VDW spheres with solid surface) of sequence (5'-D(CPGPCPGPAPAPTPTPCPGPCPG)-3'). The complex is docked in to the DNA showing intercalation between the DNA base pairs.

[Pt (L^1)Cl_2]- 1a

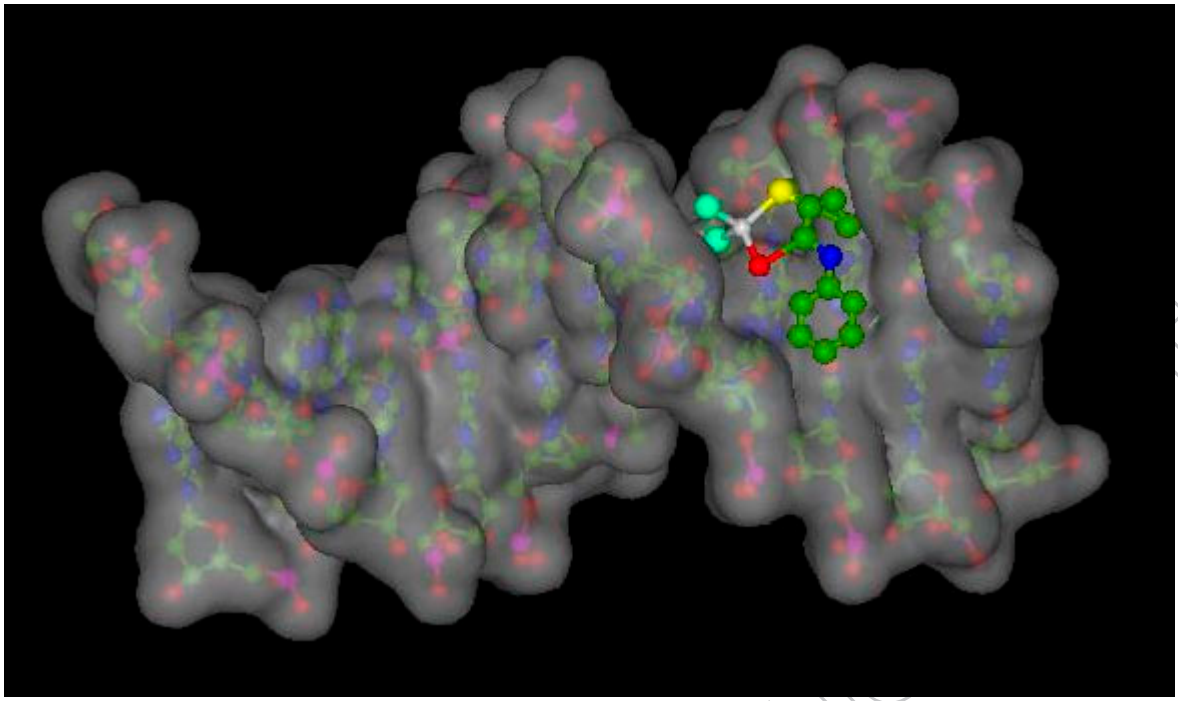

[Pt (L^2)Cl_2]- 1b

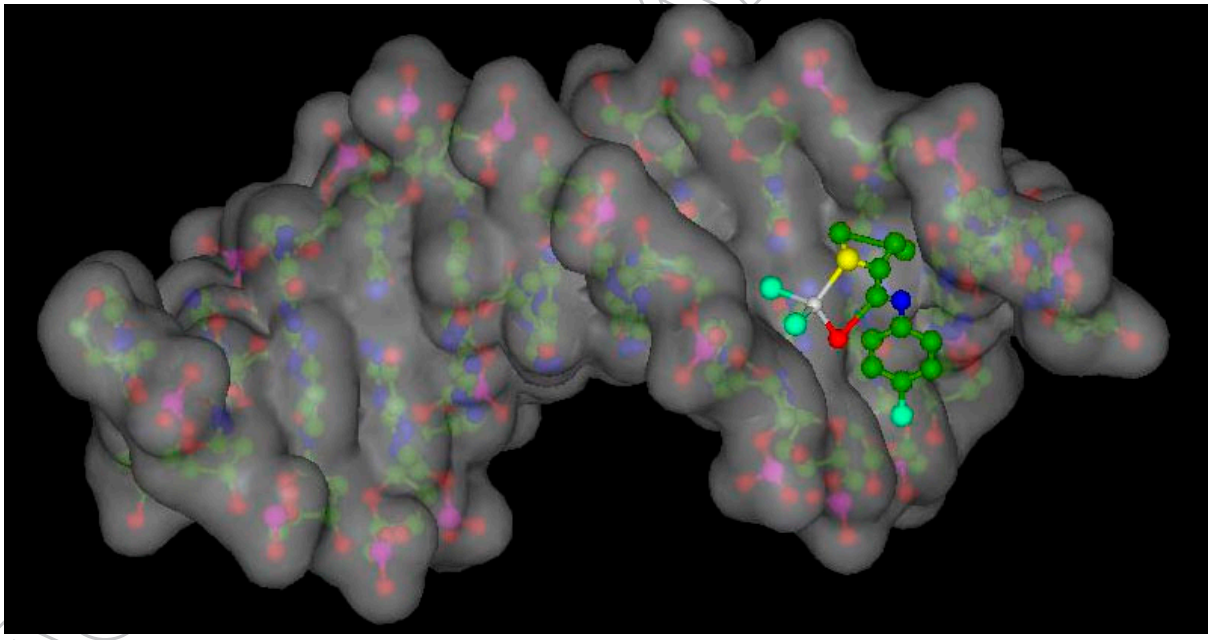

[Pt (L^3)Cl_2]- 1c

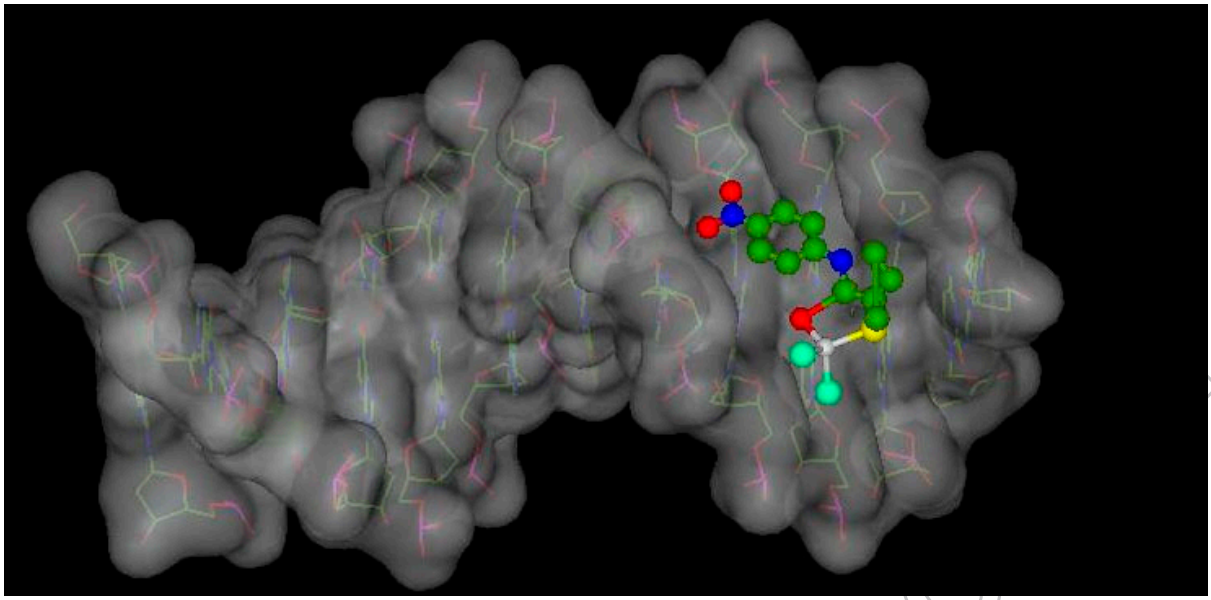

[Pt (L^4)Cl_2]- 1d

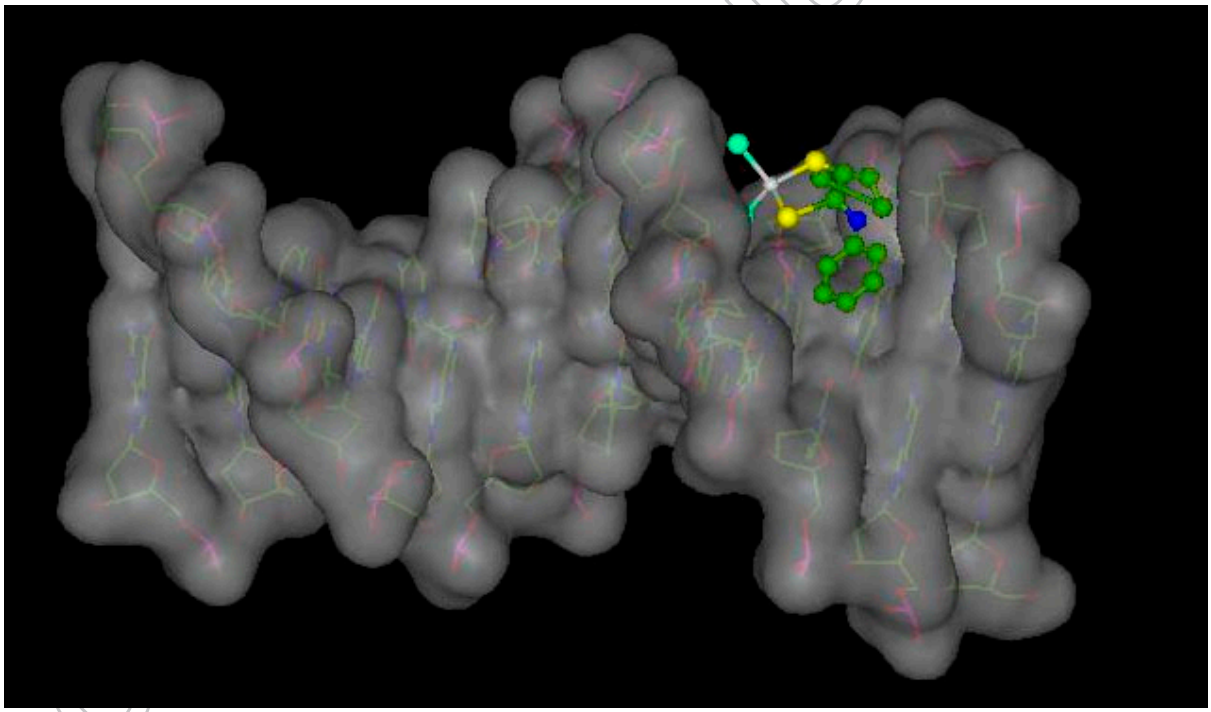

[Pt (L^5)Cl2]- 1e

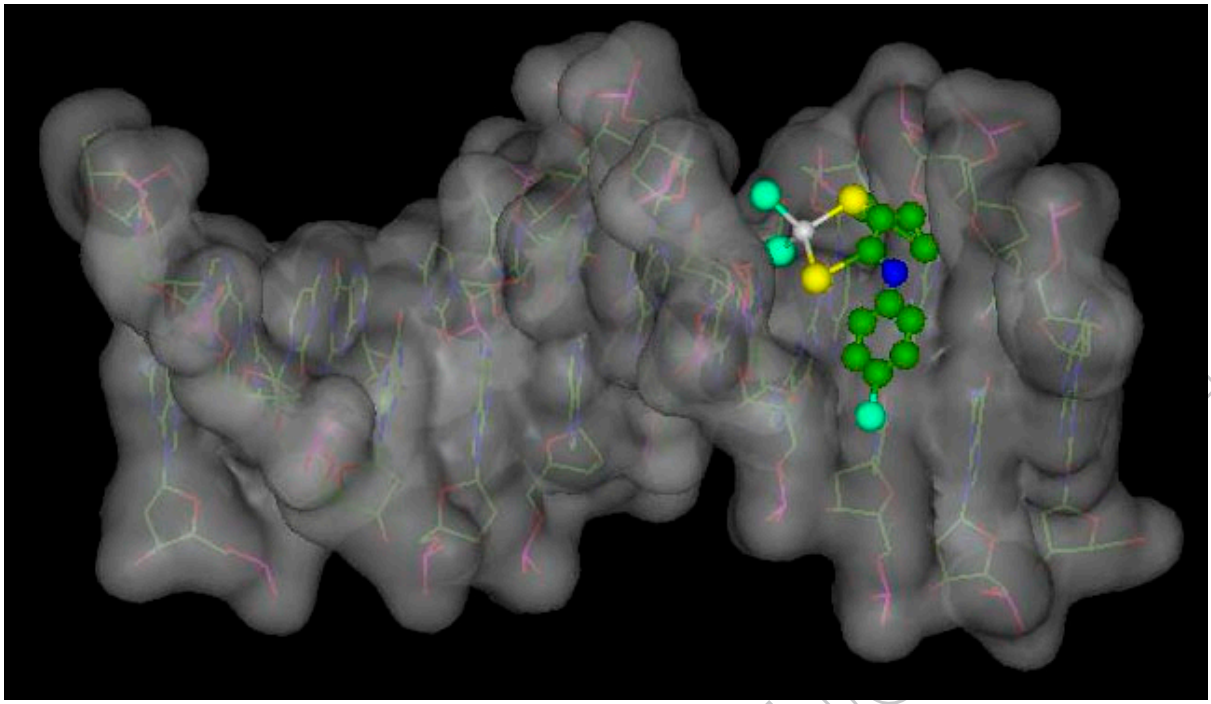

[Pt (L^6)Cl_2]- 1f

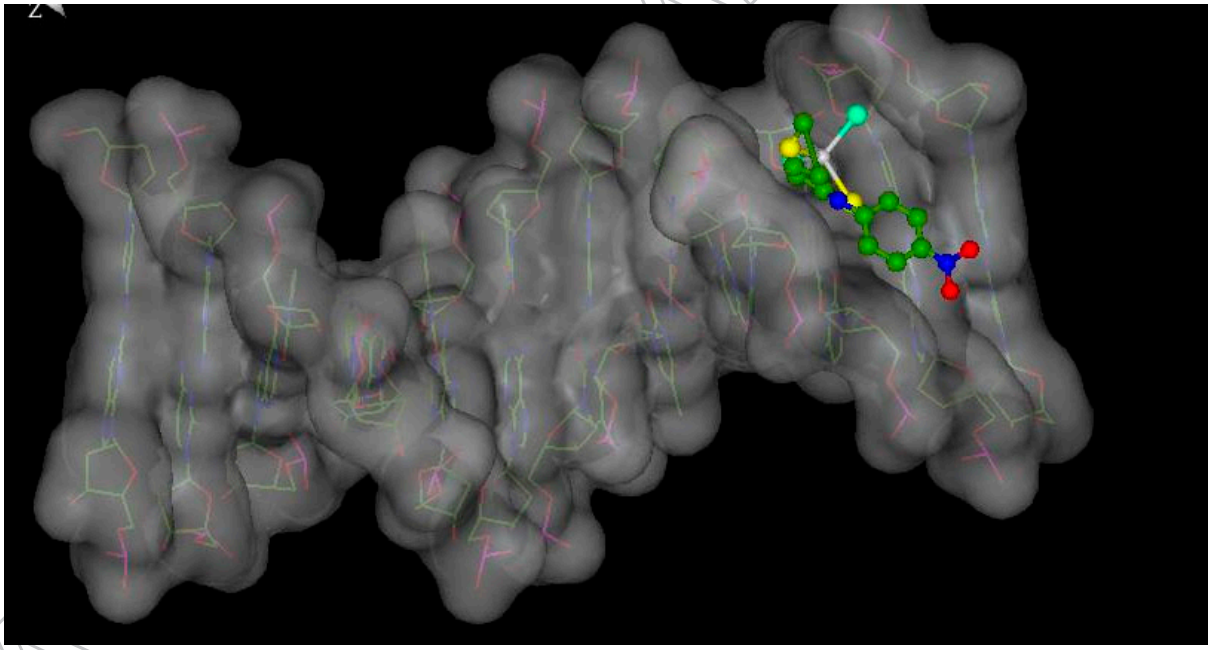

Supplementary material 12: Linear Stern-Volmer quenching constant (K_q), associative binding constant (K_a) and number of binding sites (n) calculated from plots for the interaction of Pt(II) complexes (1a-1f) with CT-DNA, and also calculated standard free energy changes (ΔG).

[Pt(L^1)(Cl_2)] (1a)

Volume (µL)	Intensity (CPS) $I_{corr.}$	Intensity (CPS) $I_{obs.}$	I_0/I	$(I_0 - I)/I$	$\log(I_0 - I/I)$	$Q \times 10^{-6}$ (µM)	log Q	K_q (M^{-1})	K_a (M^{-1})	n	ΔG(Jmol^{-1})
0	90920	90739	1.0019	0	-	0	-				
5	90721	90540	1.0041	0.0041	-2.3781	3.33	-5.47712				
10	90506	90325	1.0065	0.0065	-2.18163	6.66	-5.17609				
15	90414	90233	1.0076	0.0076	-2.11881	10	-5				
20	90240	90060	1.0095	0.0095	-2.02003	13.3	-4.87506				
25	90228	90048	1.0096	0.0096	-2.01405	16.6	-4.77815				
30	89836	89657	1.0140	0.0140	-1.85128	20	-4.69897				
35	89829	89650	1.0141	0.0141	-1.84875	23.3	-4.63202				
40	89128	88950	1.0221	0.0221	-1.65488	26.6	-4.57403				
45	88603	88426	1.0282	0.0282	-1.54975	30	-4.52288				
50	88161	87985	1.0333	0.0333	-1.47687	33.3	-4.47712				

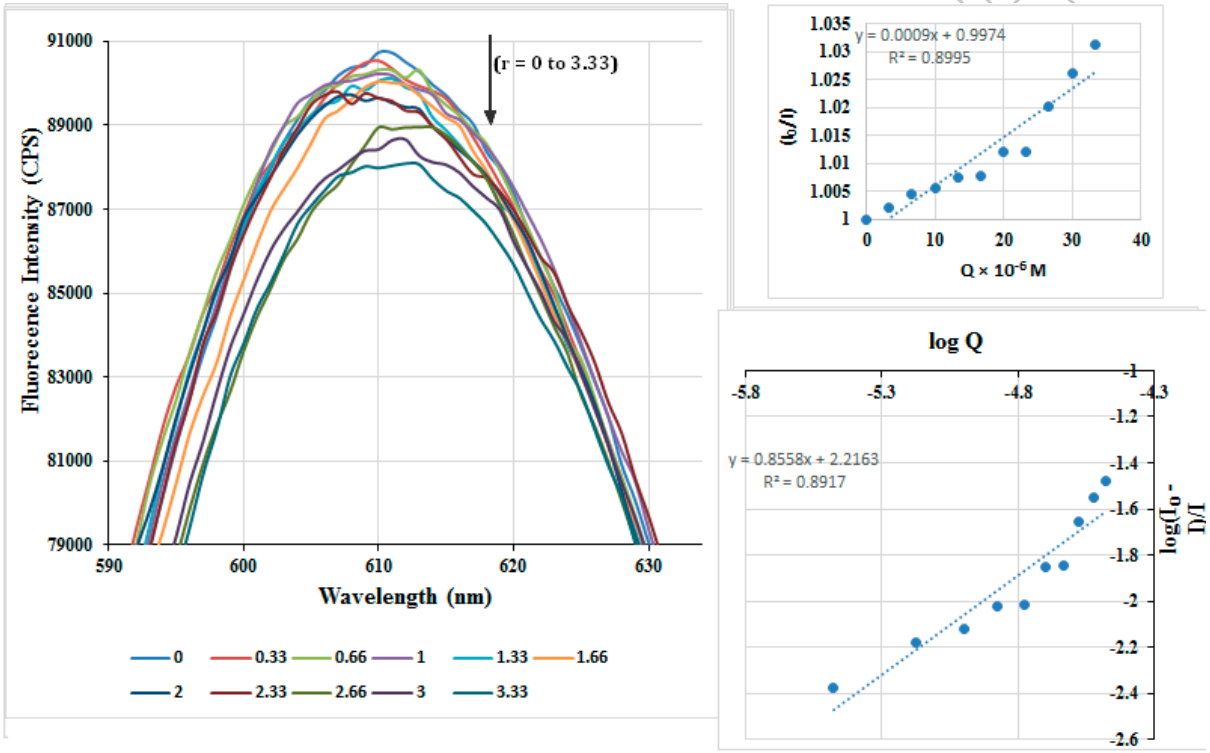

Fig. S1. Emission spectra of EB bound to DNA in the presence of Pt(II) complex **(1a)**. ([DNA] = 1.00 × 10-5 M, [EB] = 33.3 µM, [Quencher] (µM): 0 - 3.33 µM. The arrow shows the intensity changes upon gradual increasing the complex concentration. Inset: plot of I_0/I vs. [Quencher] and comparative plot of log[I_0-I/I] vs. log[Q] for the titration of CT-DNA EB system with Pt(II) complex (1a) in 1 M Tris-HCl buffer (pH 7.2) medium.

[Pt(L^2)(Cl$_2$)] (1b)

Volume (µL)	Intensity (CPS) $I_{corr.}$	Intensity (CPS) $I_{obs.}$	I_o/I	$(I_o - I)/I$	$\log(I_o - I/I)$	$Q \times 10^{-6}$ (µM)	log Q	K_q (M^{-1})	K_a (M^{-1})	n	ΔG(J mol^{-1})
0	90359	90179	1.0019	0	-	0	-				
5	90173	89993	1.0040	0.00406	-2.3914	3.33	-5.47				
10	89078	88900	1.0164	0.01640	-1.7842	6.66	-5.17				
15	88305	88129	1.0253	0.02530	-1.5968	10.00	-5.00				
20	88022	87846	1.0286	0.02860	-1.5435	13.33	-4.87				
25	87223	87049	1.0380	0.03802	-1.4199	16.66	-4.77				
30	86168	85996	1.0507	0.05073	-1.2947	20.00	-4.69				
35	85584	85413	1.0578	0.05789	-1.2373	23.33	-4.63				
40	84965	84795	1.0656	0.06561	-1.1830	26.66	-4.57				
45	83947	83780	1.0785	0.07852	-1.1049	30.00	-4.52				
50	83367	83200	1.0860	0.08603	-1.0653	33.33	-4.47	2.6×10^3	3.1×10^4	1.2383	-25,671.60

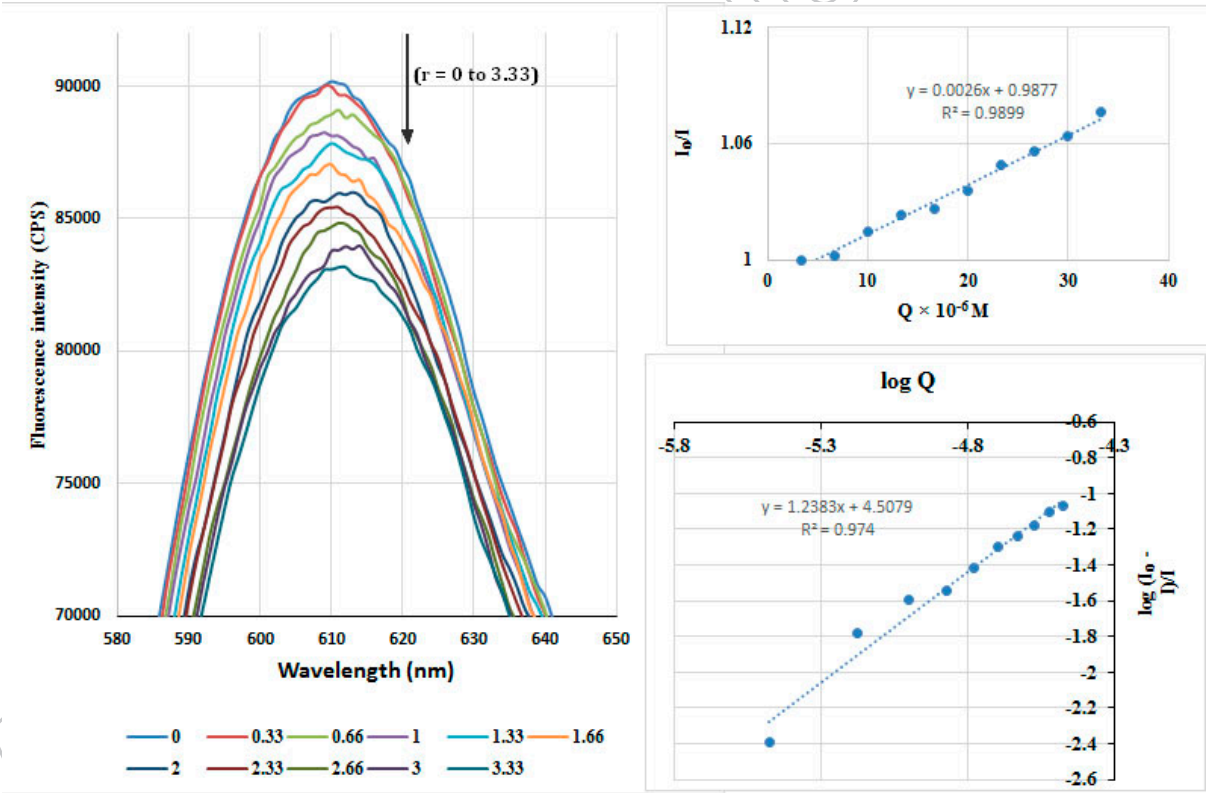

Fig. S2. Emission spectra of EB bound to DNA in the presence of Pt(II) complex **(1b)**. ([DNA] = 1.00×10^{-5} M, [EB] = 33.3 µM, [Quencher] (µM): 0 - 3.33 µM. The arrow shows the intensity changes upon gradual increasing the complex concentration. Inset: plot of I_0/I

vs. [Quencher] and comparative plot of log[I_0-I/I] vs. log[Q] for the titration of CT-DNA EB system with Pt(II) complex (1b) in 1 M Tris-HCl buffer (pH 7.2) medium.

[Pt(L^3)(Cl_2)] (1c)

Volume (µL)	Intensity (CPS) $I_{corr.}$	Intensity (CPS) $I_{obs.}$	I_o/I	$(I_o - I)/I$	$\log(I_o - I/I)$	Q × 10^{-6} (µM)	log Q	K_q (M^{-1})	K_a (M^{-1})	n	ΔG(J mol^{-1})
0	83953	83785	1.0019	0	-	0	-	2.9 ×10^3	1.73 × 10^3	0.951	-18,482.00
5	83071	82905	1.0126	0.01263	-1.8984	3.33	-5.47				
10	82812	82647	1.0157	0.01579	-1.8013	6.66	-5.17				
15	81407	81244	1.0333	0.03333	-1.4770	10	-5.00				
20	80734	80573	1.0419	0.04194	-1.3773	13.33	-4.87				
25	80828	80667	1.0407	0.04073	-1.3900	16.66	-4.77				
30	78929	78771	1.0657	0.06577	-1.1819	20	-4.69				
35	78535	78379	1.0711	0.07111	-1.1480	23.33	-4.63				
40	77918	77762	1.0796	0.07960	-1.0990	26.66	-4.57				
45	77260	77106	1.0887	0.08879	-1.0516	30	-4.52				
50	76708	76555	1.0966	0.09662	-1.0148	33.33	-4.47				

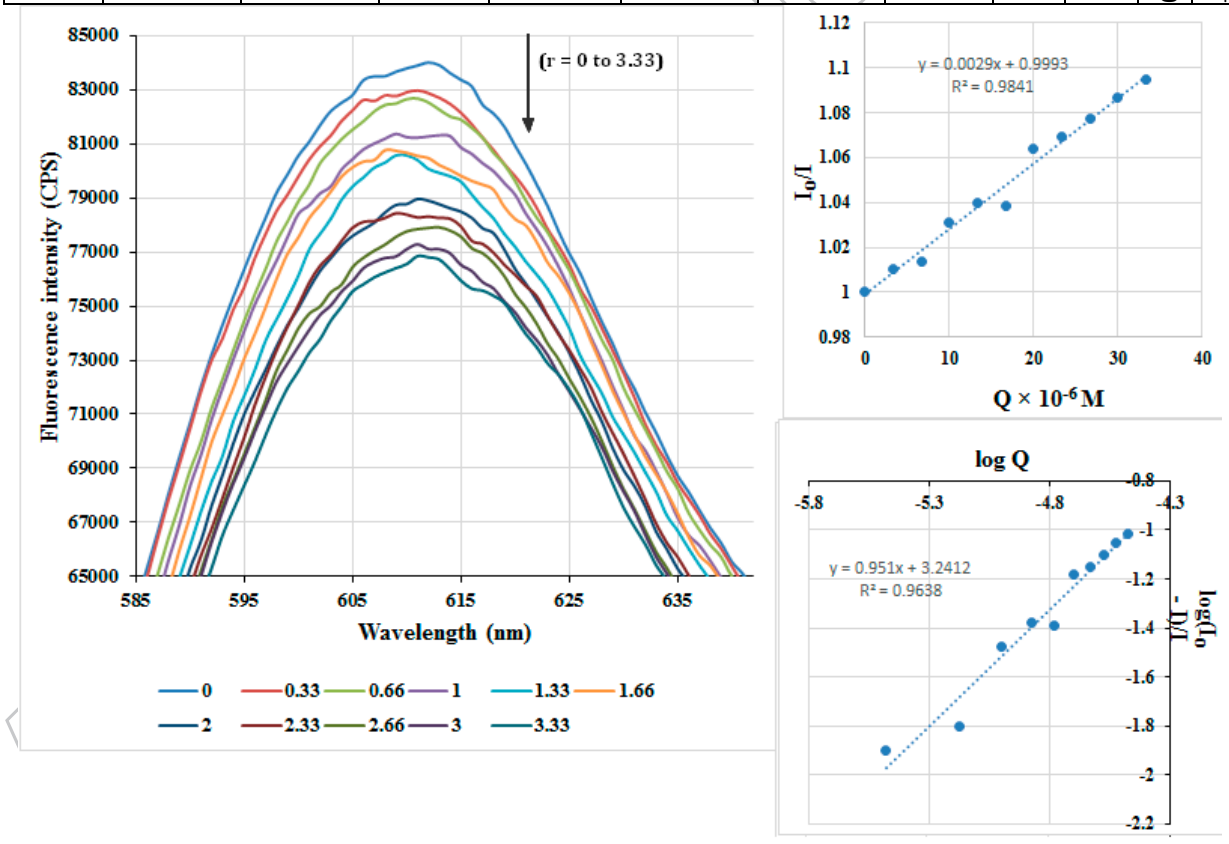

Fig. S3. Emission spectra of EB bound to DNA in the presence of Pt(II) complex **(1c)**. ([DNA] = 1.00 × 10^{-5} M, [EB] = 33.3 µM, [Quencher] (µM): 0 - 3.33 µM. The arrow shows

the intensity changes upon gradual increasing the complex concentration. Inset: plot of I_0/I vs. [Quencher] and comparative plot of log[I_0-I/I] vs. log[Q] for the titration of CT-DNA EB system with Pt(II) complex (1c) in 1 M Tris-HCl buffer (pH 7.2) medium.

[Pt(L^4)(Cl_2)] (1d)

Volume (µL)	Intensity (CPS) $I_{corr.}$	Intensity (CPS) $I_{obs.}$	I_0/I	$(I_0 - I)/I$	log(I_0 - I/I)	Q × 10^{-6} (µM)	log Q	K_q (M^{-1})	K_a (M^{-1})	n	ΔG(J mol^{-1})
0	91836	91652	1.0019	0	-	0	-				
5	90756	90575	1.0139	0.0139	-1.856	3.33	-5.47				
10	89689	89510	1.0259	0.0259	-1.585	6.66	-5.17				
15	88483	88307	1.0399	0.0399	-1.398	10.00	-5.00				
20	87537	87362	1.0515	0.0512	-1.290	13.33	-4.87				
25	86131	85960	1.0683	0.0683	-1.165	16.66	-4.77				
30	85851	85680	1.0718	0.0718	-1.143	20.00	-4.69				
35	84375	84207	1.0905	0.0905	-1.042	23.33	-4.63				
40	83567	83400	1.1011	0.1011	-0.995	26.66	-4.57				
45	82822	82657	1.1113	0.1110	-0.954	30.00	-4.52				
50	81287	81125	1.1320	0.1320	-0.879	33.33	-4.47	3.8×10^3	2.65×10^3	0.9648	-19,510.00

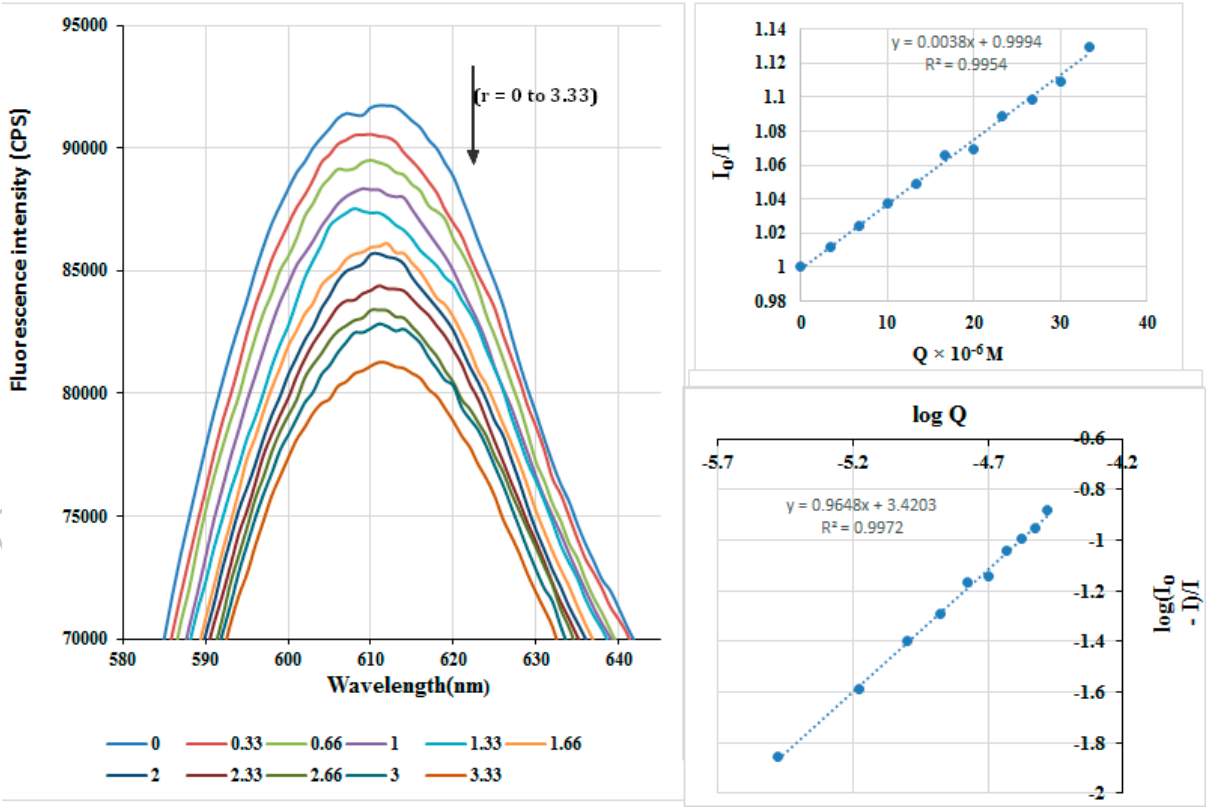

Fig. S4. Emission spectra of EB bound to DNA in the presence of Pt(II) complex **(1d).** ([DNA] = 1.00 × 10^{-5} M, [EB] = 33.3 µM, [Quencher] (µM): 0 - 3.33 µM. The arrow shows the intensity changes upon gradual increasing the complex concentration. Inset: plot of I_0/I vs. [Quencher] and comparative plot of log[I_0-I/I] vs. log[Q] for the titration of CT-DNA EB system with Pt(II) complex (1d) in 1 M Tris-HCl buffer (pH 7.2) medium.

[Pt(L^5)(Cl_2)] (1e)

Volume (µL)	Intensity (CPS) $I_{corr.}$	Intensity (CPS) $I_{obs.}$	I_o/I	$(I_o - I)/I$	log(I_o - I/I)	Q × 10^{-6} (µM)	log Q	K_q (M^{-1})	K_a (M^{-1})	n	ΔG(Jmol^{-1})
0	95277	95087	1.0019	0	-	0	-				
5	94663	94474	1.0084	0.0084	-2.079	3.33	-5.477				
10	93933	93746	1.0163	0.0163	-1.787	6.66	-5.176				
15	92888	92702	1.0277	0.0277	-1.556	10	-5				
20	92029	91845	1.0373	0.0373	-1.427	13.33	-4.875				
25	91404	91221	1.0444	0.0444	-1.352	16.66	-4.778				
30	90326	90146	1.0569	0.0569	-1.244	20	-4.698				
35	89433	89254	1.0674	0.0674	-1.170	23.33	-4.632				
40	88829	88651	1.0747	0.0747	-1.126	26.66	-4.574				
45	88678	88501	1.0765	0.0765	-1.116	30	-4.522				
50	85275	85105	1.1195	0.1195	-0.922	33.33	-4.477				
								3.1×10^3	0.698×10^4	1.083	-21,929.32

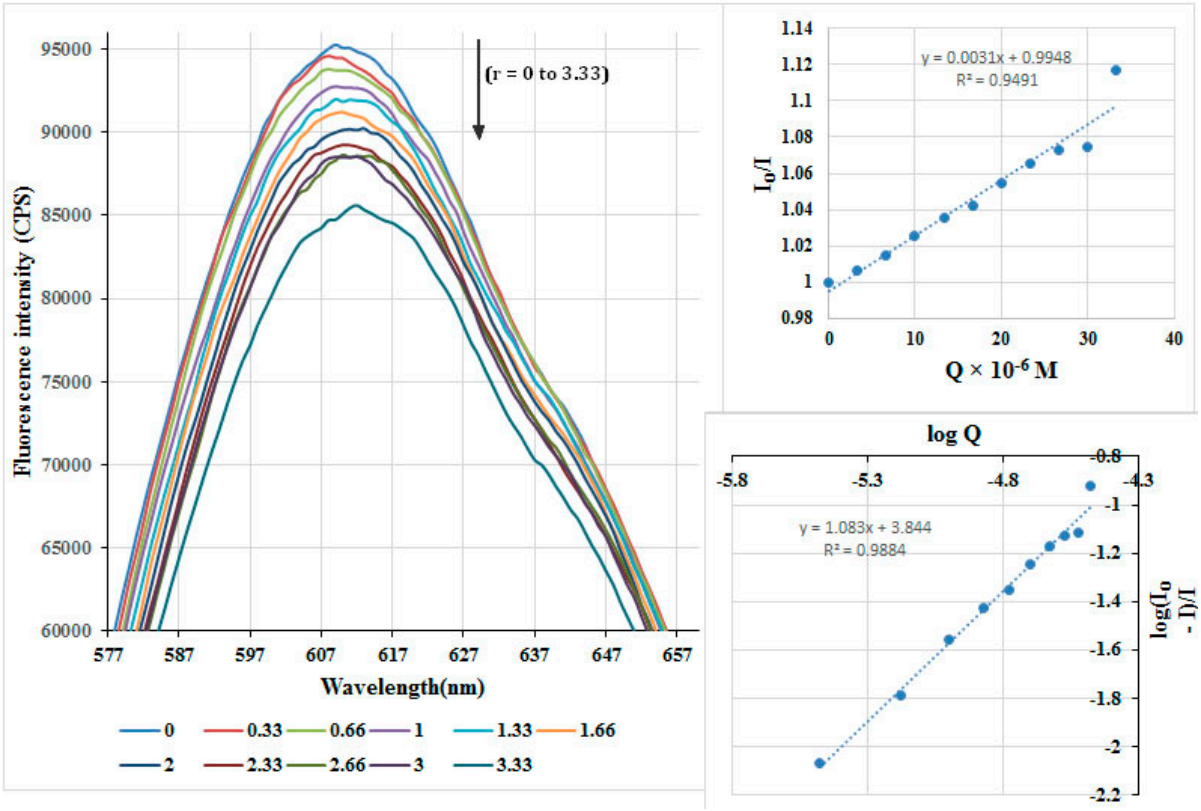

Fig. S5. Emission spectra of EB bound to DNA in the presence of Pt(II) complex **(1e)**. [DNA] = 1.00×10^{-5} M, [EB] = 33.3 µM, [Quencher] (µM): 0 - 3.33 µM. The arrow shows the intensity changes upon gradual increasing the complex concentration. Inset: plot of I_0/I vs. [Quencher] and comparative plot of $\log[I_0\text{-}I/I]$ vs. log[Q] for the titration of CT-DNA EB system with Pt(II) complex (1e) in 1 M Tris-HCl buffer (pH 7.2) medium.

[Pt(L^6)(Cl$_2$)] (1f)

Volume (µL)	**Intensity (CPS) I_{corr}**	**Intensity (CPS) $I_{obs.}$**	**I_0/I**	**$(I_0 - I)/I$**	**$\log(I_0 - I/I)$**	**$Q \times 10^{-6}$ (µM)**	**log Q**	**K_q (M^{-1})**	**K_a (M^{-1})**	**n**	**ΔG(Jmol^{-1})**
0	89975	89796	0.999996	0	-	0	-				
5	89913	89733	1.0006	0.00269	-2.57028	3.33	-5.477				
10	89821	89641	1.0017	0.00371	-2.42983	6.66	-5.176				
15	89616	89437	1.0040	0.00601	-2.22096	10	-5				
20	89494	89315	1.0053	0.00738	-2.13168	13.33	-4.875				
25	89427	89249	1.0061	0.00813	-2.08972	16.66	-4.778				
30	89201	89023	1.0086	0.01069	-1.97091	20	-4.698				
35	89178	89000	1.0089	0.01094	-1.96071	23.33	-4.632				
40	88978	88800	1.0112	0.01322	-1.87865	26.66	-4.574				
45	89017	88840	1.0105	0.01277	-1.89361	30	-4.522	4.0×10^4	0.34×10^2	0.7543	-8,757.46
50	88946	88768	1.0115	0.01359	-1.86675	33.33	-4.477				

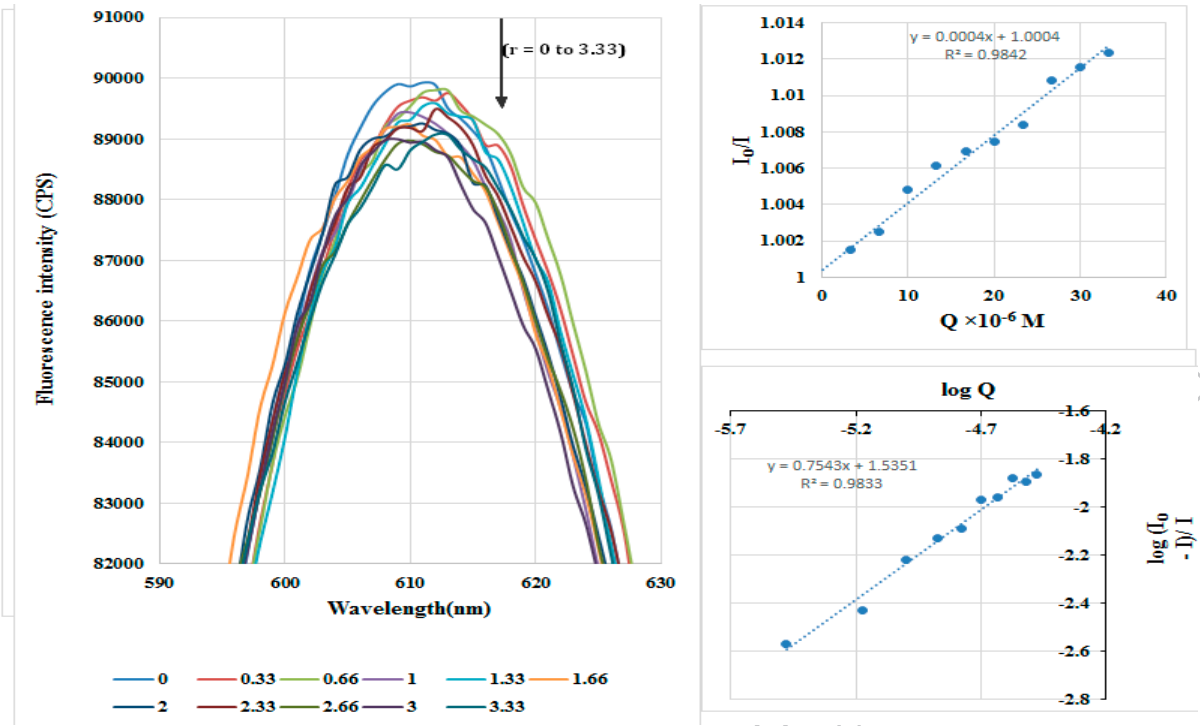

Fig. S6. Emission spectra of EB bound to DNA in the presence of Pt(II) complex **(1f)**. ([DNA] = 1.00 × 10^{-5} M, [EB] = 33.3 µM, [Quencher] (µM): 0 - 3.33 µM. The arrow shows the intensity changes upon gradual increasing the complex concentration. Inset: plot of I_0/I vs. [Quencher] and comparative plot of log[I_0-I/I] vs. log[Q] for the titration of CT-DNA EB system with Pt(II) complex (1f) in 1 M Tris-HCl buffer (pH 7.2) medium.